

1 Primary and Secondary Sources of Atmospheric Aerosol

Claudio Tomasi and Angelo Lupi

1.1

Introduction

Atmospheric aerosols are suspensions of any substance existing in the solid and/or liquid phase in the atmosphere (except pure water) under normal conditions and having a minimum stability in air assuring an atmospheric lifetime of at least 1 h. Generated by natural sources (i.e., wind-borne dust, sea spray, volcanic debris, biogenic aerosol) and/or anthropogenic activities (i.e., sulfates and nitrates from industrial emissions, wind-forced mineral dust mobilized in areas exploited for agricultural activities, fossil fuel combustion, and waste and biomass burning), aerosol particles range in size from a few nanometers to several tens of microns. As a result of internal cohesive forces and their negligible terminal fall speeds, aerosol particles can first assume sizes appreciably larger than the most common air molecules and subsequently increase to reach sizes ranging most frequently from less than 10^{-3} to no more than $100\ \mu\text{m}$ (Heintzenberg, 1994). Particles with sizes smaller than $20\text{--}30\ \text{\AA}$ ($1\ \text{\AA} = 10^{-10}\ \text{m}$) are usually classified as clusters or small ions, while mineral and tropospheric volcanic dust particles with sizes greater than a few hundred microns are not considered to belong to the coarse aerosol class, since they have very short lifetimes. Aerosol particles grown by condensation to become cloud droplets are not classified as aerosols, although a cloud droplet needs a relatively small aerosol particle acting as a condensation nucleus for its formation under normal atmospheric conditions. Similarly, precipitation elements such as rain droplets, snowflakes, and ice crystals are not classified as aerosols (Heintzenberg, 1994). Although present in considerably lower concentrations than those of the main air molecules, aerosol particles play a very important role in numerous meteorological, physical, and chemical processes occurring in the atmosphere, such as the electrical conductivity of air, condensation of water vapor on small nuclei and subsequent formation of fog and cloud droplets, acid rains, scattering, and absorption of both incoming solar (shortwave) radiation and thermal terrestrial (longwave) radiation. The interaction processes between atmospheric aerosols and the downwelling and upwelling radiation fluxes of solar

and terrestrial radiation at the surface play a major role in defining the radiation budget of our planet and, hence, the Earth's climate (Chylek and Coakley, 1974).

To give an idea of the shape of an aerosol particle suspended in dry air, a schematic representation of a particle originating from the aggregation of various kinds of particulate matter fragments is shown in Figure 1.1. It consists of several small unit structures of different chemical composition and origin (soluble acid substances, sodium chloride crystals of marine origin, ammonium sulfates, insoluble carbonaceous matter, insoluble mineral dust, and insoluble organic substances), held together by interparticle adhesive forces in such a way that an aerosol particle behaves as a single unit in suspension. Thus, the same particle often contains distinct homogeneous entities, which are internally mixed to form aggregates of different components.

The insoluble carbonaceous and organic substances often consist of gas-borne particulate matter pieces from incomplete combustion, which predominantly contain carbon and other combustion-produced materials. When the surrounding air relative humidity (RH) increases to reach values higher than 65–70%, the same particle (containing soluble substances) grows gradually by condensation of water vapor to become a water droplet in which pieces of insoluble matter are suspended, as can be seen in the (b) of Figure 1.1 (see also Hänel, 1976), while the various soluble materials reach different solution states as a result of their appreciably differing deliquescence properties. In this way, an internally mixed particle evolves assuming the characteristics of an aggregate consisting of different particulate phases. Figure 1.1 also shows that dry aerosol particles can often exhibit irregular shapes, which can considerably differ from the spherical

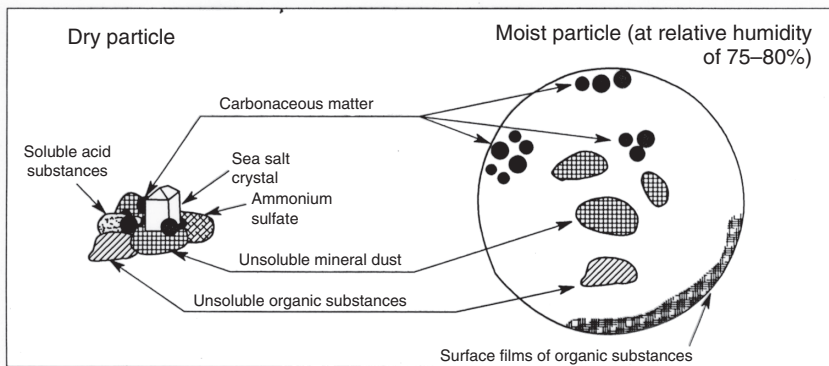


Figure 1.1 Schematic representation of an aerosol particle for dry air conditions (left) and humid air (for relative humidity (RH) = 75–80% conditions (right), consisting of particulate matter pieces of soluble (i.e., soluble acid substances, sea-salt crystal, ammonium sulfates) and insoluble substances (carbonaceous matter, mineral

dust, organic substances), which remain suspended inside the moist particle gradually growing by condensation until becoming a water droplet with soluble salts, acids, and organic compounds. (Adapted from a draft presented by Gottfried Hänel in a seminar given in 1985 at the FISBAT-CNR Institute, Bologna, Italy.)

one. Thus, the size of each real aerosol particle is generally evaluated in terms of an “equivalent” diameter a , for which the volume of such an ideal spherical particle is equal to that of the real particle.

Aerosol particles cover a size range of more than five orders of magnitude, with “equivalent” sizes ranging from 5×10^{-3} to $2.5 \mu\text{m}$ for fine particles and greater than $2.5 \mu\text{m}$ for coarse particles (Hinds, 1999). The fine particles include both (i) the so-called Aitken nuclei, having sizes mainly ranging from 5×10^{-3} to $5 \times 10^{-2} \mu\text{m}$, and (ii) the so-called “accumulation” particles having sizes ranging from 5×10^{-2} to about $2 \mu\text{m}$. In this classification, it is worth mentioning that (i) the nuclei constitute the most important part of the so-called ultrafine particles (which have sizes $< 10^{-1} \mu\text{m}$) and mainly form through condensation of hot vapors during combustion processes and/or nucleation of atmospheric gaseous species to form fresh particles and (ii) the accumulation particles are mainly generated through coagulation of small particles belonging to the nuclei class and condensation of vapors onto existing particles, inducing them to grow appreciably. Consequently, the particle concentration within this size subrange increases, and the accumulation mode becomes gradually more evident, so named because the particle removal mechanisms are poorly efficient in limiting the concentration of such an intermediate-size class of particles. Therefore, such particles have longer residence times than the nuclei, and their number concentration tends to increase through “accumulation” of these particles within such a size class. Among the coarse particles, those having sizes ranging from $10 \mu\text{m}$ to the previously established upper limit of $100 \mu\text{m}$ are often called “giant” particles. They mainly contain man-made, sea-salt, and natural dust aerosols, being subject to sufficiently high sedimentation velocities and, hence, very efficiently removed in rather short times.

As shown in Figure 1.2, aerosols with diameters ranging from 10^{-3} to $2 \times 10^{-1} \mu\text{m}$ can play an important role in cloud and precipitation physics, because water and ice aerosols form cloud droplets and ice crystals with diameters varying mainly from about 2×10^{-2} to more than $10^3 \mu\text{m}$. These growth processes lead to the incorporation of particulate matter into cloud droplets during the formation of precipitation and hence contribute to removing aerosols from the atmosphere through the so-called wet deposition processes.

Aerosols also play a fundamental role in enhancing the electricity characteristics of the atmosphere, mainly due to molecular aggregates carrying an electric charge. These particles are called ions and are divided into (i) small ions, with sizes varying from 3×10^{-4} to no more than $10^{-3} \mu\text{m}$, and (ii) large ions, with sizes varying from 10^{-3} to about $5 \times 10^{-1} \mu\text{m}$. The presence of these ions determine the electrical conductivity of air. Therefore, their increase in concentration can change the magnitude of the fair weather atmospheric electric field. In the lower atmosphere, ions are mainly produced by cosmic rays and, to a lesser extent, by ionization due to crustal radioactive materials within the surface layer of the atmosphere. Ions are removed from the atmosphere through the combination of ions of opposite sign. Small ions are not much larger than molecules and have electrical mobility (defined as their velocity in an

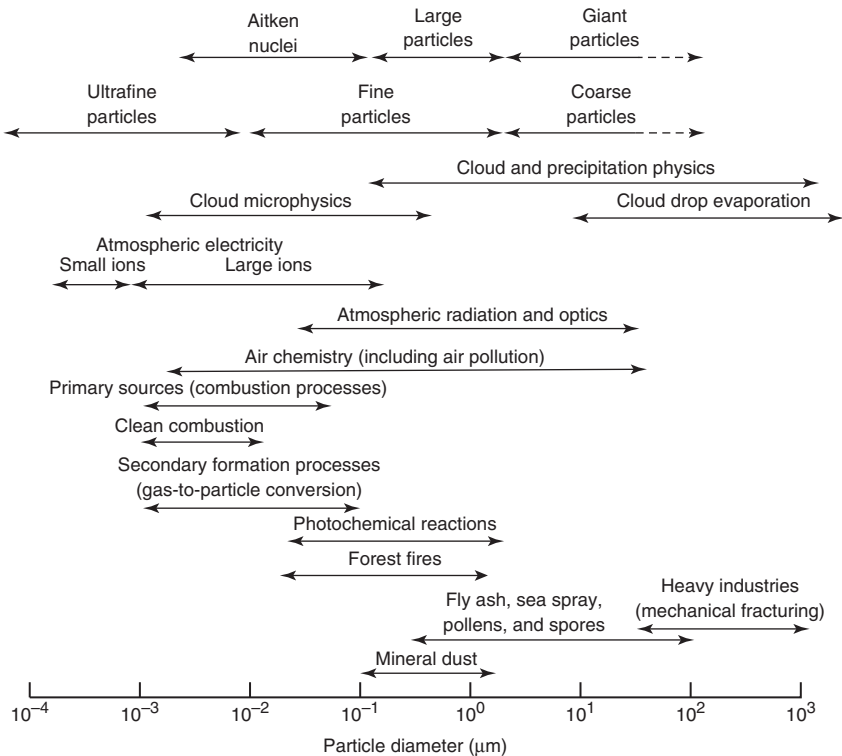


Figure 1.2 Size range of aerosol particles in the atmosphere and their role in atmospheric physics and chemistry.

electric field equal to 1 V m^{-1}) ranging from about 1 to $2 \times 10^4 \text{ m s}^{-1}$ at normal temperature and pressure (NTP) conditions. Conversely, the electrical mobility of large ions is very low, generally varying from 3×10^{-8} to $8 \times 10^{-7} \text{ m s}^{-1}$. Thus, the concentration of small ions usually varies from about 40 to 1500 cm^{-3} at sea level, and that of large ions from about 200 cm^{-3} in maritime air to more than $8 \times 10^5 \text{ cm}^{-3}$ in the most polluted urban areas. Electrical conductivity of the air is proportional to the product of ion mobility by ion concentration, so it is generally produced by small ions in unpolluted areas. Conversely, the concentration of small ions in polluted urban areas tends to decrease as a result of their capture by both large ions and uncharged aerosols, which all exhibit very high concentrations in highly polluted areas. Consequently, the electrical conductivity of air associated with fair weather atmospheric conditions assumes the lowest values for the highest concentrations of large ions. In this view, the decrease of at least 20% in the electrical conductivity of the air, as observed over the Northern Atlantic Ocean during the twentieth century, is currently attributed to a doubling in the concentration of particles with sizes ranging from 0.02 to $0.2 \mu\text{m}$, resulting from the increase in background pollution

conditions measured in North America and Europe (Wallace and Hobbs, 2006).

Combustion aerosols produced by forest fires have sizes ranging for the major part from 10^{-3} to 10^{-1} μm , while mineral dust particles generated by soil erosion and wind-forced mobilization present sizes mainly varying from 10^{-1} to no more than 5 μm . Figure 1.2 shows that fly ash, sea spray, pollens, and spores cover all together the size range from 5×10^{-1} to 10^2 μm , while industrial man-made aerosols fall within the range from 5×10^1 to more than 10^2 μm . Chemical processes involve particles mainly generated by air pollution processes, with sizes in general varying from 10^{-3} to 10^1 μm . More precisely, the aerosol polydispersions of different origins usually cover the following size intervals:

- From less than 10^{-3} to 5×10^{-2} μm , for aerosols generated by primary combustion processes
- From 10^{-3} to 10^{-2} μm , for aerosols produced by clean combustion
- From 10^{-3} to 10^{-1} μm , for secondary aerosols formed through gas-to-particle (g-to-p) conversion processes
- From 5×10^{-2} to about 2 μm , for aerosols originated by photochemical reactions

Aerosol radiative effects on solar and terrestrial radiation are produced more efficiently by particles with sizes ranging from 5×10^{-2} to 5×10^1 μm , which are able to cause marked scattering and absorption of incoming shortwave radiation at wavelengths varying from 0.4 to 2.2 μm (Charlson *et al.*, 1991). As a result of these interactions, nonabsorbing aerosol layers generally produce significant cooling effects, especially when poorly absorbing particles are suspended above low-reflectance surfaces, such as those of the oceanic regions (Bush and Valero, 2002). By contrast, appreciable warming effects can be induced near the surface by strongly absorbing particle layers suspended above bright surfaces, such as those covered by glaciers and snow fields in Greenland and Antarctica (Chylek and Coakley, 1974). The most intense radiative effects are mainly induced directly through scattering and absorption of incoming solar radiation, but appreciable exchanges of infrared radiation between the surface and the atmosphere can occur in the presence of dense aerosol layers near the surface, usually causing rather marked cooling effects within the ground layer. Besides these direct effects induced by aerosol particles on the shortwave and longwave radiation budget of the surface–atmosphere system (Charlson *et al.*, 1992; Penner, Dickinson, and O’Neill, 1992), aerosols exert an important influence on climate inducing various indirect effects, which can appreciably modify the size-distribution curves of cloud droplets and ice crystals, enhance the liquid water content (LWC) of clouds, favor longer cloud life, and strongly influence the heterogeneous chemistry of the atmosphere (Schwartz *et al.*, 1995; Jensen and Toon, 1997; Lohmann and Lesins, 2002).

The preceding remarks clearly indicate that aerosol is unique in its complexity among the atmospheric constituents and strongly influences the Earth’s climate system. Airborne particulate matter is not only generated by particle direct emission mechanisms but can also form from emissions of certain gases that either

condense as particles directly or undergo chemical transformations to gaseous species, which subsequently become particles by condensation. The variety of the morphological, optical, and chemical composition properties of airborne aerosols closely depends on the formation processes of particulate matter and their subsequent aging processes occurring in the atmosphere. Considering only the formation processes of primary and secondary aerosols, the present study describes the various physicochemical processes acting as sources of marine, wind-borne (dust), volcanic, biological, combustion and anthropogenic and/or industrial aerosols, and the chemical reactions leading to the formation of secondary aerosols of both natural and anthropogenic origin. This chapter is divided into the following five sections:

Section 1.1, presenting the primary sources of natural aerosols (mineral dust, sea salt, tropospheric volcanic dust, biogenic aerosols, and forest fire and biomass burning smokes generated by natural processes).

Section 1.2, describing the formation of secondary aerosols of natural origin, like sulfate particles in the troposphere from natural SO_2 and sulfur compounds, natural nitrates from tropospheric nitrogen oxides, organic aerosols from biogenic volatile organic compounds (VOCs), and stratospheric sulfates formed from SO_2 of volcanic or marine origin.

Section 1.3, dealing with the primary sources of anthropogenic aerosols (industrial dust, fossil fuel combustion particles, including carbonaceous (soot) substances, and waste and biomass burning particulate matter).

Section 1.4, describing the main chemical processes forming secondary anthropogenic aerosols (mainly sulfates from SO_2 , nitrates from NO_x , and organic aerosols).

Section 1.5, providing the most reliable estimates of the global annual emission fluxes of particulate matter associated with the various primary and secondary formation processes. The estimates were in part taken from the literature of the past 20 years and in part calculated by assuming that they agree with the most realistic evaluations of the global atmospheric mass burdens of the various types of natural and anthropogenic particles.

1.2

A General Classification of Aerosol Sources

Airborne aerosol particles are directly generated by surface sources or through a combination of physical and chemical and sometimes biological processes occurring in the atmosphere and in the adjacent reservoirs. Among these processes, three general types of sources are commonly distinguished:

1. "Bulk-to-particle (b-to-p) conversion," leading to the production of (i) mineral dust particles when the Earth's crust provides the solid base material; (ii) maritime (sea-salt) particles when the liquid base material is constituted by the natural marine water reservoirs; and (iii) biological aerosols when

the particulate solid material is furnished by plants (mainly plant debris and pollens) and animals. It is evident that a variety of physical, chemical, and biological precursors are necessary in all these b-to-p conversion processes for the division of the bulk material into particles before its emission into the atmosphere.

2. "G-to-p conversion" in which condensable vapors lead to either the nucleation of new particles or the condensational growth of existing particles. In these cases, both physical and chemical processes are necessary for the accretion of precursors (most frequently molecules), which are by themselves too small to be initially counted as particles.
3. "Combustion" processes which are assumed to constitute a third typological class of particle sources, even though they are, strictly speaking, a combination of the first two types of formation processes. The main difference between the combustion processes and the b-to-p and g-to-p conversions lies in the high temperatures at which the combustion processes take place, which facilitate the formation of such particles presenting shapes and composition features that cannot be achieved solely through the first two source processes mentioned earlier.

Emitted directly as particles (primary aerosol) through b-to-p conversion processes or originating in the atmosphere through g-to-p conversion processes (secondary aerosol), atmospheric aerosols of both natural and anthropogenic origin present composition characteristics closely dependent on their formation processes, with number concentration generally decreasing rapidly as their sizes gradually increase (Junge, 1963).

1.3

Primary Aerosols of Natural Origin

Significant natural surface sources of primary aerosol particles include the emission of sea spray, release of soil and rock debris (mineral dust) and biogenic aerosols, emission of biomass burning smoke, and injection of volcanic debris at tropospheric altitudes by violent eruptions. A negligible contribution to the overall atmospheric aerosol loading is also given by space, in the form of cosmic aerosols, but these fine particles are deemed to exert only a very weak influence on the aerosol characteristics of the high-altitude atmospheric regions, where particle concentration is always very low. Thus, cosmic rays do not substantially alter the air properties of the low stratosphere and the human environment conditions observed in the troposphere. The aforementioned primary mechanisms that generate the different types of particles formed at the terrestrial surface are each characterized by well-diversified morphological features, chemical composition, optical properties, and deposition patterns. They are described in detail in the following subsections.

1.3.1

Sea-Salt Particles

The oceans constitute the main source of sea-salt aerosols. They are estimated to originate a very large amount of particulate matter per year, including the coarse particles (having sizes $a \geq 2.5 \mu\text{m}$), which are generally be transported over short distances because of their rapid removal due to gravitational settling. Abundance of sea-salt particles is second only to mineral dust in contributing to the overall global particulate mass content of the troposphere (Andreae and Rosenfeld, 2008), in which hygroscopic salts, such as NaCl, KCl, CaSO_4 , and $(\text{NH}_4)_2\text{SO}_4$ provide about 3.5% of the overall tropospheric water mass. Relatively high percentage mass concentrations of various salt ions are estimated to furnish relative mass percentages equal to 55.0% Cl^- , 30.6% Na^+ , 7.7% SO_4^{2-} , 3.7% Mg^{2+} , 1.2% Ca^{2+} , 1.1% K^+ , and 0.7% due to other ions. Pósfai *et al.* (1995) collected a large variety of sea-salt aerosols during the Atlantic Stratocumulus Transition Experiment/Marine Aerosol and Gas Exchange (ASTEX/MAGE) field campaign undertaken in June 1992 over North Atlantic and studied their morphological characteristics using transmission electron microscopy (TEM) techniques. They found that oceanic aerosols may have different composition features in clean, intermediate, and dirty samples. The major species present in clean samples included NaCl molecules with mixed cations (Na^+ , Mg^{2+} , K^+ , and Ca^{2+}), sulfate ions, and to a lesser extent NaNO_3 , presenting uniform composition features of sea-salt mode particles. The excess in sulfate and nitrate concentrations is reasonably due to the oxidation of SO_2 in the sea-salt aerosol water and the reactions of NO_x with NaCl. The same compounds were also found to be present in intermediate samples in which compositional groups characterized by low and high losses of Cl^- ions from sea salt were distinguished, with most Cl^- losses compensated by NaNO_3 formation. Several compositional groups were found in the dirty samples, including Na_2SO_4 (with minor contents of Mg, K, and Ca), $(\text{NH}_4)_2\text{SO}_4$, and silicates, in addition to the particle types present in clean and intermediate samples. The distinct compositional groups monitored in the dirty samples revealed that long-range transport of continental air masses has favored the mixing of aerosols, while ozone oxidation and cloud processing could have contributed to the formation of excess sulfate in such samples.

During the Aerosol Characterization Experiment 2 (ACE-2) conducted in summer 1997 over the North Atlantic, Li, Anderson, and Buseck (2003a) found that the major maritime aerosol types include fresh and partly or completely reacted sea salt consisting of NaCl, mixed cations (Na, Mg, K, and Ca), sulfate (Na_2SO_4), and nitrate (NaNO_3), confirming the Pósfai *et al.* (1995) evaluations. In addition to the aforementioned marine components, particles of industrial origin, including $(\text{NH}_4)_2\text{SO}_4$, soot, fly ash, silica, Fe oxide, and CaSO_4 , were found in the samples, together with minor mineral dust contents. Li, Anderson, and Buseck (2003a) also pointed out that (i) only a sea-salt mass fraction of 0–30% remains unreacted along the Atlantic Ocean coasts of southern Portugal with the anthropogenic aerosol transported from Europe – while the rest was

partly reacted or converted to sulfates and nitrates – and (ii) the sea-salt mass fraction sampled at Punta del Hidalgo (Canary Islands) was much less affected by industrial pollution, with only 5% of the particles that were completely reacted, demonstrating that the dilution of pollution varies considerably as a function of the distance of samplings from sources.

More generally, in the most remote areas of our planet, just above the ocean surface, sea salts are generally found to dominate the mass of both submicrometer and supermicrometer particles. Sea-salt aerosols are generated by various physical processes, especially the rising of entrained air bubbles to the sea surface and the subsequent bursting of such bubbles during whitecap formation, through effectiveness features that strongly depend on wind speed (Blanchard and Woodcock, 1957). These aerosol particles are often the dominant cause of solar light scattering and the main contributor of cloud nuclei in the atmosphere above the most remote oceanic regions, provided that wind speed is high enough and the other aerosol sources are weak (O'Dowd *et al.*, 1997). In fact, sea-salt particles can grow considerably as a function of RH due to their usually high hygroscopic properties (Pósfai *et al.*, 1998) and often act as very efficient cloud condensation nuclei (CCNs), creating major cloud nucleating effects (O'Dowd *et al.*, 1997). Therefore, the characterization of the maritime aerosol production processes occurring at the oceanic surface is of great importance to achieve correct evaluations of their indirect chemical effects in the marine atmosphere, especially those induced by particles with diameters $a < 200$ nm (Leck and Bigg, 2005).

The maritime particles are ejected into the air through the bubble bursting mechanism occurring at the ocean surface during whitecap formation (Monahan, Spiel, and Davidson, 1986), as can be seen looking at the schematic sequence presented in Figure 1.3. It shows that bubbles with $a \geq 2$ mm first reach the ocean surface (in parts (1)–(3)), each of them ejecting 100–200 film droplets into the air when the upper portion of the air bubble film bursts (see part (4)). These small “film droplets” subsequently evaporate, leaving behind sea-salt particles with $a \leq 0.3$ μm (as can be seen in part (5)). One to five larger drops break away from each jet that forms when a bubble bursts (as shown in part (6)), and these jet drops are thrown about 15 cm up into the air. Some of these drops subsequently evaporate and leave behind sea-salt particles with $a > 2$ μm , containing not only sea salts but also organic compounds and bacteria that are already present in the surface layer of the ocean. This is due to the fact that the surface microlayer of the ocean is enriched in microorganisms, viruses, and extracellular biogenic material, which can enter the atmosphere through such a bubble bursting mechanism. Consequently, sea-salt particles usually contain about 10% organic matter (OM) (Middlebrook, Murphy, and Thomson, 1998), but currently it is not well known whether these biogenic constituents are internally mixed with sea salt or whether they also form agglomerate pools of externally mixed organic particles (Bigg and Leck, 2008).

As a result of the mechanisms described in Figure 1.3, sea-salt particles cover a wide size range from about 0.05 to 10 μm , presenting in general bimodal size-distribution curves with a first mode centered at $a_c \approx 0.1$ μm and consisting of

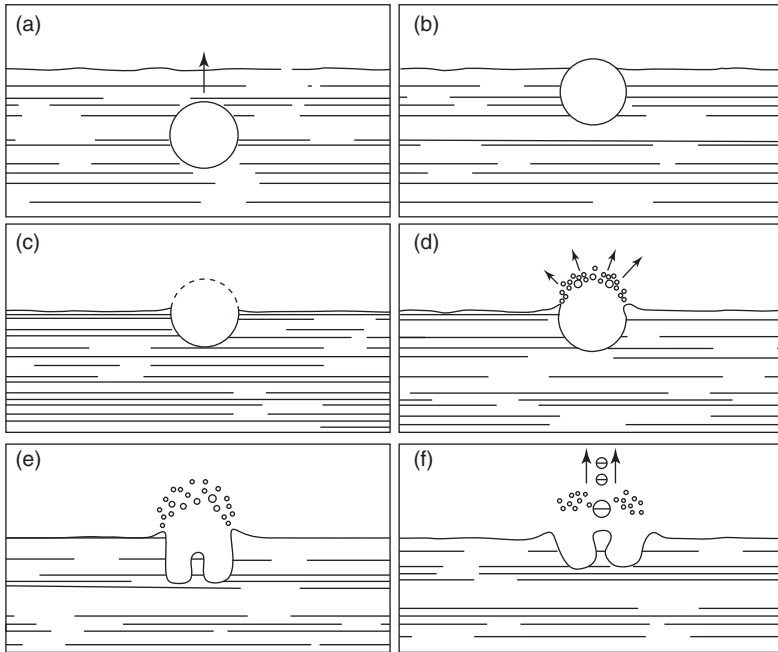


Figure 1.3 Schematic sequence of the various phases through which the film droplets and jet drops are produced when an air bubble bursts at the sea surface: (a) the air bubble is coming to sea surface; (b) the air bubble reaches the surface; (c) the sea water film starts to break; (d) droplets of $\sim 5\text{--}30\ \mu\text{m}$ diameter form when the upper portion of

the bubble film bursts; (e) film droplets start to evaporate leaving sea-salt particles and other materials in the air; and (f) when the bubble bursts, 1–5 large drops (of sizes equal to about 15% the air bubble diameter) break away from the jet formed during the bubble burst. The time between phases (c) and (f) is $\sim 2\ \text{ms}$.

particles originated from film drops and the second mode centered at $a_c \approx 2.5\ \mu\text{m}$ and containing particles forming from the jet drops (Mårtensson *et al.*, 2003). These particles exhibit a wide range of lifetime Δt_L , depending on the large variety of sea-salt particle sizes. In fact, the largest droplets fall rapidly to the ground within their area of origin, while only the smallest aerosol particles formed at the ocean surface play a major role in determining maritime aerosol properties on a large scale. The particles are originated by bubble bursting and have sizes ranging approximately from 0.1 to $1\ \mu\text{m}$, therefore having residence times in the atmosphere long enough to allow sampling in high concentrations even at continental sites (Sinha *et al.*, 2008).

The average global value of sea-salt particle production in the oceanic regions is estimated to be close to $100\ \text{cm}^{-2}\ \text{s}^{-1}$, including the large drops formed from windblown spray and foam. As mentioned earlier, the coarse sea-salt particles have rather short lifetimes Δt_L in the air, due to their large sizes. Some scanning electron microscopy (SEM) images of maritime aerosol particles consisting of pure sea-salt (halite) crystals or containing NaCl and other sea-salt cubic crystals alone

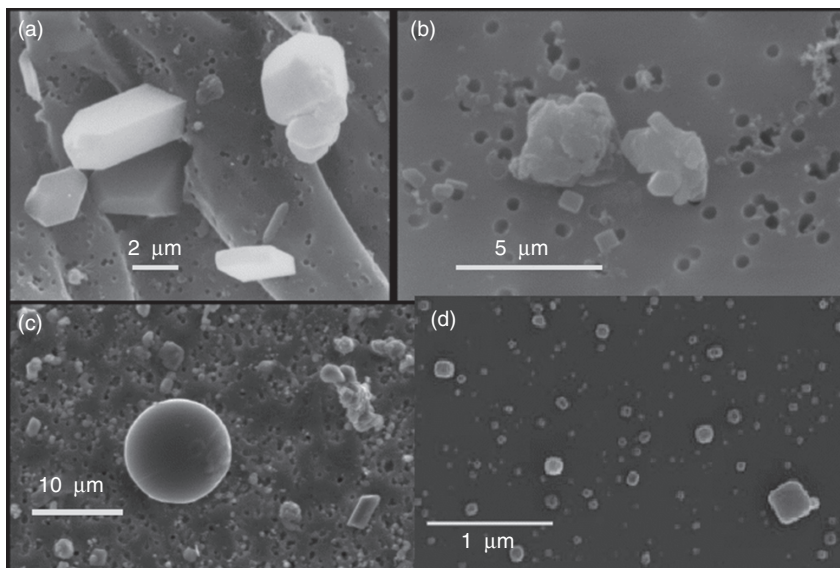


Figure 1.4 SEM images of sea-salt and other maritime particles: (a) particles sampled off the shore of Sardinia (Italy); (b) aggregates of sea-salt (halite) particles and numerous small sea-salt crystals of about $1\ \mu\text{m}$ sizes, with a large-size ($\sim 4\ \mu\text{m}$) particle on the left, containing sea-salt crystals and mineral dust, and a large-size ($\sim 4\ \mu\text{m}$) particle on the right, consisting of various sea-salt crystals; (c) sea-salt and anthropogenic particles sampled off the shore of Malta (Mediterranean Sea), including some sea-salt crystals of cubic

shape and a larger irregular-shaped particle (on the right) formed by aggregation of marine particles, together with a large-size spherical particle (having a diameter of $\sim 14\ \mu\text{m}$) in the middle, presumably due to coal combustion (from the intense ship traffic in the Sicily Channel, near Malta); and (d) several submicron sea-salt cubic crystals sampled near the island of Malta. (Reproduced with permission of Alessandra Bonazza, ISAC-CNR Institute, Bologna, Italy.)

or aggregated with sulfate and nitrate particles are shown in Figure 1.4, as obtained by examining some particulate samples collected at various sites in Sardinia (Italy) and in the Sicily Channel, near the island of Malta. Interesting SEM images of sea-salt cubic crystals of various sizes and aged sea-salt particles have been shown by Sinha *et al.* (2008), obtained for samples collected in the surroundings of Mainz (Germany), that is, in an area very far from the Atlantic Ocean. SEM images of sea-salt particles have also been provided by Li, Anderson, and Buseck (2003a), sampled at Sagres (southern Portugal) and Punta del Hidalgo (Canary Islands, Spain) during the ACE-2, which show evidence of the morphological characteristics of (i) a sea-salt particle consisting of euhedral NaCl with tabular Na_2SO_4 , (ii) a particle of euhedral NaCl with mixed-cation sulfate rims, and (iii) a completely converted sea-salt crystal consisting of Na_2SO_4 and NaNO_3 .

The dry sea-salt particles transported away by winds can very easily form solution droplets in all cases where RH exceeds 65–70%. Ambient gases (e.g., SO_2 and CO_2) are also taken up by these droplets, changing their ionic composition.

For example, the reaction of OH (gaseous phase) with sea-salt particles generates OH⁻ ions in the liquid droplets and can lead to an increase in the production of SO₄²⁻ ions (in liquid phase) by aqueous-phase reactions and a concomitant reduction in the concentration of Cl⁻ ions (in liquid phase). Consequently, the ratio of Cl⁻ to Na⁺ ions in sea-salt particles collected in the atmosphere is generally much lower than in seawater. The excess SO₄²⁻ ions (in liquid phase) over those of bulk seawater is referred to as “nonsea salt (nss) sulfate.”

The oxidation of Br⁻ and Cl⁻ ions in liquid phase, occurring in solutions of sea-salt particles for both these ions, can produce BrO_x and ClO_x species. But catalytic reactions involving BrO_x and ClO_x, similar to those observed also in the stratosphere, turn out to destroy O₃ through a mechanism postulated to explain the depletion of O₃ from about 40 to less than 0.5 ppbv, as occasionally observed over periods of hours to days in the Arctic boundary layer, usually starting at polar sunrise and continuing during the early spring period.

In order to analyze the emissions and atmospheric distribution of the maritime aerosol components and evaluate the mechanisms forming sea-salt aerosols and the atmospheric content of such particles, it is necessary to use size-resolved models. A semiempirical formulation was proposed by Gong *et al.* (1998) to establish a relationship between the size-segregated surface emission rate of sea-salt aerosols and the wind field intensity over the particle diameter range from 0.06 to 16 μm. On the average, the complex mechanism described in Figure 1.3 leads to a number concentration of sea-salt particles with diameters $a > 0.2$ μm varying from 0.1 to 25 cm⁻³ near the surface. As can be seen, the sea-salt particle formation process generates a broad range of particle sizes. Consequently, the particle production rate is strongly size dependent, as demonstrated by Monahan, Spiel, and Davidson (1986), who proposed the following parameterization for a size-dependent production rate J_{s-s} (expressed in m⁻² μm⁻¹ s⁻¹) of sea-salt particles at the surface level:

$$J_{s-s} = 1.373 \text{ WS}^{3.41} (a/2)^{-3} [(1 + 0.057(a/2)^{1.05})] 10^{1.19 \exp(B)}, \quad (1.1)$$

where a is measured in micrometer at RH = 80%, WS is the wind speed measured in meter per second at the altitude $z = 10$ m above sea level (a.m.s.l.), and $B = \{[0.38 - \ln(d/2)]/0.65\}^2$.

The dependence features of total mass concentration M_{s-s} of sea-salt particles produced by winds on the surface-level wind speed was parameterized by Jaenicke (1988) in terms of the following two empirical formulas defined over different ranges of height z and wind speed WS:

$$M_{s-s} = 4.26 \exp(0.160 \text{ WS}) \quad (1.2)$$

over the $5 \leq z \leq 15$ m and $1 \leq \text{WS} \leq 21$ m s⁻¹ ranges and

$$M_{s-s} = 2.82 \exp(0.152 \text{ WS}) \quad (1.3)$$

over the $10 \leq z \leq 600$ m and $5 \leq \text{WS} \leq 35$ m s⁻¹ ranges.

For the present-day climate, estimates of the overall global annual emission flux Φ_e of sea-salt particles from ocean to atmosphere have been made over the

past three decades. Flux Φ_e was evaluated to be of 300 Tg per year by SMIC (1971) over the range $a < 20 \mu\text{m}$ and to (i) range from 5×10^2 to 2×10^3 Tg per year by Jaenicke (1988) over the whole size range, (ii) vary from 10^3 to 3×10^3 Tg per year by Erickson and Duce (1988), (iii) be equal to 5.9×10^3 Tg per year (Tegen *et al.*, 1997), and (iv) vary from 10^3 to 10^4 Tg per year by Seinfeld and Pandis (1998, 2006), assuming an average global value of 1.3×10^3 Tg per year for sea-salt coarse particles only. Partial flux values were proposed by the IPCC (2001) equal to 54 Tg per year for fine particles with $a < 1 \mu\text{m}$ and 3.29×10^3 Tg per year for coarse particles over the $1 \leq a \leq 16 \mu\text{m}$ range, leading to a value of $\Phi_e = 3344$ Tg per year, which was very close to the value of 3.3×10^3 Tg per year assumed by Jaenicke (2005), while higher evaluations were proposed by Gong, Barrie, and Lazare (2002) ($\Phi_e = 1.01 \times 10^4$ Tg per year) and Tsigaridis *et al.* (2006) ($\Phi_e = 7.804 \times 10^3$ Tg per year). Taking these estimates into account, Andreae and Rosenfeld (2008) provided a reasonable range of Φ_e for sea-salt particles from 3×10^3 to 2×10^4 Tg per year, as reported in Table 1.1.

1.3.2

Mineral Dust

Mineral dust originates mainly from desert and semiarid land surfaces as a result of the wind forces that mobilize the soil particles. The main dust mobilization regions include the Sahara desert and other desert regions that constitute the dust belt, a chain of arid regions extending not only over North Africa but also over South Africa, and the Middle East Asia and China (Gobi Desert), besides some wide high-altitude desert regions in South America. In addition, dry lakes and lakebeds and other once-wet areas act also as particularly efficient sources of atmospheric dust (Prospero, 1999). Consequently, dust particles constitute the major component of the atmospheric aerosol content in the subtropical regions of the planet. This is due to the fact that all the aforementioned arid and semiarid regions of the Earth acting as dust sources occupy about one-third of the global land area, desert dust being the dominant particle type even in air masses thousands of kilometers away from the source. Estimates of the annual emission flux Φ_e of mineral dust made over the global scale vary from 10^3 to 5×10^3 Tg per year (Duce, 1995), presenting marked spatial and temporal variations from one region of the Earth to another, because such dust source regions also include semiarid desert fringes and dry land areas, where the vegetation cover was seriously disturbed by human activities.

Particle reactions and internal mixing during transport of mineral dust can substantially change the composition of the original aerosol. For instance, mineral particles become internally mixed with sea-salt components, perhaps through cloud processing (Trochkin *et al.*, 2003). In other cases, Saharan minerals were associated with sulfur and OM transported from both urban and agricultural pollution areas (Falkovich *et al.*, 2001) and with organics contained in combustion smokes and anthropogenic particulate matter (Gao, Anderson, and Hua, 2007),

Table 1.1 Estimates of the annual emission fluxes (measured in teragram per year (being $1 \text{ Tg yr}^{-1} = 10^6 \text{ ton yr}^{-1}$)) of natural aerosols on a global scale from various sources, as found in the literature over the past 15 years.

Natural particles	Annual global emission flux (Tg yr^{-1})
Sea salt (total, sizes $<16 \mu\text{m}$)	3344 (IPCC, 2001)
Sea salt (sizes $<1 \mu\text{m}$)	54 (IPCC, 2001)
Sea salt (1–16 μm size range)	3290 (IPCC, 2001)
Sea salt (overall)	10 100 (Gong, Barrie, and Lazare, 2002), 3300 (Jaenicke, 2005), 7804 (Tsigaridis <i>et al.</i> , 2006), ranging from 3000 to 20 000 Tg yr^{-1} (Andreae and Rosenfeld, 2008)
Mineral (soil) dust (total, sizes $<20 \mu\text{m}$)	2150 (IPCC, 2001)
Mineral (soil) dust (sizes $<1 \mu\text{m}$)	110 (IPCC, 2001)
Mineral (soil) dust total (1–2 μm size range)	290 (IPCC, 2001)
Mineral (soil) dust total (2–20 μm size range)	1750 (IPCC, 2001)
Mineral dust (0.1–10 μm size)	1000–2150 (average = 1490) (Zender, Brian, and Newman, 2003)
Mineral dust (overall)	2000 (Jaenicke, 2005), 1704 (Tsigaridis <i>et al.</i> , 2006), ranging from 1000 to 2150 Tg yr^{-1} (Andreae and Rosenfeld, 2008)
Volcanic dust (coarse particles only)	30 (Seinfeld and Pandis, 1998)
Sulfates from volcanic SO_2	10 (Hobbs, 2000)
Volcanic sulfates (as NH_4HSO_4)	21 (IPCC, 2001)
Volcanic SO_2	9.2 (Tsigaridis <i>et al.</i> , 2006)
Cosmic dust in the upper mesosphere	3×10^{-2} to 1.1×10^{-1} (Plane, 2012)
Cosmic dust in the middle atmosphere	2×10^{-3} to 2×10^{-2} (Plane, 2012), 1.5×10^{-4} to 4×10^{-2} (Gardner <i>et al.</i> , 2014)
Biogenic aerosol	1000 (Jaenicke, 2005)
Biogenic sulfate (as NH_4HSO_4)	57 (IPCC, 2001)
Biogenic carbonaceous aerosol (sizes $>1 \mu\text{m}$)	56 (IPCC, 2001)
Biogenic primary organic aerosol	15–70 (Andreae and Rosenfeld, 2008)
Biogenic VOC compounds	16 (IPCC, 2001)
Secondary organic aerosol from biogenic VOC	11.2 (Chung and Seinfeld, 2002)
Secondary organic aerosol	2.5–83 (Andreae and Rosenfeld, 2008)
Sulfates (from all the natural primary and secondary sources)	107–374 (Andreae and Rosenfeld, 2008)
Nitrates (overall, from natural primary and secondary sources)	12–27 (Andreae and Rosenfeld, 2008)
Secondary sulfates from DMS	12.4 (Liao <i>et al.</i> , 2003), 18.5 (Tsigaridis <i>et al.</i> , 2006)
Carbonaceous aerosols from biomass burning (sizes $<2 \mu\text{m}$)	54 (IPCC, 2001)
Primary organic aerosol	44.4 (Tsigaridis <i>et al.</i> , 2006)
Biomass burning organic	26–70 (Andreae and Rosenfeld, 2008)
Total natural particles over the whole size range	5875 (IPCC, 2001) 4200–22 800 (Andreae and Rosenfeld, 2008), including the United Nations (1979) estimate of volcanic debris

suggesting that mineral dust is a potential cleansing agent for organic pollutants (Pósfai and Buseck, 2010).

Dust deflation occurs in a source region when the frictional wind speed at the surface exceeds a threshold value, which is a function of surface roughness elements, grain size, soil moisture, and surface geological characteristics. The mobilized desert dust can be then transported by winds over long distances, even thousands of kilometers from their source areas. Crusting of soil surfaces and limitation of particle availability can contribute efficiently to reduce the dust release from a source region. In addition, the disturbance of such surfaces by human activities can strongly enhance the dust mobilization potentiality of these land areas. Up to 50% of the current atmospheric dust load has been estimated to originate from disturbed soil surfaces and should therefore be considered anthropogenic in origin (Tegen and Fung, 1995). Dust deflation can change in response to currently occurring natural climate events: for instance, Saharan dust transport to Barbados was estimated to increase during the El Niño years (Prospero and Nees, 1986), and dust export to the Mediterranean and North Atlantic was found to be closely correlated with the North Atlantic Oscillation (Moulin *et al.*, 1997). Further information on dust mobilization, transport, and interannual variability are available in the literature, as given by various models over regional global scales (Marticorena *et al.*, 1997; Tegen and Miller, 1998).

As shown in Table 1.1, the estimate of the average range of annual global emission flux Φ_e made by Zender, Brian, and Newman (2003, 2004) for mineral dust over the whole size range from 0.1 to 10 μm is from 1000 to 2150 Tg per year, giving an average value of 1490 Tg per year. This estimate substantially agrees with the maximum estimate of 1800 Tg per year made by Jaenicke (1988) and the soil dust range of 1000–5000 Tg per year given by Duce (1995) and that of 1000–3000 Tg per year proposed by Seinfeld and Pandis (1998, 2006), with an average value of 1500 Tg per year defined for the coarse particles of soil dust. Values of annual global emission flux Φ_e of mineral dust were evaluated by the IPCC (2001) to be equal to 2150 Tg per year over the whole range of particle diameter range $a < 20 \mu\text{m}$, of which 110 Tg per year was attributed to the range $a < 1 \mu\text{m}$, 290 Tg per year to the range $1 \leq a \leq 2 \mu\text{m}$, and 1750 Tg per year to the range $2 \leq a \leq 20 \mu\text{m}$. More recent evaluations of Φ_e for mineral dust were provided over the last decade, yielding values of 2000 Tg per year (Jaenicke, 2005) and 1704 Tg per year (Tsigaridis *et al.*, 2006), which are very close to the upper limit of 2150 Tg per year determined by Zender, Miller, and Tegen (2004) and subsequently confirmed by Andreae and Rosenfeld (2008).

Large uncertainties exist in explaining the mineral dust emission processes, which arise not only from the complexity of the processes raising dust into the atmosphere under wind forcing but also on the nature of the arid and semiarid surfaces and the atmospheric turbulence fields capable of involving the mobilized dust and transporting it over long distances. Soil particles are mobilized by wind forcing. The threshold value of the frictional wind speed at the ground is estimated to be equal to $\sim 0.2 \text{ m s}^{-1}$ for particles with equivalent diameter a ranging from 50 to 200 μm and for soils containing 50% clay or tilled soils,

because smaller particles adhere better to the surface and cannot be mobilized (Mullins *et al.*, 1992). To reach a frictional speed of 0.2 m s^{-1} , the wind speed WS must be higher than several meters per second at the height of a few meters above the ground. A major source of relatively smaller particles (with a ranging from ~ 10 to $100 \mu\text{m}$) is saltation, in which the larger grains become airborne, fly a few meters, and then land on the ground, creating a burst of smaller dust particles, as shown in the schematic representation of Figure 1.5.

The formation of crustal particles can be considered an important b-to-p conversion process that generates sand particles from crustal material through a two-stage sequence, the first consisting of the physicochemical erosion processes dividing the bulk material into small grains and the second causing the wind-forced ejection of such particles into the atmosphere:

1. Two physical models represent the first stage. The first assumes slow processes, which divide each grain randomly into two different parts, leading to a size distribution that tends to assume a lognormal analytical form after many repetitions. The second model assumes faster processes, which divide each grain randomly into a certain number of parts, giving an overall exponential mass size-distribution curve, resulting from the envelope of different unimodal size distributions, as shown in the example of Figure 1.6 suggested by Junge (1979). It is worth noting that the first model is a special case of the second one and both these modeled processes are expected to act simultaneously on the natural sands.
2. The second stage of the desert dust formation process consists of particle ejection. It is much harder to model this physical mechanism. For grains

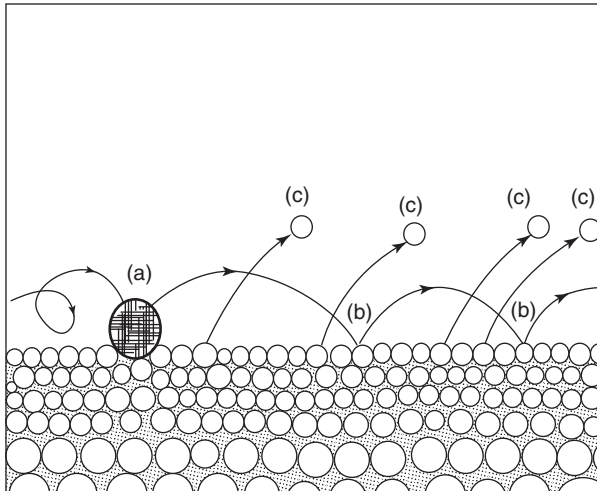


Figure 1.5 Schematic representation of the saltation mechanism through which sand particles are mobilized by wind: a large particle (a) is lifted by wind and then lands on the ground (b), creating a burst of smaller dust particles (c).

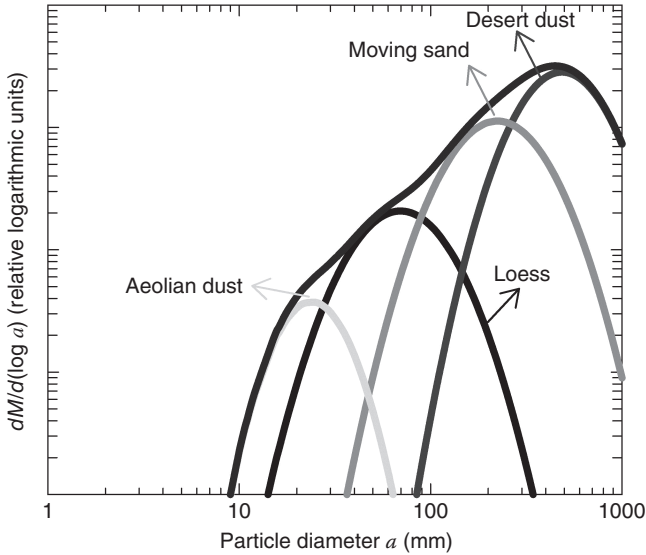


Figure 1.6 Schematic picture of the mineral dust particle mass size distributions generated in different ground sands, characterized by multimodal features associated with the various mobilization processes. (Adapted from a graph of Junge (1979).)

with $a > 100 \mu\text{m}$, critical flow velocities for the ejection have been proposed in the literature, establishing that all grains become airborne for wind speed $WS > 1 \text{ m s}^{-1}$ at the ground. Consequently, airborne particle size distributions are independent of grain sizes, and, hence, all grain sizes are involved in such mobilization processes. On this matter, Jaenicke (1988) evaluated that the airborne mass concentration M_c of crustal material near the surface varies as a function of wind speed WS according to the following mean relationship:

$$M_c = 52.77 \exp(0.30 WS), \quad (1.4)$$

assumed to be valid over the $0.5 \text{ m s}^{-1} < WS < 18 \text{ m s}^{-1}$ range.

Closely depending on the geological characteristics of the mobilization areas, the morphological features of mineral dust particles can vary widely, presenting features that change appreciably with the chemical composition and mineralogical characteristics of the bulk material forming such crustal aerosols. The main species found in soil dust are quartz, clays, calcite, gypsum, and iron oxides, with optical properties depending on the relative abundance of the various minerals. Some SEM images of wind-forced dust particles and soil particles consisting of smectite, illite, and gypsum and sampled at different localities in Italy are shown in Figure 1.7. More details on the composition of such soil dust samples collected in the Mediterranean area are presented by Molinaroli *et al.* (1999). Numerous SEM and TEM images of mineral dust particles are available in the literature, such as (i) those sampled by Sinha *et al.* (2008) in central Europe (at

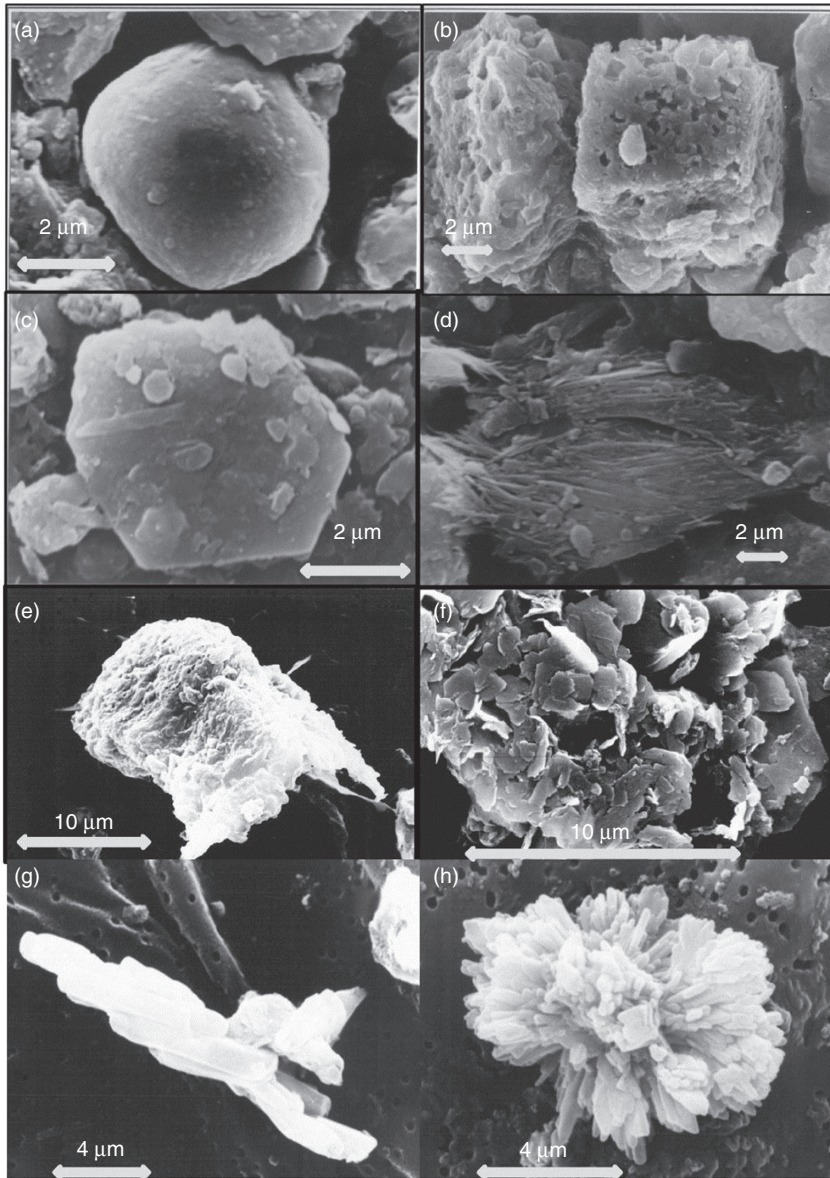


Figure 1.7 Scanning electron microscopy (SEM) images of mineral (aeolian) dust particles consisting of (a) quartz, (b) dolomite, (c) kaolinite, (d) palygorskite of Saharan origin, (e) smectite, (f) illite, and (g), and

(h) gypsum (calcium sulfate dihydrate) in both cases. (Reproduced with the permission from Emanuela Molinaroli, Ca' Foscari University, Dept. of Environmental Sciences, Venice, Italy.)

Mainz, Germany), consisting of silicates, primary and secondary gypsum, calcium carbonate, and iron oxide; (ii) those sampled by Li, Anderson, and Buseck (2003a) at Sagres (southern Portugal), during the June–July 1997 ACE-2 campaign conducted over the North Atlantic Ocean, regarding an aluminosilicate sphere mixed with Na_2SO_4 crystals, an aggregate of euhedral magnetite crystals, a quartz crystal, a smectite particle, and a kaolinite particle coated with ammonium sulfate; (iii) some silicate mixed particles with small NaCl and Na_2SO_4 aggregated crystals, sampled by Li, Anderson, and Buseck (2003a) at Punta del Hidalgo (Canary Islands, Spain) during the ACE-2; and (iv) and those sampled by Li *et al.* (2003b) in mineral dust collected for hazy conditions in South Africa, showing muscovite particles with aggregated small tar balls and a quartz particle aggregated with smectite and organic particles.

Most dust particles are not soluble in water. Therefore, major changes in the shape and morphological characteristics of such aerosols due to high RH conditions of air are rarely observed. However, the mineral core of such airborne particles can be covered by a water or ice shell when transported at high altitudes within highly moist air masses. These changes in the structural features of dust particles can lead to marked modifications in the radiative properties of dust particles, with lower values of the real part of the refractive index than those usually found for dust particles suspended in dry air.

Significant variations in the optical properties of mineral dust can also be caused by changes in the chemical composition of these particles often occurring when mineral dust is mixed with aerosols having different composition features during their transport over long distances. Examples of these variations have been, for instance, documented in cases where (i) calcite and halite particles relatively close to the source partially react to sulfate during dust storms (Okada and Kai, 2004); (ii) mineral dust types containing a significant fraction of carbonate minerals in certain desert areas act as effective sinks for nitric acid to form nitrates (Krueger *et al.*, 2004); (iii) carbonate minerals convert to sulfate particles or mixed (sulfate and nitrate) particles (Sobanska *et al.*, 2003) or nitrates only (Matsuki *et al.*, 2005); (iv) dust particles mixed internally with sea-salt aerosols, when transported within clouds over oceans (Trochkin *et al.*, 2003); (v) desert dust is associated with sulfur compounds and OM from surrounding urban and agricultural polluted areas (Falkovich *et al.*, 2001); (vi) desert dust particles mixed with organics from combustion products over oceans, acting as cleansing agent for organic pollutants (Gao, Anderson, and Hua, 2007); and (vii) mineral dust contributing to stimulate phytoplankton growth (Cwiertny *et al.*, 2008), playing an important role in the global biogeochemical cycle of iron, which is a significant limiting nutrient in many oceanic ecosystems (Jickells *et al.*, 2005).

The mineral dust particles mobilized in desert regions can be transported over long distances, as frequently observed over the Mediterranean by means of satellite-based observations made by TOMS, SEVIRI, MODIS, MISR, and other sensors, which gather information on such transport episodes from North Africa toward Europe (Karam *et al.*, 2010). More intense desert dust transport episodes, during which dust particles can be transported thousands of kilometers away

from their sources, are frequently observed in various areas of the planet: (i) from Sahara-Sahel toward Atlantic Ocean and the Caribbean region (Prospero, 1999), (ii) from mid-eastern Asia toward the Persian Gulf and Indian Ocean, and (iii) from the Gobi Desert and Central Asia toward the Northern Pacific Ocean, as shown by the POLDER/ADEOS-1 observations performed by Deuzé *et al.* (1999). It is also important to mention that plumes of Asian dust are often detected over Alaska by means of satellite observations and in the Arctic region by means of ground-based sun-photometer measurements performed mainly in spring (Stone *et al.*, 2007). Therefore, mineral dust is expected to cause important direct and indirect effects on the terrestrial climate system.

The transport of mineral dust particles is in general accompanied by sharp and marked changes in the multimodal size-distribution curves of columnar aerosol polydispersions, especially within the size range typical of coarse particles, associated with significant changes in the optical properties of these aerosols. Gravitational settling and wet deposition act as the major removal processes of mineral dust from the atmosphere, limiting the atmospheric lifetimes Δt_L of such particles to no more than 2 weeks on average. It is obvious that the lifetime Δt_L of mineral dust particles depends closely on particle size, since large particles are quickly removed from the atmosphere by gravitational settling, while submicron particles can remain suspended in air over periods of several weeks.

1.3.3

Biogenic Aerosols

Primary biogenic aerosols are solid and liquid particles released into the atmosphere from plants and animals. They consist of plant debris (cuticular waxes, leaf fragments), microbial particles (living and dead viruses, bacterial cells, fungi, spores, pollens, algae, seeds, etc.), insects, humic matter, and other biogenic debris, such as marine colloids and pieces of animal skins. Due to their highly different origins, biological aerosol particles exhibit a large variety of shapes and cover a wide size range from less than $0.1 \mu\text{m}$ to at least $250 \mu\text{m}$. For instance, fungal spores have sizes mainly ranging from 1 to $30 \mu\text{m}$, while (i) most pollens present sizes varying usually from 20 to $60 \mu\text{m}$, and (ii) bacteria, algae, protozoa, fungi, and viruses have sizes generally smaller than a few micrometers, those of viruses varying in general from 0.1 to $0.3 \mu\text{m}$ and those of bacteria from $0.2 \mu\text{m}$ to no more than $8.0 \mu\text{m}$.

Figure 1.8 shows some SEM images of aerodiffuse biological particles sampled at rural sites in the Po Valley (Italy) by the ISAC-CNR. The images show some pollen samples, with nearly spherical shapes and sizes varying mainly from 15 to $60 \mu\text{m}$, and a spherical-shaped fungus spore, with a diameter of $\sim 15 \mu\text{m}$. TEM images of biogenic particles sampled in Southern Africa in the Madikwe Game Reserve were shown by Pósfai *et al.* (2003a), presenting a group of brochosomes (C-, O-, and Si-bearing particles secreted by leaf-hopping insects) showing spherical shapes with a equal to $\sim 250 \text{nm}$. Other interesting TEM images of biogenic particles have been presented by Pósfai and Buseck (2010), including an atypical

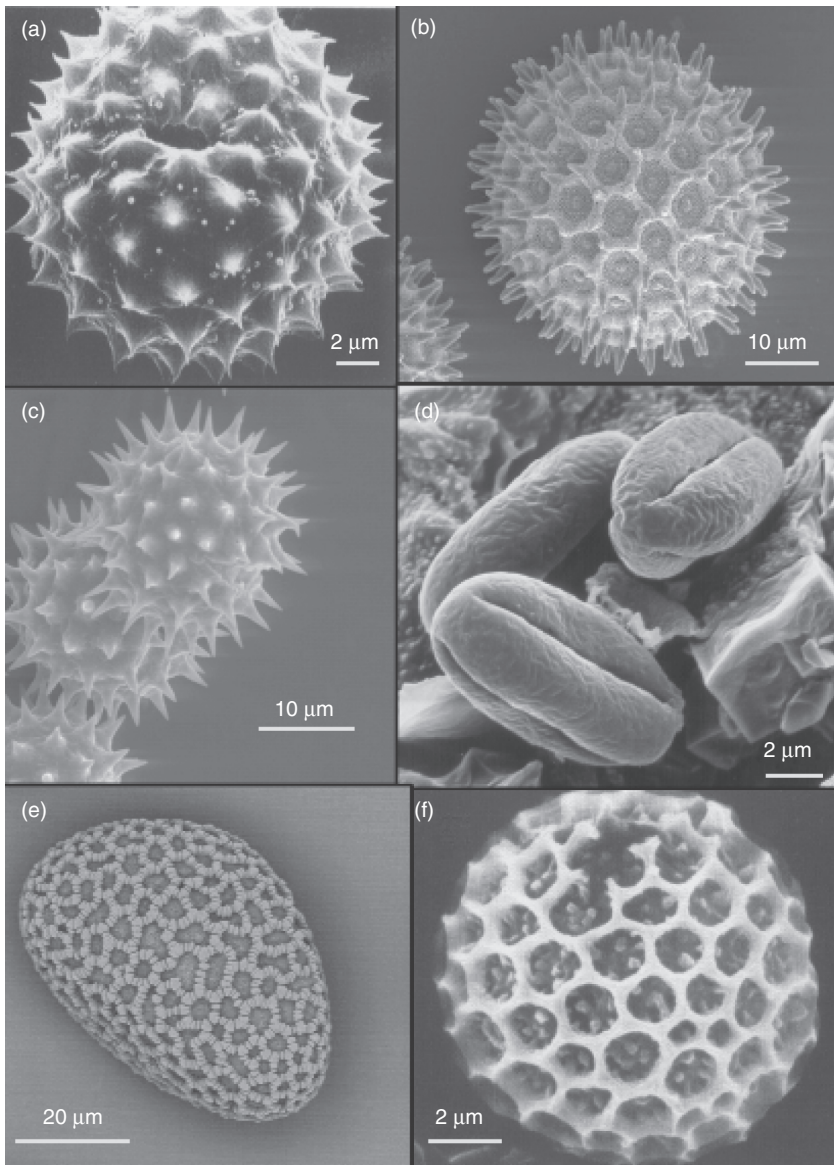


Figure 1.8 SEM images of aerodiffuse biological particles sampled at rural sites of the Po Valley (northern Italy): (a) pollen of *Ambrosia* sp. (Po Valley), (b) pollen of Convolvulaceae sp. (Po Valley), (c) pollen of Asteraceae (Helian.) (Po Valley), (d) pollen of

Castanea sativa sp. (Po Valley), (e) pollen of Liliaceae sp. (Po Valley), and (f) fungus spore of *Ustilago* sp. (Po Valley). (Reproduced with the permission from Paolo Mandrioli, ISAC-CNR Institute, Bologna, Italy).

oceanic microorganism sampled at Cape Grim with sizes of $\sim 1 \mu\text{m}$ and biogenic debris consisting of several plant fragments collected at a rural site in Hungary, with sizes varying from 2 to $10 \mu\text{m}$.

As a result of the large variability of sources and typologies, the number density concentrations of biogenic aerosol particles are close to 1% of the total aerosol concentration in remote oceanic regions and equal to around 2–3% in continental environments (Pósfai *et al.*, 2003b; Winiwarter *et al.*, 2009), but can reach percentage values of $\sim 25\%$ in continental aerosol (Matthias-Maser and Jaenicke, 1994) and 35% in Amazonia (Elbert *et al.*, 2007), presenting wide variations related to the source and particle type. These remarks show that the relative contribution of biological aerosols can be very high in densely vegetated regions, particularly in the moist tropical regions (Simoneit, Cardoso, and Robinson, 1990). Conversely, biological aerosols suspended in an urban midlatitude temperate environment can contribute to the total aerosol mass concentration by percentages of 10–30% over the submicron and supermicron size ranges (Matthias-Maser and Jaenicke, 1995). The number density concentration of biological aerosols can vary appreciably with season, location, and altitude. Low number concentrations are usually measured at midlatitudes in mountain locations during winter, and very low concentrations are recorded usually at polar latitudes in all seasons. Typical concentrations of biological particles in the midlatitude regions were found to be (i) higher than 200 m^{-3} for grassy pollens, (ii) ranging from about 100 to 400 m^{-3} for fungal spores (in water), (iii) equal to $\sim 0.5 \text{ m}^{-3}$ for bacteria over remote oceans (Pósfai *et al.*, 2003b), (iv) varying from 80 to 800 m^{-3} for bacteria in the urban New York City area, and (v) close to about 10^4 m^{-3} for bacteria over sewage treatment plants. Jaenicke (2005) estimated that the average annual global emission flux Φ_e from biospheric sources is approximately equal to 1000 Tg per year for atmospheric primary particles, compared to the estimates of 2000 Tg per year for mineral dust and 3300 Tg per year for sea-salt particles (see Table 1.1).

Biogenic aerosols can sometimes occupy up to 30% of the total atmospheric aerosol volume at a given location, especially in the remote tropical continental areas covered by pluvial forests, and exhibit at least three times lower concentrations in the remote oceanic regions (Elbert *et al.*, 2007). Nevertheless, inland biogenic aerosols can travel very long distances owing to their low density, often being collected thousand kilometers from their origin area. The occurrence of such long-range transport episodes is commonly used for the identification of the origin of a certain air mass at a given location (Mandrioli *et al.*, 1980). The biogenic aerosols are in general widespread and occupy the whole troposphere, presenting highly variable number concentrations with altitude. For instance, spores of a number of molds were identified at 11 km altitude in the atmosphere (Cadle, 1966), suggesting that the primary biological particles can efficiently participate in the cloud and ice nucleation processes. Many problems in atmospheric science are related to the primary biological particles, including the spread of pathogens and the roles of microorganisms in cloud and ice nucleation (Morris *et al.*, 2011). Biogenic aerosols can easily penetrate the respiratory systems of animals and humans,

while pollens can cause serious allergologic pathologies affecting various biological functions of humans. Viruses and bacteria can be attached to other particles (e.g., dust grains, pollens, and spores) and transported over large distances by them and by the cloud particles that were grown on biogenic nuclei. Some bacteria are also suspected to be active in cloud droplets, governing the biological activities occurring inside these droplets (Sattler, Puxbaum, and Psenner, 2001).

In evaluating the optical effects induced by biological aerosols, it is important to take into account that most of these particles are not spherical (Pósfai *et al.*, 2003a; Niemi *et al.*, 2006; Pósfai and Buseck, 2010). In particular, many bacteria are rod shaped and are not characterized by just one size. Bacteria also have an internal structure and cannot be considered homogeneous objects in light scattering studies. More generally, bioaerosols often have quite complex shapes and variable internal structures. Therefore, it is very difficult to simulate their optical characteristics, even using advanced computers. In addition, the refractive index of these particles needed for the theoretical modeling of their optical effects is poorly known. Due to the fact that only left-handed amino acids and right-handed sugars exist in nature, it is clear that the biological aerosols are mostly chiral. This implies that the refractive index depends on the sense of rotation of incident electromagnetic circularly polarized waves (Kokhanovsky, 2003). The presence of humic-like substances makes these aerosol particles light absorbing, especially in the ultraviolet (UV)-B wavelength range (Havers *et al.*, 1998). It is currently known that many biological particles not only absorb and scatter light but can also fluoresce when zapped with a beam of UV light. Due to their relatively low background number concentrations, however, biological particles are deemed to produce in general rather low direct radiative effects on the Earth's climatic system. As mentioned earlier, there is evidence that primary biogenic particles can efficiently act as cloud droplets and ice nuclei (Schnell and Vali, 1976). Thus, biogenic particles are expected to play a not negligible role in inducing indirect climatic effects since they favor the formation of cloud particles. Quantitative estimates of these effects currently deserve closer investigation.

1.3.4

Forest Fire Smoke

Biomass burning smoke is emitted into the atmosphere by intense fires of forests, savannah grass, and other types of vegetation, occurring most frequently in the tropical regions during drought periods. Emissions from burning vegetation include elemental carbon (EC) and organic carbon (OC) as well as other particulate substances, together with gases such as CO_2 , CO , NO_x , CH_4 , and nonmethane hydrocarbons (NMHCs). The term EC refers to the most refractory part of the carbonaceous aerosol particles, which oxidize above a certain threshold in combustion experiments. However, it is often called "free carbon" or "graphitic" and most frequently "black carbon" (BC), being a combustion product capable of strongly absorbing the incoming solar radiation over the whole visible wavelength range. The acronyms BC and EC are inappropriate and it is better to

use the term “soot” to indicate the primary particles produced by combustion processes (Andreae and Gelencsér, 2006; Bond and Bergstrom, 2006). These particles have a distinctive structure consisting of graphene-like layers that are wrapped into (i) spherules having diameters equal to tens of nanometer and resembling nano-onions and (ii) aggregates of spherules into branching or compact clusters. Numerous examples of such complex layered structures and aggregates of soot spherules are available in the literature illustrated by means of both SEM and TEM images made for particle samples collected during different fire episodes by (a) Li *et al.* (2003b) during the Madikwe Game Reserve fire (South Africa) on August 20, 2000, showing SEM images of a tar ball (arrowed) in young smoke and soot aggregates in young smoke; (b) Li *et al.* (2003b) in the Timbavati (South Africa) region during the fire of September 7, 2000, showing TEM images of (i) tar balls from aged smoke, collected downwind from the Timbavati fire, together with potassium-salt particles having organic coatings and most of the KCl crystals in the young smoke that were transformed into potassium sulfate and nitrate with the aging of the smoke, and (ii) potassium salts that have formed inclusions within organic particles; and (c) Pósfai *et al.* (2003a) in the Kruger National Park (South Africa) during the fire of August 17, 2000, observed in the presence of both smoke and haze particles, showing TEM images of (i) a typical portion of a sample of young smoke from a smoldering and flaming fire, in which most particles are carbonaceous (organic) with inorganic K-sulfate inclusions, (ii) individual spherules consisting of graphitic layers, and (iii) a few nanometer-sized graphite nucleus within a soot globule.

Three distinct types of carbonaceous particles were mostly found by Pósfai *et al.* (2003a) in the smoke samples collected at the Kruger National Park in August 2000: (i) particles with inorganic (K-salt) inclusions; (ii) the so-called tar balls, which constitute a new and distinctive type of particles produced by biomass burning emissions (Pósfai *et al.*, 2003b, 2004); and (iii) soot particles. It is worth mentioning that the large variety of soot particles, carbonaceous particulate aggregates, graphitic nanoparticles, and the so-called tar balls are all generated by forest and savannah fires, which can be clearly observed using high-resolution transmission electron microscopy (HRTEM) techniques (Pósfai *et al.*, 1999), since this instrument can provide useful diagnoses for soot identification in complex internally mixed particles. Pósfai *et al.* (2003a) showed that the relative number density concentrations of organic particles assumed the highest values in young smoke, whereas tar balls were dominant in slight smoke from smoldering fire, with $\Delta t_L = \sim 1$ h. Flaming fires were evaluated to emit relatively more soot particles than smoldering fires, but soot was a minor constituent of all such studied plumes. Further aging effects were observed to cause the accumulation of sulfate on organic and soot particles, as indicated by the large number of internally mixed organic/sulfate particles recorded in the haze cases. Externally mixed ammonium sulfate particles were found to dominate in the boundary layer hazes, whereas organic/sulfate particles were the most abundant type in the upper hazes. The measurements also showed that the elevated haze layers were affected more strongly by biomass smoke and those in the boundary layer less

apparently. Particles of all the aforementioned kinds are usually found in high concentrations for stable meteorological conditions persisting in the atmospheric ground layer over the regions involved by forest and savannah fires.

The analysis of smoke particles sampled by Li *et al.* (2003b) during the SAFARI 2000 experiment conducted in South Africa provided evidence that potassium salts and organic particles were the predominant species, whereas more K_2SO_4 and KNO_3 particles were found in aged smoke. This difference indicates that with the aging of the smoke, KCl particles from the fires were converted to K_2SO_4 and KNO_3 through reactions with sulfur- and nitrogen-bearing species from biomass burning as well as other sources. More soot was found in smoke from flaming grass fires than bush and wood fires, probably due to the prevailing flaming combustion in grass fires. The high abundance of organic particles and soluble salts was deemed to affect the hygroscopic properties of biomass burning aerosol, thereby also influencing the potentiality of such particles to act as CCNs.

The effect of gaseous emissions from biomass burning on atmospheric chemistry and climate is critically important. Biomass burning is one of the major sources of atmospheric aerosols, mainly consisting of small smoke particles containing primarily organic compounds and EC, mainly having submicron sizes. In fact, combustion processes generate in general (i) a very high number concentration of small particles, with $a < 0.2 \mu\text{m}$; (ii) a high number of accumulation mode particles with sizes ranging from 0.2 to $1 \mu\text{m}$; (iii) a relatively low number of coarse particles, with sizes varying from 1 to $2 \mu\text{m}$; and (iv) only a few coarse-mode particles, with sizes greater than $2 \mu\text{m}$. This implies that a large fraction of smoke particles can easily penetrate the respiratory system of humans causing various health problems. Most of these submicron aerosols are produced by large-scale savannah burning and forest fires occurring during the dry season in Africa, the Amazon Basin, and southwestern Asia, which can also induce sharp increases in the surface-level ozone concentration on a regional scale, to such an extent as to approach the O_3 concentration level measured in urban industrialized regions and observed to vary often from 60 to 100 ppbv. Such forest fire particles are rapidly uplifted to high altitudes and transported over long distances, with major effects on air quality, biogeochemical distribution of nutrients, and climate. The climatic effects are mainly associated with an appreciable decrease in surface reflectance and a decrease in the single scattering albedo of columnar aerosols, which both appreciably contribute to cause local warming effects in the atmosphere.

Vegetation is predominantly composed of cellulose, hemicellulose, and lignin and constitutes the major fuel consumed in natural biomass burning. Therefore, the combustion of biomass organic components involves a complex sequence of physical transformations and chemical reactions, including pyrolysis, depolymerization, water elimination, fragmentation, oxidation, char formation, and volatilization. During the earlier stages of combustion, known as flaming combustion, hydrocarbons volatilized from the decomposing biomass are rapidly oxidized in a flame upon mixing with air. When the flux of these combustible volatile compounds falls below a critical level, flaming expires and

smoldering or glowing combustion starts to occur. Taking place at such lower temperatures, these combustion processes involve a gradual gas–solid phase reaction between oxygen and the remaining reactive char, thus emitting large amounts of incompletely oxidized pyrolysis products. Many of these compounds have sufficiently low vapor pressures to be found in the particulate phase when released into the ambient atmosphere. Therefore, OM often constitutes the major fraction of smoke aerosols, sometimes accounting for more than 90% of the total aerosol mass (Graham *et al.*, 2002), while the fraction of water-soluble organic compounds consists of a complete mixture of oxygenated substances derived primarily from biomass burning.

Smoke aerosols may cause a number of spectacular optical atmospheric effects, such as the blue moon and Sun. As mentioned earlier, smoke aerosols contain a large fraction of soot substances. These particles consist in part of aggregates and in part of small aerosols, of which (i) the aggregates generally have sizes greater than 1 μm , and are formed by coalescence of ultimate or primary small particles having sizes mainly varying from 50 to 100 nm, and (ii) small aerosols exhibit sizes that are mainly smaller than 0.2 μm . As mentioned previously, soot particles are often assembled in chain-like structures. This makes it impossible to use spherical particle models to estimate their radiative properties, because the complex refractive index of soot varies as a function of its structure and production chain, presenting relatively high values of its real part at visible and near-infrared wavelengths varying mainly from 1.74 to 1.83 and values of its imaginary part usually close to 0.4–0.5, therefore considerably higher than those typical of maritime, mineral dust, and secondary water-soluble aerosols.

Several million grams of particles can be released by the burning of one tropical forest hectare (10^4 m^2). On a global scale, SMIC (1971) estimated that forest fires and slash-burning debris contributed to give a global annual average production flux of aerosol particle mass varying from 3 to 150 Tg per year, with the fraction of forest fire smoke particles with $a < 20 \mu\text{m}$ that provides a value of Φ_e not exceeding 50 Tg per year (United Nations, 1979). Accordingly, flux Φ_e including the whole smoke atmospheric load from forest fires was estimated to range from 5 to 150 Tg per year by Jaenicke (1988). On the basis of most recent evaluations, it was estimated by the IPCC (2001) that about 54 Tg per year of carbonaceous aerosols with $a < 2 \mu\text{m}$ is released into the atmosphere each year by natural biomass burning, of which 28 Tg per year in the northern hemisphere and 26 Tg per year in the southern hemisphere. This estimate of emission flux Φ_e is relatively small in comparison to that of overall aerosols formed from all the natural and anthropogenic sources. A fraction of Φ_e equal to about 10% and, hence, to ~ 6 Tg per year, is attributed to carbonaceous particles, consisting mainly of EC, which does not usually volatilize below the temperature of 550 $^\circ\text{C}$. As reported in Table 1.1, Tsigaridis *et al.* (2006) calculated that overall flux Φ_e of primary organic aerosol from forest fires is equal to 44.4 Tg per year, while the flux Φ_e for biomass burning organic particles was estimated by Andreae and Rosenfeld (2008) to range from 26 to 70 Tg per year. This evaluation agrees very well with that of OM different from EC, equal to about 48 Tg per year on a global scale.

Aerosols emitted from forest fires consist mainly of submicron particles giving form to an accumulation particle mode, usually peaked at $a \approx 0.1 \mu\text{m}$, and containing relatively high concentrations of EC that may have major light absorption effects. Smoke has important local effects on the environment: (i) provoking serious diseases in humans, animals, and plants; (ii) affecting the Earth albedo through deposition of soot particles at the surface, at the same time causing a marked lowering of the overall single scattering albedo of airborne aerosols, which may consequently induce pronounced warming effects in the atmosphere; (iii) causing the decrease of local and regional visibility because of their light scattering and absorption properties; (iv) acting as efficient CCNs, which can considerably modify the cloud droplet size distribution and the cloud reflectance characteristics; and (v) efficiently changing the cloud microphysical processes, leading to major variations in precipitation patterns. On a global scale, the combined direct and indirect radiative effects induced by these aerosols are estimated to be responsible for a net radiative forcing comparable to that induced by sulfate aerosols. In particular, boreal forest fires are estimated to contribute as much as 20–50% to the observed BC concentrations in the Arctic during summer. When deposited at the ground in these polar regions covered by sea ice, snow fields, and glaciers, smoke particles originated from summer forest fires in North America and Siberia are often transported toward Northern Canada, Greenland, the Svalbard islands, and other Arctic land regions, causing considerable changes in the surface albedo (Stohl *et al.*, 2006). For instance, over 5 million hectares of boreal forests burned in Alaska and Canada during summer 2004, and an enormous transport of smoke particles toward the Arctic followed. During this episode, values of aerosol optical thickness higher than 0.2–0.3 at the visible wavelengths were measured at Summit (Greenland) and Ny-Ålesund (Svalbard) in June and July 2004 (Tomasi *et al.*, 2007), showing some very high peaks exceeding the unit value at Barrow (Alaska) in June 2004 (Stone *et al.*, 2008). The combined mechanism of transport of the forest fire aerosols toward higher latitudes (Paris *et al.*, 2009) and the subsequent deposition on high-albedo surfaces is estimated to cause a reduction of the snow-covered areas in the Arctic and a not negligible decrease in the surface albedo of such polar regions, leading to significant variations in the radiation budget of the surface–atmosphere system (Flanner *et al.*, 2011).

1.3.5

Volcanic Dust in the Troposphere

Volcanoes emit both particles and gases into the troposphere during their moderate eruptions and inject considerable amounts of gases into the lower stratosphere during the most violent episodes, at altitudes most frequently between 15 and 25 km. In these often dramatic circumstances, volcanic eruptions can play an important role in stratospheric chemistry, causing chemical processes that are described in detail in Section 1.4.4 dealing with the formation of natural marine

secondary and volcanic sulfate aerosols in the stratosphere. Two components of volcanic emissions contribute mainly to the formation of volcanic aerosol particles at tropospheric altitudes, primarily consisting of dust and sulfates formed from gaseous sulfur. Estimates of the global annual flux Φ_e of volcanic dust injected into the troposphere were made in the 1990s by Jones, Charlson, and Rodhe (1994), who proposed values ranging from 4 to 10^4 Tg per year (evaluated for extremely explosive eruption episodes). An average estimate of the annual volcanic aerosol emission flux Φ_e equal to ~ 33 Tg per year was proposed by Andreae (1995), which agrees closely with other evaluations of Φ_e for volcanic debris, giving a range from 25 to 150 Tg per year (SMIC, 1971; United Nations, 1979) and a range from 4 to 90 Tg per year (Jaenicke, 1988), for which an average value of 30 Tg per year was determined by Kiehl and Rodhe (1995). On the basis of these evaluations, all reported in Table 1.1, we assumed that the tropospheric volcanic dust emission rate Φ_e ranged from 4 to 150 Tg per year over the past 50 years, with an average value of 30 Tg per year.

Volcanic sources contribute significantly to the sulfate aerosol burden in the upper troposphere, where they might take part to the formation of ice particles, therefore representing an important potential for inducing strong indirect radiative effects (Graf, Feichter, and Langmann, 1997). Support for this contention lies in the evidence of cirrus cloud formation from volcanic aerosols (Sassen, 1992) and arises from the results achieved by Song *et al.* (1996), indicating that the interannual variability of high-altitude clouds is currently associated with explosive eruption episodes. Graf, Feichter, and Langmann (1997) estimated that the radiative effects of volcanic sulfates are only slightly weaker than those induced by anthropogenic sulfates, even though the anthropogenic SO_2 source intensity is about five times greater. This surprising impact capability on climate arises from the higher efficiency of volcanic sulfur in producing sulfate aerosols, evaluated to be 4.5 times higher than that of anthropogenic sulfur. This is because SO_2 molecules released from volcanoes at high tropospheric altitudes have a longer residence time, mainly due to their appreciably lower dry deposition rate with respect to that typical of anthropogenic SO_2 emitted at the surface level (Benkovitz *et al.*, 1994).

The coarse solid matter particles (like powder-size matter, volcanic ash, or other igneous rock materials) blown into the air by an erupting volcano have generally short residence times in the troposphere, not exceeding a few weeks, as observed during the Eyjafjallajökull eruption in Iceland during April 2010 and the subsequent spread over Europe and North Atlantic in the second half of April and early May (Campanelli *et al.*, 2012). In this view, the term “volcanic dust” is here more appropriately referred to powder-size material than to fly ash particles most commonly having very large sizes, although both powder-size and fly ash particles usually cover the size range from 0.3 to more than 30 μm , having mass density close to $2.5 \times 10^6 \text{ g m}^{-3}$. Some TEM images of volcanic ash particles of various sizes were shown by Schumann *et al.* (2011), as sampled inside the plume emitted by the Eyjafjallajökull volcano in April 2010 and penetrating the North Atlantic

on May 2, 2010. They exhibit irregular shapes with jagged edges and sizes ranging from 0.7 to more than 20 μm . Silicates and mixed particles with $a < 500$ nm were found to constitute the most abundant groups. Such sampling measurements also provided evidence of sulfur-containing particles inside the Eyjafjallajökull plume, clearly indicating that the aerosol content in the size range $a < 500$ nm was dominated by secondary particles mainly consisting of ammonium sulfates and nitrates. Numerous submicron particles of ammonium sulfate were also sampled in very high concentration, together with supermicron particles having irregularly prismatic shape (with sizes of ~ 2 μm), and small droplets of sulfuric acid. In addition, numerous agglomerates were observed, consisting of (i) rather large silicate particles having sizes of ~ 10 μm and containing predominantly mixtures of various minerals, feldspars, amphiboles/pyroxenes, and pure SiO_2 minerals and (ii) smaller ammonium sulfate particles having sizes $a < 1$ μm , often crystallized out as droplets.

The residence times of the fly ash particles (mainly with $a < 1$ μm) forming drifting volcanic clouds can range from days to weeks, while the ash particles with sizes mainly ranging from 1 to 20 μm can remain suspended at atmospheric altitudes only for short times, varying from a few hours to 2 days. Due to these relatively long residence times in the atmosphere, both fine and coarse ash particles can produce locally relevant optical effects, which can be realistically evaluated using the Mie (1908) theory applied to scattering by spherical particles. Being insoluble in water, the larger volcanic ash particles exhibit in general sizes ranging from 20 μm to about 1 mm, presenting most frequently irregular shapes with sharp and jagged edges, as shown by Muñoz *et al.* (2004) for particles sampled during the volcanic eruptions of Mt St Helens on May 18, 1980, Mt Redoubt in 1989 and 1990, and Mt Spurr in August and September 1992.

The ash particles having sizes equal to several tens of micrometer fall not far from the volcano, having residence times of no more than 1–2 h. Therefore, they are estimated to produce only negligible radiative effects on climate. Volcanic ash particles of giant sizes look like grained fragments with sizes of 1–2 mm and consist mostly of broken glass shards and variable amounts of broken crystal and lithic fragments. However, having lifetimes of no more than a few hours and sizes greater than 1 mm, they cannot be classified as aerosols, being largely beyond the upper size limit commonly defined for aerosols (Rose and Durant, 2009). Most of the particles ejected from volcanoes in the form of dust and ash consist of water-insoluble substances (minerals, silicates, and metallic oxides such as SiO_2 , Al_2O_3 , and Fe_2O_3) and remain for the most part confined to the troposphere.

Finally, it is important to emphasize that volcanic eruptions can play an important role in modifying the sulfate aerosol load of the upper troposphere, where they act as condensation nuclei for ice particles. Therefore, they can significantly favor cirrus cloud formation, thus contributing to produce relevant indirect radiative forcing effects. Satellite-based observations of volcanic aerosol and clouds confirm that an interannual variability link exists between explosive

volcanic eruptions and high-level cloud formation and cloudiness index (Graf, Feichter, and Langmann, 1997).

1.3.6

Cosmic Dust

Cosmic dust in the solar system is mainly constituted by small particles having sizes ranging from a few molecules to $0.1\ \mu\text{m}$. In the solar system, cosmic dust is formed from comet dust, asteroidal dust, Kuiper belt dust, and interstellar dust, the last component causing the zodiacal light. Examining spacecraft measurements of the cosmic dust flux, it was estimated by Zook (2001) that as many as $4 \times 10^4\ \text{t}$ of cosmic dust reach the Earth's surface every year, with nearly all of the meteoritic mass residing in grains with masses ranging from 10^{-19} to $10^{-7}\ \text{g}$. Less than 25% of this mass is believed to derive from asteroids. Data from the spacecrafts of Pioneer 8 and 9 missions gave evidence for a flux of submicron dust grains leaving the solar system under radiation pressure at the rate of about $10\ \text{tons}\ \text{s}^{-1}$, while a mass flux of interstellar grains equal on average to $3 \times 10^{-19}\ \text{g}\ \text{s}^{-1}$ has been estimated to pass through the solar system on the basis of the measurements taken on board the spacecrafts of Galileo and Ulysses missions. Kwok and Zhang (2011) reported that cosmic dust contains complex OM (consisting of amorphous organic solids with a mixed aromatic–aliphatic structure) that could be created naturally, and rapidly, by stars. More recently, examining a set of zodiacal cloud observations and measurements made with a spaceborne dust detector, Plane (2012) found that the daily mass input of interplanetary dust particles entering the Earth's atmosphere ranges from 100 to 300 t, in agreement with the accumulation rates of cosmic-enriched elements (Ir, Pt, Os, and superparamagnetic Fe) evaluated in polar ice cores and deep-sea sediments. In contrast, it was estimated by Plane (2012) from measurements in the middle atmosphere conducted with radar, LIDAR, high-flying aircraft, and satellite remote sensing techniques that the annual input flux Φ_e varies between 5 and 50 tons per day. The previous evaluations lead to obtain values of cosmic dust Φ_e ranging from 3×10^{-2} to $1.1 \times 10^{-1}\ \text{Tg}$ per year at around 100 km altitude and from 2×10^{-3} to $2 \times 10^{-2}\ \text{Tg}$ per year at the 50 km altitude. These estimates are two to three orders of magnitude smaller than those given by the weaker surface-level sources, as can be seen in Table 1.1. It is important to take into account that cosmic dust particles enter the atmosphere at high speeds and undergo significant ablation passing through the atmosphere. The resulting metals injected into the atmosphere are involved in a diverse range of phenomena, including (i) the formation of layers of metal atoms and ions; (ii) the nucleation of noctilucent clouds, which are a sensitive marker of climate change; (iii) impacts on stratospheric aerosols and ozone chemistry, which need to be considered against the background of a cooling stratosphere and geoengineering plans to increase sulfate aerosol; and (iv) fertilization of the ocean with bioavailable Fe, which has potential climate feedbacks. Gardner *et al.* (2014) estimated that the global influx of cosmic dust ranges from 0.4 to 110 t per day and therefore from

1.5×10^4 to 4×10^{-2} Tg per year, for which the average global flux of cosmic dust entering the Earth's atmosphere can be evaluated as equal to 2×10^{-2} Tg per year.

1.4

Secondary Aerosols of Natural Origin

Natural secondary aerosols originate in the atmosphere as a result of *in situ* g-to-p conversion processes. They are composed mostly of sulfates and nitrates formed through condensation of sulfur- and nitrogen-containing gases and may (i) condense onto existing particles, thereby increasing the mass (but not the number) of particles, such a process being favored when the surface area of existing particles is high and the supersaturation of the gases is low, or (ii) form new particles, with sizes smaller than $0.01 \mu\text{m}$ in general. The amount of aerosols produced by g-to-p conversions is comparable to that generated by direct emissions of natural aerosols and exceeds that due to direct emissions of anthropogenic aerosols. Three major families of chemical species can be identified in such g-to-p conversion processes, involving natural gaseous compounds containing sulfur, nitrogen, and organic and carbonaceous molecules. In fact, various organic substances (originating, e.g., from gases emitted by plants) can additionally furnish a large contribution to the total aerosol mass (Seinfeld and Pandis, 1998). In particular, SO_2 is oxidized to H_2SO_4 and the rate of conversion is influenced by the presence of heavy metal ions (e.g., Fe, Mn, V). Among the proposed reactions, the following six are commonly estimated to be the most important:



The particles forming through these reactions generally exhibit spherical shapes, with number density concentrations usually ranging from 3×10^3 to $7 \times 10^3 \text{ cm}^{-3}$, but sometimes reaching values exceeding $1.5 \times 10^4 \text{ cm}^{-3}$ for the heaviest pollution conditions occurring in urban areas. The size distributions of these aerosols are in general realistically represented by lognormal curves with geometrical standard deviations assuming values close to 0.70. The mass concentration of these particles can vary considerably as a function of RH conditions of the surrounding air. Due to their relatively high number concentration at locations all over the world, secondary particles play an important role in the global

aerosol budget, also due to the remarkable contribution from anthropogenic gaseous emissions.

1.4.1

Natural Sulfate Particles from Tropospheric SO₂ and Sulfur Compounds

Sulfate aerosols are produced by chemical reactions in the atmosphere involving gaseous precursors, with the exception of sea-salt sulfate and gypsum dust particles. Together with those formed from anthropogenic sources through secondary processes (which are described in Section 1.6.1), sulfate particles have compositions ranging from sulfuric acid droplets to ammonium sulfates and constitute a major aerosol type in the troposphere. The key controlling variables for the production of sulfate aerosols from its precursors are (i) the source strength of the precursor substance, (ii) the fraction of precursors removed before conversion to sulfate, and (iii) the chemical transformation rates along with the gas-phase and aqueous chemical pathways for sulfate formation from SO₂. The atmospheric burden of sulfate aerosol is then regulated by the interplay of production, transport, and wet and dry deposition processes. Sulfate aerosols nucleate homogeneously or form on existing particles from gaseous precursors. Natural aerosols are formed from SO₂ emitted by volcanoes into the atmosphere and from dimethyl sulfide (i.e., CH₃SCH₃, or referred to as DMS) emitted by biogenic sources, especially marine plankton.

Natural sulfur is mainly assimilated by living organisms and is then released into the atmosphere as one of the final metabolism products. The most important atmospheric sulfur gases are sulfur dioxide (SO₂), hydrogen sulfide (H₂S), DMS, carbonyl sulfide (COS), and carbon disulfide (CS₂). Among them, the three following reduced sulfur gases of biogenic origin are the most important in the formation of sulfate aerosols:

1. H₂S, which is produced by sulfate-reducing bacteria and is mainly emitted from swamps and sediments. Here, microbial degradation of dead OM, occurring through biogenic reactions in soils, marshland, and plants, contributes together with halocarbons to release H₂S in the air, which is then rapidly converted to SO₂.
2. DMS, which is emitted from marine phytoplankton together with dimethyl disulfide and is then oxidized to SO₂ and sulfate aerosols.
3. COS, which is released in much smaller amounts from the biosphere but remains in the atmosphere during much longer lifetimes of 44 years on average.

All three gaseous species serve as precursor gases for sulfate aerosol production. The regions of the ocean with high organic content and biological productivity (i.e., upwelling regions, coastal waters, and salt marshes) constitute the major sources of CS₂ and COS, where various biogenic reactions in the oceans act as sources of DMS, COS, and CS₂, primarily due to phytoplankton. Released into the atmosphere, DMS and COS are first oxidized to SO₂. In

particular, DMS is oxidized by free radicals that contain oxygen (such as NO_3^- and OH^-). Since OH^- forms during the day via photochemical processes, the reaction with OH^- during sunlight hours is the primary process leading to DMS oxidation. Intermediate oxidation products are methanesulfonic acid ($\text{CH}_3\text{SO}_3\text{H}$), dimethyl sulfoxide, and dimethyl sulfone. DMS is not subject to dry deposition and can therefore be converted to SO_2 far enough from the ground to avoid large deposition losses. For this reason, DMS is the main precursor of SO_2 in remote oceanic air. In polluted atmospheres, NO_3 can build up at night and lead to the $\text{DMS} + \text{NO}_3$ reaction, from which SO_2 is formed near the ground. The reactivity of COS in the troposphere is low, allowing COS to enter the stratosphere by diffusion. At these low stratospheric levels, oxidation of COS dominates the production of stratospheric sulfate aerosol during periods of weak volcanic activity, when direct injection of SO_2 into the stratosphere is negligible.

Sulfur compounds exist in both reduced and oxidized states, with oxidation numbers from -2 to $+6$. When these reduced sulfur gases are released into the oxygen-rich atmosphere, they are mainly oxidized by more than 65% to the $+6$ oxidation state of H_2SO_4 (i.e., oxidized to SO_4^- with S(VI)), while the remainder of the SO_2 is oxidized to the $+4$ oxidation state of SO_2 (i.e., S(IV)), and a small percentage is removed by dry deposition. In fact, the $+6$ oxidation state is the stable form of sulfur in the presence of oxygen. Oxidation of sulfur compounds illustrates an effect that often applies to other compounds, for which the more oxidized species generally have a high affinity for water (e.g., sulfuric acid). Consequently, such oxidized species are removed very rapidly and efficiently from the atmosphere by wet processes.

As mentioned earlier, the principal natural sources of SO_2 are the oxidation processes of DMS and H_2S . For example, H_2S reacts with OH to form H_2O and HS and then forms SO_2 through the following sequence of reactions:



Volcanoes, biomass burning, and forest fires are also natural sources of tropospheric SO_2 , although the strongest source of SO_2 all over the world is fossil fuel combustion, estimated to yield an annual average global flux $\Phi_e = 75 \text{ Tg(S)}$ per year of sulfur, against $\Phi_e = 10 \text{ Tg(S)}$ per year of volcanic sulfur, and $\Phi_e = 3 \text{ Tg(S)}$ per year of sulfur from biomass burning, as can be seen in Table 1.2, where the estimates of atmospheric content of sulfur compounds (H_2S , SO_4^{2-} , SO_2 , CS_2 , DMS, and COS) are given together with those of the emission and removal annual global fluxes from the principal sources and sinks of sulfur-containing

Table 1.2 Principal sources and sinks of sulfur-containing species on a global scale, defining the sulfur reservoirs of the surface–troposphere system where continents contain 2×10^{10} Tg(S) and oceans 1.6×10^9 Tg(S) (Hobbs, 2000) (being $1 \text{ Tg} = 10^6 \text{ t}$).

Reservoir	Atmospheric mass content (Tg(S))	Entering annual global flux (Tg(S) yr ⁻¹)	Outgoing annual global flux (Tg(S) yr ⁻¹)
H ₂ S	0.03	7 (from soils and marshlands)	7 (toward the SO ₂ reservoir)
SO ₄ ²⁻	1.20 ^{a)}	3 (volcanoes)	10 (dry deposition)
		80 (SO ₂ reservoir)	73 (wet deposition)
SO ₂	0.30	7 (H ₂ S reservoir)	80 (toward the SO ₄ ⁻ reservoir)
		3 (biomass burning)	40 (dry deposition)
		10 (volcanoes)	—
		75 (anthropogenic activities and fossil fuel combustion)	—
		25 (DMS reservoir)	—
		0.5 (CS ₂ reservoir)	—
CS ₂	0.10	0.7 (soils, plants and industry)	0.5 (toward the SO ₂ reservoir)
		0.3 (biogenic processes in oceans)	0.5 (toward the COS reservoir)
DMS	0.05	25 (biogenic processes in oceans)	25 (toward the SO ₂ reservoir)
COS	2.50	0.3 (biogenic processes in oceans)	0.9 (dry deposition)
		0.3 (soils)	0.2 (toward the stratosphere)
		0.5 (CS ₂ reservoir)	—

a) 40–320 Tg(S) of SO₄²⁻ are involved in the sea-salt cycle (emission and removal in atmosphere–ocean exchanges).

species, respectively (Hobbs, 2000). Estimates of the entering global flux Φ_e of SO₂ defined by the IPCC (2001) are presented in Table 1.4 for comparison. The value of $\Phi_e = 75 \text{ Tg(S)}$ per year of SO₂ proposed by Hobbs (2000) as due to fossil fuel combustion is in close accordance with the value of $\Phi_e = 76 \text{ Tg(S)}$ per year provided by Benkovitz *et al.* (1996), while the estimate of Φ_e made by Hobbs (2000) for Φ_e for the sulfur from biomass burning was appreciably higher than that estimated by Spiro, Jacob, and Logan (1992) around 2.2 Tg(S) per year. The entering global flux of particulate matter sulfur from volcanoes was estimated by Andres and Kasgnoc (1998) to be 9.3 Tg(S) per year (including H₂S) and, hence, slightly lower than the Hobbs (2000) value. A total entering annual global flux of SO₂ equal to 88 Tg(S) per year was therefore assumed by the IPCC (2001), including a small contribution of 0.06 Tg(S) per year from aircraft traffic (Penner *et al.*, 1998). The entering annual global flux of DMS from biogenic processes in

the oceans was evaluated by Hobbs (2000) to be 25 Tg(S) per year, in accordance with the overall estimate of IPCC (2001) including also H₂S, consisting of 24 Tg(S) per year from oceans (Kettle and Andreae, 2000) and 1.0 Tg(S) year from land biota and soils (Bates *et al.*, 1992; Andreae and Jaeschke, 1992), as reported in Table 1.4.

In the gas phase, SO₂ is oxidized through the following sequence of three reactions:



where M is a third molecule to which the exothermal energy is transferred;



yielding SO₃, which then reacts with water in the final reaction; and



which may also occur in cloud water to form a sulfuric acid molecule.

The main sources of H₂S are emissions from soils, marshlands, oceans, and volcanoes. The only significant sink for H₂S is oxidation to SO₂, through the four reactions in Eqs 1.11–1.14. Biological reactions in the oceans involving phytoplankton emit several sulfur gases, of which DMS exhibits the largest emission rate, being then removed from the atmosphere primarily by its reaction with OH to produce SO₂. The sulfur gas with the highest concentration in the unpolluted atmosphere is COS (~0.5 ppbv), due to biogenic sources and oxidation of CS₂ by OH. Molecules of COS are very stable in the troposphere and can be transported into the stratosphere, where they constitute the dominant source of sulfate particles during the quiescent periods between two consecutive violent and strong volcanic eruptions, which are capable of injecting sulfur gases into the stratosphere through the mechanisms described in Section 1.4.4.

The preceding remarks state that various sulfur gases (e.g., H₂S, CS₂, COS, DMS) can be oxidized to SO₂, which is then oxidized to sulfate (SO₄²⁻), the dominant gas-phase routes being the reactions defined in Eqs. 1.15–1.17. It is estimated that H₂S oxidizes to SO₂ within about 2 days on average at tropospheric levels, during the sulfate particle formation processes.

An important role is played by sulfuric acid in the formation of sulfates by ammonia (NH₃), which is the principal basic gas in the atmosphere originating from soils, animal waste, fertilizers, and industrial emissions, having residence time in the lower troposphere of ~10 days. Ammonia neutralizes acid species through reactions such as



This implies that the primary removal mechanisms for NH₃ involve its conversion to ammonium-containing aerosols, which are then removed from the atmosphere and transported to the ground by wet and dry deposition. However, on a

global scale, heterogeneous reactions of SO_2 in cloud water dominate the conversion of SO_2 to ammonium-containing droplets. Over the oceans, sulfates derived from DMS contribute to the growth of existing particles. Sulfates are also produced in and around clouds, the subsequent evaporation of cloud water releasing these sulfate particles into the air, as reported in Table 1.2.

The chemical pathway of precursors converted to sulfate is important because it changes the radiative effects. Most SO_2 is converted to sulfate either in the gas phase or in cloud droplets that later evaporate. Model calculations suggest that aqueous-phase oxidation is dominant over the global scale. Both processes produce sulfate mostly in submicron aerosols, which act as efficient light scatterers, but the size distribution of sulfate in aerosols is different for gas phase and aqueous production. The size distribution of sulfate particles formed in the gas-phase process also depends on the interplay of nucleation, condensation, and coagulation processes. Two types of chemical interaction have been recognized to reduce the radiative impact of sulfate aerosols by causing some to condense onto larger particles with lower scattering efficiencies and shorter atmospheric lifetimes: (i) heterogeneous reactions of SO_2 on mineral aerosols (Andreae and Crutzen, 1997) and (ii) oxidation of SO_2 to sulfate in sea-salt-containing cloud droplets and deliquesced sea-salt aerosols. The second process forms a substantial fraction of nss sulfate particles that numerically predominate over that of coarse sea-salt particles, especially under conditions where the rate of photochemical H_2SO_4 production is low and the amount of sea-salt aerosol surface available is high (Sievering *et al.*, 1992). Sulfate in aerosol particles is present as sulfuric acid, ammonium sulfate, and intermediate compounds, depending on the availability of gaseous ammonia to neutralize the sulfuric acid formed from SO_2 . In a modeling study, Adams, Seinfeld, and Koch (1999) estimated that the global mean $\text{NH}_4^+/\text{SO}_4^{2-}$ mole ratio is close to unit, in good agreement with experimental data. This not only increases the mass of sulfate aerosol by some 17% but also changes the hydration behavior and refractive index of the aerosol. The overall effects are of the order of 10%, which is relatively low if compared with the uncertainties discussed earlier.

On this matter, an interesting hypothesis on the existence of a DMS global climate feedback formulated by Charlson *et al.* (1987), called the CLAW hypothesis from the initials of the four coauthors' surnames, is worth mentioning. This theory states that biogenic DMS production by marine phytoplankton influences global climate through a feedback mechanism involving sulfate aerosols and clouds through the following 10 steps:

1. DMS diffuses from the sea surface to the atmosphere.
2. DMS is oxidized to a sulfate aerosol.
3. Sulfate aerosols act as the main source of CCNs over the oceans.
4. Cloud albedo increases.
5. Global temperature is lowered.
6. Phytoplankton production decreases.
7. DMS emissions decrease.
8. Atmospheric load of sulfate aerosols decreases.

9. Cloud albedo decreases.
10. Global temperature rises, increasing both phytoplankton production and DMS emissions.

1.4.2

Natural Nitrate Particles from Tropospheric Nitrogen Oxides

Nitrogen molecules (N_2) constitute more than 99.99% of the nitrogen present in the atmosphere and have an overall atmospheric content of 2×10^9 Tg(N). Nitrous oxide (N_2O) is one of the most important greenhouse gases and contributes to provide most of the remaining nitrogen, giving a considerably lower atmospheric content of 1.3×10^3 Tg(N). The other nitrogen species in the atmosphere are therefore present in very low trace concentrations, yielding an overall content of 0.75 Tg(N). Nonetheless, they are of crucial importance in atmospheric chemistry, since they participate in important aerosol formation processes. Ammonium (NH_3), for example, is the only basic gas in the atmosphere responsible for neutralizing acids produced by the oxidation of SO_2 and NO_2 . The ammonium salts of sulfuric and nitric acid formed through these processes become atmospheric aerosols, mainly through the reactions involving nitrogen oxides NO and NO_2 in both tropospheric and stratospheric chemistry processes. All of the nitrogen-containing gases in the air are involved in biological nitrogen fixation and denitrification. "Fixation" refers to the reduction and incorporation of nitrogen from the atmosphere into living biomass. This transformation is accomplished by bacteria that have special enzymes for this task, usually producing NH_3 . The term "fixed nitrogen" refers to nitrogen contained in chemical compounds that can be used by plants and microorganisms. Under aerobic (i.e., oxygen-rich) conditions, other specialized bacteria can oxidize ammonia to nitrite (NO_2^-) ions and then to nitrate (NO_3^-) ions through a process referred to as "nitrification." Most plants use nitrate taken through their roots to satisfy their nitrogen needs. Some of the nitrate undergoes bacterial reduction to N_2 and N_2O (termed "denitrification"), which returns fixed nitrogen from the biosphere to the atmosphere. In this case, nitrate acts as the oxidizing agent. Therefore, denitrification generally occurs under anaerobic conditions, where oxygen is not available. Fixed nitrogen can also be returned from plants to the atmosphere in the form of N_2O . Biomass burning returns fixed nitrogen to the atmosphere such as N_2 , NH_3 , N_2O , and NO_x .

The oxides of nitrogen, that is, nitric oxide (NO) and nitrogen dioxide (NO_2), which together are referred to as NO_x , play a very important role in atmospheric chemistry, contributing to determine the entering and outgoing global annual fluxes of nitrogen estimated in Table 1.3, because they take part in all the formation and removal processes of nitrogen-containing compounds occurring in the atmosphere. The nitrogen oxides are produced by fossil fuel combustion and biomass burning and originated from soils, lightning, NH_3 oxidation, aircraft emissions, and transport from the stratosphere. Nitrogen oxides are emitted into the troposphere primarily as NO , but during the day NO rapidly establishes an

Table 1.3 Principal sources and sinks of nitrogen-containing species on a global scale, defining the nitrogen reservoirs of the surface-troposphere system where continents contain 9×10^9 Tg(N) and oceans 1.1×10^7 Tg(N) (Hobbs, 2000) (being 1 Tg = 10^6 t).

Reservoir	Atmospheric mass content (Tg(N))	Entering annual global flux (Tg(N) yr ⁻¹)	Outgoing annual global flux (Tg(N) yr ⁻¹)
N ₂	2×10^9	100 (denitrification at the ocean surface) 140 (denitrification by bacteria in plants, soils, and water)	100 (fixation at the ocean surface) 140 (fixation by bacteria in plants, soils, and water)
N ₂ O	1.3×10^3	2 (from oceans) 0.5 (biomass burning) 4 (fossil fuel consumption and industrial activities) 6 (soil emissions due to nitrification, denitrification, and fertilizers)	9 (toward the stratosphere) — — —
NO _x	0.15	6 (soil emissions due to nitrification, denitrification, and fertilizers) 12 (biomass burning) 20 (fossil fuel combustion) 3 (reservoir of NH ₃ and NH ₄ ⁺) 5 (lightning in clouds) 7 (from oceans)	20 (dry removal of NO _x) 25 (wet removal of NO _x) — — —
NH ₃ and NH ₄ ⁺	0.60	2 (biomass burning) 12 (soil emissions including fertilizer loss) 26 (decomposition of proteins), of which 23 in urea from domestic animals and 3 in urea from wild animals	— 15 (dry removal of NO ₃ and NH ₄ ⁺) 32 (wet removal of NO ₃ and NH ₄ ⁺) 3 (toward the NO _x reservoir) — — —

equilibrium with NO_2 through the null cycle consisting of the following two reactions:



where M represents an inert molecule, capable of absorbing the excess molecular energies. Once NO is converted to NO_2 , a number of reaction paths are available. During the night, NO_x is present only as NO_2 due to the reaction represented in Eq. (1.19), while in the daytime the principal sink for NO_x is given by the following reaction:



Nitric acid (HNO_3) is removed in about 1 week by dry and wet deposition. During the night hours, NO_2 is oxidized by O_3 to NO_3 , and the NO_3 then reacts with NO_2 to produce N_2O_5 , which reacts subsequently with water on particles and cloud droplets to form HNO_3 . The evaporation of cloud water releases these nitrate particles into the air, so that the resulting residence time of NO_2 is of about 1 day.

Examining the data given in Table 1.3, Hobbs (2000) estimated that the overall entering annual global flux of NO_x was equal to 46 Tg(N) per year, while the IPCC (2001) estimated a flux of ~ 41 Tg(N) per year, of which:

1. 5.5 Tg(N) per year is due to soil emissions associated with nitrification and denitrification as well as to the effects arising from the use of fertilizers (Yienger and Levy, 1995), such an overall flux being subdivided into ~ 2.2 Tg(N) per year coming from agricultural soils and ~ 3.2 Tg(N) per year from natural soils, while Hobbs (2000) evaluated this overall flux as equal to 6 Tg(N) per year.
2. 6.4 Tg(N) per year is given by biomass burning (Lioussé *et al.*, 1996) against the estimate of 12 Tg(N) per year made by Hobbs (2000).
3. 21 Tg(N) per year is due to fossil fuel combustion (Benkovitz *et al.*, 1996) in place of the Hobbs (2000) estimate equal to 20 Tg(N) per year.
4. 7.0 Tg(N) per year (Price, Penner, and Prather, 1997) is due to lightning against the estimate of 5.0 Tg(N) per year made by Hobbs (2000).

All these estimates are given in Table 1.4, while those of Hobbs (2000) are presented in Table 1.3. The main discrepancies resulting from such a comparison are due to the fact that the IPCC (2001) neglected the contribution made by the reservoir of NH_3 and NH_4^+ , while Hobbs (2000) assumed a value of 3 Tg(N) per year for evaluating such a contribution and neglected the aircraft traffic contribution, which was evaluated by Penner *et al.* (1999) to be equal to 58 Tg(N) per year. The overall entering annual global flux of nitrogen from NH_3 was estimated by the IPCC (2001) to be 54 Tg(N) per year (Bouwman *et al.*, 1997), while Hobbs (2000) assumed a total value of 47 Tg(N) per year. The partial contributions were attributed by Bouwman *et al.* (1997) to (i) domestic animals (21.6 Tg(N) per year),

Table 1.4 Estimates of the annual emission fluxes of natural and anthropogenic aerosol precursors (measured in Tg(S), Tg(N), and Tg(C) per year) on a global scale, as estimated by the IPCC (2001) and determined by various authors over the past two decades.

Emissions from natural precursors	Estimates and references
DMS and H ₂ S from oceans	24 Tg(S) yr ⁻¹ (Kettle and Andreae, 2000)
DMS and H ₂ S from land biota and soils	1.0 Tg(S) yr ⁻¹ (Andreae and Jaeschke, 1992)
NH ₃ (natural overall)	10.7 Tg(N) yr ⁻¹ (IPCC, 2001)
NO _x from natural soils and lightning	10.2 Tg(N) yr ⁻¹ (IPCC, 2001)
VOCs from isoprene	467.5 Tg(C) yr ⁻¹ (Tsigaridis <i>et al.</i> , 2006)
VOCs from monoterpenes	120.8 Tg(C) yr ⁻¹ (Tsigaridis <i>et al.</i> , 2006)
Aromatic VOCs	14.3 Tg(C) yr ⁻¹ (Tsigaridis <i>et al.</i> , 2006)
Overall VOCs	250.9 Tg(C) yr ⁻¹ (Tsigaridis <i>et al.</i> , 2006)
Emissions from anthropogenic precursors	
SO ₂ (anthropogenic overall)	78.3 Tg(S) yr ⁻¹ (IPCC, 2001)
NO _x (anthropogenic overall)	30.2 Tg(N) yr ⁻¹ (IPCC, 2001)
NH ₃ (anthropogenic overall)	42.8 Tg(N) yr ⁻¹ (IPCC, 2001)

(ii) agriculture (12.6 Tg(N) per year), (iii) humans (2.6 Tg(N) per year), (iv) biomass burning (5.7 Tg(N) per year), (v) fossil fuel combustion and industry (0.3 Tg(N) per year), (vi) natural soils (2.4 Tg(N) per year), (vii) wild animals (0.1 Tg(N) per year), and (viii) oceans (8.2 Tg(N) per year).

Aerosol nitrate is closely tied to the relative abundances of ammonium and sulfate. If ammonia is available in excess of the amount required to neutralize sulfuric acid, nitrate can form small-size radiatively efficient aerosol particles. In the presence of an accumulation mode of aerosols containing sulfuric acid, nitric acid is deposited on alkaline mineral or sea-salt particles having larger sizes. Because coarse-mode particles are less efficient in causing light scattering per unit mass, this process reduces the radiative impact of nitrate particles in practice. The global burden of ammonium nitrate aerosols was estimated by Andreae (1995) to be 0.24 Tg from natural sources and 0.40 Tg (as NH₄NO₃) from anthropogenic sources, finding that anthropogenic nitrates cause only 2% of the total direct aerosol-induced forcing on a global scale. Similar estimates of global burden were derived by Jacobson (2001), who estimated that the global mean direct radiative forcing induced by anthropogenic nitrates is equal to $-2.4 \times 10^{x2} \text{ W m}^{-2}$ on average. Adams, Seinfeld, and Koch (1999) obtained an even lower value of 0.17 Tg (as NO₃⁻ ions) for the global nitrate burden. Part of the difference with respect to the Andreae's (1995) evaluation was plausibly attributed to the fact that the Adams, Seinfeld, and Koch (1999) model did not include nitrate deposition on sea-salt aerosol. Estimates obtained from other studies indicate that direct radiative forcing due to ammonium nitrate is about 1/10 of the sulfate forcing. However, the importance of aerosol nitrate will probably increase appreciably over the twenty-first century, because it was forecast that NO_x emissions will more than triple over such a period, while the emissions of SO₂ will decline

slightly. Thus, assuming an increase in agricultural emissions of ammonia, it is conceivable that direct forcing by ammonium nitrate could become comparable in magnitude to that induced by sulfates within the next 50 years (Adams *et al.*, 2001).

1.4.3

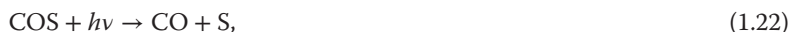
Organic Aerosols from Biogenic Volatile Organic Compounds

Organic and carbonaceous aerosols are formed by g-to-p conversion involving gases released from the biosphere and VOCs, such as crude oil leaking to the Earth's surface. As pointed out in Section 1.3.5, natural carbonaceous particles are emitted directly into the atmosphere, mainly during the biomass combustion processes occurring in forest and savannah areas. Therefore, they contain both EC and OC. In addition to biomass burning products, the main natural sources of carbonaceous aerosols are atmospheric oxidation of biogenic VOCs, which mainly consist of isoprene and terpene emitted by terrestrial plants (Claeys *et al.*, 2004), as reported in Table 1.4. Photooxidation of VOCs reduces their vapor pressure, while organic gases condense onto existing aerosol particles. Polymerization continues in the condensed phase and results in semi- or nonvolatile organic species (Gelencsér, 2004). Several thousands of VOCs are emitted not only by plants but also by numerous other biogenic sources into the atmosphere, providing a contribution which is globally predominant over that provided by anthropogenic sources (Tsigaridis and Kanakidou, 2007). In fact, it was estimated in the IPCC (2001) report that the overall volatile organic emissions are equal to 236 Tg(C) per year, of which 127 Tg(C) per year is from terpenes (i.e., ~54%) (Guenther *et al.*, 1995) and 10^9 Tg(C) per year from anthropogenic sources (equivalent to ~46%) (Piccot, Watson, and Jones, 1992), the second sources being mainly constituted by (i) motor vehicles that are in practice the primary source of VOCs in the most polluted areas of our planet, because of the incomplete combustion and vaporization of fuel producing hydrocarbons, and (ii) evaporation of solvents, evaluated to be the second most important anthropogenic source of VOCs in the world. Some of the more important VOCs are isoprene (C_5H_8), ethane (C_2H_4), and monoterpenes, yielding the global annual emission fluxes reported in Table 1.4, according to Tsigaridis *et al.* (2006). Isoprene accounts for about 50% of the NMHC. The photooxidation of isoprene can produce compounds having vapor pressures so low as to condense onto preexisting particles. This process could account for about 5–20% of the annual secondary organic aerosol (SOA) production from biogenic sources. Terpenes constitute a class of hydrocarbons that evaporate from leaves. About 80% of these emissions oxidize to organic aerosols within about 1 h. Emissions from vegetation constitute a significant source of hydrocarbons, which can react photochemically with NO and NO₂ to produce O₃, thereby playing a central role in atmospheric chemistry. Estimates of the annual emission fluxes of these aerosol precursors on a global scale are given in Table 1.4, as determined for both natural and anthropogenic sources.

1.4.4

Sulfate Particles from Marine and Volcanic SO₂ Formed in the Stratosphere

Stratospheric aerosols are composed of an aqueous solution of 60–80% sulfuric acid for temperatures varying from -80 to -45 °C, respectively (Shen, Wooldrige, and Molina, 1995). The source of the globally distributed background stratospheric aerosol, formed in the absence of perturbations caused by violent volcanic eruptions, is given by the emission of COS at the ocean surface, as a result of metabolism in marine areas, producing a high content of COS molecules near the surface, which are subsequently transported across the tropopause and then oxidized at stratospheric altitudes. Besides this sulfur compound, the transport from the troposphere to the stratosphere also involves other chemical species, such as (i) chlorine (Cl), whose major natural source is methyl chloride (CH₃Cl), which derives in part from biological activities in seawater, wood molds, and biomass burning, and (ii) halogen compounds (e.g., chlorine and bromine species) produced by biological activities in the oceans. COS is chemically inert and water insoluble and therefore has a long tropospheric residence time. For this reason, it diffuses into the stratosphere, where it is photolytically dissociated by solar UV radiation to form sulfuric acid through the following reaction:



where the incoming photons $h\nu$ belong to the UV radiation spectral range from 200 to 260 nm (Lin, Sim, and Ono, 2011), followed by these reactions:



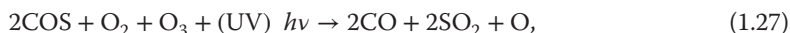
and



or



both leading to oxidation of SO into SO₂. The sequence of reactions (1.22–1.26) leads to the net result:



which contributes efficiently to form stratospheric SO₂, from which natural aerosols are formed at these altitudes. Alternatively, but with less efficiency, COS can react with a hydroxyl OH to yield SO₂.

As a result of the overall conversion defined in Eq. (1.27), the mixing ratio of COS decreases with height, passing from about 0.4 ppbv at the tropopause level to 0.02 ppbv at around 30 km altitude. Consequently, the SO₂ concentration remains roughly constant with height, assuming rather stable values of ~ 0.05 ppbv. The production of stratospheric sulfate aerosols at these altitudes primarily occurs

through oxidation of SO_2 by OH, through the reactions described in Eqs. (1.15) and (1.16) to form HO_2 and SO_3 . In the stratosphere, an alternative path for the formation of SO_3 is also given by the reaction



in which the exothermal energy is transferred to the third molecule M. Subsequently, SO_3 is combined with H_2O in the reaction of Eq. (1.17) leading to the formation of sulfuric acid molecules. The subsequent conversion of the H_2SO_4 vapor to liquid H_2SO_4 can occur because of the following two main mechanisms: (i) the combination of molecules of H_2SO_4 and H_2O (i.e., *homogeneous bimolecular nucleation*) and/or the combination of H_2SO_4 , H_2O , and HNO_3 to form new (primarily sulfuric acid) droplets (i.e., *homogeneous heteromolecular nucleation*) and (ii) vapor condensation of H_2SO_4 , H_2O , and HNO_3 onto the surfaces of preexisting particles with sizes $>0.30 \mu\text{m}$ (i.e., *heterogeneous heteromolecular nucleation*).

Model calculations indicate that the second mechanism is the more likely route in the stratosphere. The tropical stratosphere is probably the major region where the nucleation processes occur, and the aerosols are then transported to higher latitudes by large-scale atmospheric motions. As a result of the aforementioned chemical processes, the concentration of H_2SO_4 liquid droplets assumes a peak at around 20 km. The previous explanation based on the conversion of COS in SO_2 and the subsequent formation of H_2SO_4 is supported by the fact that other sulfur-containing species, such as SO_2 , DMS, and CS_2 , do not persist long enough in the troposphere to be transported to the stratosphere. Therefore, their role in the formation of stratospheric sulfuric acid droplets is wholly negligible. The background amount of stratospheric sulfate is mainly due to UV photolysis of organic COS forming SO_2 , although the direct contribution of tropospheric SO_2 injected in the stratosphere across the tropical tropopause region plays a significant role in forming sulfates at the lower stratospheric levels and accounts for about one-third of total stratospheric sulfate mass content. This quantity is currently estimated to be equal to $\sim 0.15 \text{ Tg(S)}$ during volcanically quiet periods, therefore accounting for no more than 15% of the overall sulfate content in the troposphere and stratosphere.

Sulfur direct emissions in the stratosphere occur mainly in the form of SO_2 , even though other sulfur species may be present in the volcanic plume, predominantly SO_4^{2-} ions and H_2S , which were evaluated to assume percentage concentrations of around 1% of the total amount and only in some cases to exceed percentages of around 10–20%. In these less frequent cases, H_2S oxidizes to SO_2 in about 2 days at the tropospheric levels and within 10 days at the lower stratospheric levels. The state of unperturbed background stratospheric aerosol was relatively rare during the past decades because several very violent volcanic eruptions took place during the past 50 years, in which significant amounts of SO_2 were directly injected into the lower and middle stratosphere, as occurred during the series of Gunung Agung eruptions in 1963–1964 in Bali (Indonesia), the El Chichón volcano eruption of April 1982 in Mexico, and Mt Pinatubo eruption in the

Philippines (June 1991). The observations of these volcanic eruption events indicated that the associated transient climatic effects may be very important in such circumstances, showing that the trends in the frequency of volcanic eruptions can constitute an efficient climatic factor capable of strongly influencing the average surface temperature, as was understood by analyzing the well-documented data set recorded during the evolution of the Pinatubo plume, from which valuable information was achieved by the scientific community on the climate effects that can be caused by a violent volcanic eruption.

In all these episodes, a few months after the direct injection of large amounts of SO_2 and lower concentrations of minor gases into the stratosphere, small particles were formed at relatively low stratospheric altitudes consisting of sulfuric acid ($\sim 75\%$) and liquid water ($\sim 25\%$). These droplets were transported globally during the subsequent months, producing rather high values of stratospheric aerosol optical depth with respect to the globally average background conditions of this optical parameter, causing pronounced cooling effects on the tropospheric and stratospheric temperatures (McCormick, Thomason, and Trepte, 1995). To give a measure of the strong changes in the aerosol optical thickness caused by the formation of Mt Pinatubo aerosol layers in the stratosphere, Figure 1.9 shows the time patterns of the daily mean values of aerosol optical thickness $\tau_a(\lambda)$ measured at various visible and near-infrared wavelengths and the corresponding atmospheric turbidity parameters α and β (Ångström, 1964) obtained from the sun-photometer measurements performed at the CNR Pyramid Laboratory (5050 m a.m.s.l.) in the Himalayan region (Nepal) on several clear-sky days during summer 1991 and summer 1992 (Tomasi, Vitale, and Tarozzi, 1997). These spectral dependence patterns were found to be very similar to those measured by Russell *et al.* (1993) at the Mauna Loa Observatory during the same months. The results recorded at the CNR Pyramid Laboratory provided evidence of the sharp increase in $\tau_a(\lambda)$ at all wavelengths λ and the corresponding decrease in α and the simultaneous increase in β due to the arrival of the stratospheric volcanic aerosol layers on July 27 above this high-altitude observation site. Evaluations of the vertical mass loading M_S of volcanic aerosols suspended in the low stratosphere, made using the average multimodal size distributions defined by Pueschel *et al.* (1993) from measurements performed at the Mauna Loa Observatory (Hawaii), indicated that M_S increased from less than 0.04 to more than 0.07 g m^{-2} within a few days in late July 1991, due to the arrival of the Mt Pinatubo stratospheric particles.

Figure 1.9 shows that the decay of aerosol extinction features recorded 1 year later caused a decrease of $\tau_a(0.50 \mu\text{m})$ from more than 0.20 in summer 1991 to around 0.17 in summer 1992, presenting decay features similar to those observed by Pueschel *et al.* (1993) at the Mauna Loa Observatory. These variations in the Himalayan region occurred with (i) the gradual decrease of α from about 0.8 to 0.5, caused by the growth of the coarse particles; (ii) the decrease of β from more than 0.12 to less than 0.10, due to the decreasing trend of $\tau_a(\lambda)$; and (iii) the appreciable decrease of M_S from 0.07 g m^{-2} in summer 1991 to less than 0.05 g m^{-2} in summer 1992. These findings clearly showed that the columnar particulate mass content M_s decreased from more than 0.03 g m^{-2} in summer 1991 to about 0.02 g m^{-2} in

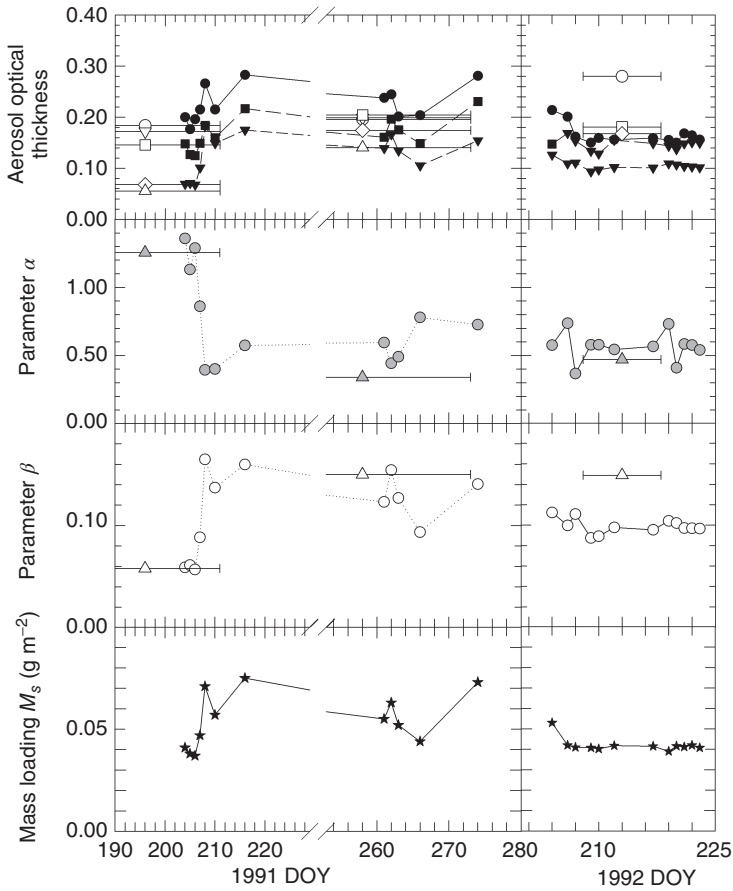


Figure 1.9 Upper part: time patterns of the daily mean values of aerosol optical thickness $\tau_a(\lambda)$ measured by us at the 380 nm (solid circles), 500 nm (solid squares), and 875 nm (solid triangles) wavelengths (Tomasi, Vitale, and Tarozzi, 1997) at the Pyramid Laboratory (5050 m a.m.s.l.) in Nepal, during summer 1991 (left-hand side) and summer 1992 (right-hand side), and of the monthly mean values of $\tau_a(\lambda)$ measured by Pueschel *et al.* (1993) at the Mauna Loa Observatory (Hawaii) in July and September 1991 (left-hand side) and in July and August 1992 (right-hand side) at the 382 nm (open circles), 451 nm (open down triangles), 528 nm (open squares), 865 nm (open up triangles), and 1060 nm (open diamonds) wavelengths. Middle part: time patterns of the daily mean values of Ångström's (1964) exponent α (solid circles) and atmospheric turbidity parameter

β (open circles), determined at the Pyramid Laboratory during summer 1991 (left-hand side) and during summer 1992 (right-hand side) and compared with the monthly mean values of α and β (open triangles) determined by Pueschel *et al.* (1993) in July and September 1991 at the Mauna Loa Observatory. Lower part: time patterns of the daily mean values of the Pinatubo aerosol mass loading M_s , as determined by us from the spectral values of $\tau_a(\lambda)$ measured during summer 1991 and summer 1992, in terms of variable linear combinations of background aerosol model and bimodal extinction model defined by Pueschel *et al.* (1993) for volcanic particles a few months old (summer 1991) and the trimodal model of Pueschel *et al.* (1993) for an aged population of Pinatubo particles (summer 1992).

summer 1992, indicating that the mean half-time was considerably longer than one year. The time patterns of $\tau_a(\lambda)$ shown in Figure 1.9 give a measure of the sharp increase in aerosol extinction within the stratospheric region below the 25 km altitude a few months after the eruption. Such an increase in $\tau_a(\lambda)$ arose from the formation of stratospheric particles mainly due to the injection of sulfur-containing volcanic gases and the subsequent reactions defined in Eqs. (1.15–1.17). The following increase in M_s occurred as a result of the gradual aging of the Mt Pinatubo sulfate aerosols at altitudes ranging from 8 to 26 km.

These pronounced evolutionary patterns in the size-distribution parameters of volcanic particles were observed at all latitudes of the two hemispheres over a period of 2–3 years after the eruption, as shown by the latitudinal and temporal patterns of the stratospheric aerosol depth $\tau_a(1.02 \mu\text{m})$ derived by Thomason *et al.* (2008) from the SAM II, SAGE, SAGE II, and SAGE III satellite-borne measurements performed over the period from January 1985 to the end of 2005 and completed with supplementary LIDAR data. This study provided evidence of (i) the gradual decrease in the atmospheric extinction observed in 1985 and early 1986 after the El Chichón eruption of 1982 and (ii) the formation of the Mt Pinatubo volcanic particle cloud in 1991 a few months after the eruption, followed by a slow decrease from 1991 to 1996. They confirm that the total removal period of the Pinatubo aerosol loading in the stratosphere lasted about 4 years, leading to an average estimate of the residence time of these aerosol particles in the low stratosphere equal to around 2.5 ± 1.2 years. It was evaluated that the Mt Pinatubo eruption of June 15, 1991, ejected very large amounts of ash and gases into the atmosphere so strongly that the volcano's plume penetrated into the stratosphere.

The aerosol mass loading ejected by this violent volcanic eruption was estimated to be about 1.5×10^7 t of SO_2 into the stratosphere, where it reacted with hydroxyl and water to form sulfuric acid droplets, yielding an overall stratospheric aerosol mass content of about 30 Tg on a global scale. The Mt Pinatubo eruption caused an abrupt increase in stratospheric aerosol optical depth by a factor of 10–100 times that measured before the eruption. Three months after the eruption, it was found that the stratospheric region at midlatitudes near the Philippines had warmed suddenly by 2.5–3.0 °C due to the increased aerosol concentration. In the following few months, a huge stratospheric load of sulfuric acid droplets was observed to accumulate, leading to the formation of a dense layer of volcanic particles around the planet. This abrupt increase was gauged to cause a decrease of about 5 °C in the temperature of the midlatitude tropospheric region above the Philippines and an overall average decrease in the global surface temperature of about –0.5 °C over the subsequent 2 years. A value of 2 years was therefore assumed to be a reliable estimate of the stratospheric relaxation time to background conditions (McCormick, Thomason, and Trepte, 1995). Volcanic stratospheric particles can persist for up to a few years since they are not efficiently removed by wet deposition, having very low fall speeds at those altitudes. Bearing in mind that only one strong volcanic eruption occurs every 10 years on average, it can be stated that stratospheric aerosol is only rarely in a totally unperturbed state by volcanic emissions.

Volcanic eruptions can have a strong impact on the stratospheric load of aerosol particles. The lifetime of coarse particles (dust and ash) directly injected into the stratosphere is relatively short (not longer than 1–2 months) due to the efficient removal of settling coarse particles. About 3 months of post-eruptive aging are needed for chemical and microphysical processes to form the stratospheric layer of sulfate particles, causing the sharp increase in volcanic aerosol mass and aerosol optical thickness shown in Figure 1.9 at the end of July 1991 (209th DOY). The analysis of satellite observations made by Thomason *et al.* (2008) estimated that (i) the average stratospheric $\tau_a(1.02\ \mu\text{m})$ was equal to 0.1 over the entire global scale (for latitudes from 80°N to 80°S) during the first 6 months of 1992 and (ii) a total time of ~ 4 years was needed to return to an average background value of $\tau_a(1.02\ \mu\text{m}) = 3 \times 10^{-3}$. An analysis of these observations indicated that the Pinatubo stratospheric particles produced a mean radiative cooling forcing of about $-4\ \text{W m}^{-2}$ over a global scale at the beginning of 1992, that is, about 6–8 months after the eruption. This average radiative forcing effect decayed exponentially over the subsequent years until reaching a value of around $-0.1\ \text{W m}^{-2}$ at the end of 1996.

The trend observed in the frequency of volcanic eruptions during the past 50 years has been estimated to have a major impact on the temperature conditions of the low stratosphere, because the sulfur emissions from volcanoes can produce a strong increase in the stratospheric load of aerosol particles. Considering that the volcanic aerosols efficiently reflect the shortwave solar radiation and absorb the longwave terrestrial radiation, the formation and growth of volcanic particles cause an increase in the planetary albedo, giving rise to important climatic effects: satellite measurements revealed a 1.4% increase in solar radiation reflected from the atmosphere toward space over a period of several months after the Mt Pinatubo eruption.

Such emissions occur mainly in the form of SO_2 , even though other sulfur species may be present in the volcanic plume, predominantly sulfate ions and H_2S , the latter being the second molecular species that is oxidized to SO_2 in about 10 days at stratospheric altitudes. Estimates of the emission of sulfur-containing species from quiescent degassing and eruptions vary on average from 7 to 14 Tg(S) per year. The historical record of SO_2 emissions by erupting volcanoes shows that over 100 Tg of SO_2 can be emitted in a single event, such as the Mt Tambora (Sumbawa, Indonesia) eruption in 1815, which presumably led to very strong transient cooling effects evaluated to range from -0.1 to at least $-0.3\ ^\circ\text{C}$. Estimates of the global annual flux Φ_e of sulfate volcanic aerosols formed in the stratosphere were recently made by Toohey *et al.* (2011), who determined a value of 17 Tg per year for the Mt Pinatubo eruption in June 1991. Therefore, considering also the years with only weak eruptions, a reasonable range from 2 to 17 Tg per year was assumed for the events occurring during the past 20 years, with an average value equal to about half the Mt Pinatubo value.

Within the stratospheric layers of sulfuric acid droplets, the concentration of Aitken nuclei is higher at the low stratospheric altitudes and generally decreases slowly with height. In contrast, particles with sizes ranging from about 0.2 to 4 μm

reach a maximum concentration of $\sim 0.1 \text{ cm}^{-3}$ at altitudes of around 17–20 km at midlatitudes. This part of the low stratosphere, where background layers of sulfate particles can persist over long periods, is called the “stratospheric sulfate layer” or also the “Junge layer,” to honor the memory of Christian Junge who discovered these thin aerosol layers in the late 1950s. As mentioned earlier, the most significant source of SO_2 in the stratosphere is given by the major volcanic eruptions, which inject SO_2 into the stratosphere. This molecule is then converted to H_2SO_4 , mainly through the reactions defined in Eqs. (1.15–1.17), in which SO_2 is oxidized to SO_3 and SO_3 is then combined with water to form sulfuric acid. As mentioned previously, the oxidation of SO_2 to form SO_3 may also occur through the reaction of Eq. (1.28) in the presence of an external molecule. Finally, H_2SO_4 vapor is then converted to liquid H_2SO_4 through the homogeneous heteromolecular nucleation and heterogeneous heteromolecular nucleation processes, among which the heterogeneous processes are evaluated to be more efficient at stratospheric levels.

The enhancement of the stratospheric sulfate layer originated from volcanic eruptions can cause depletions in stratospheric O_3 , due to the fact that H_2SO_4 droplets act to modify the distribution of catalytically active free radicals. For example, the eruption of Mount Pinatubo caused dramatic depletions in stratospheric ozone, which caused an indirect radiative forcing estimated to be equal to about -0.1 W m^{-2} and hence considerably smaller than the direct aerosol-induced radiative forcing. The observed stratospheric load of sulfate particles is estimated to be $\sim 0.14 \text{ Tg(S)}$ during volcanically quiet periods. Calculations with global climate models suggest that the radiative forcing of volcanic sulfate particles is only slightly smaller than that induced by anthropogenic sulfates suspended in the troposphere, even though the anthropogenic SO_2 source intensity is about five times greater. The main reason is that SO_2 is released from volcanoes at higher altitudes and therefore has a longer residence time than anthropogenic sulfates. Relatively dense stratospheric layers of sulfate aerosols were estimated to cause general cooling effects on the climate system. Theoretical studies have been developed on the possibility of artificial production of sulfate aerosols in the stratosphere with the aim of increasing the planetary albedo and hence slowing down the current global warming trends (Crutzen, 2006). The benefits and disadvantages of such efforts need to be carefully discussed before entering the field of artificial modifications of climate, but the idea first proposed by Budyko (1977) is itself very stimulating.

1.5

Primary Anthropogenic Aerosols

A significant fraction of tropospheric aerosol particles is anthropogenic and consists of both primary particles (mainly due to diesel exhaust and vehicular traffic dust) and secondary particles formed from the gases emitted by urban and industrial activities. Anthropogenic aerosol emissions arise primarily from the following four source categories: (i) fuel combustion, (ii) industrial processes, (iii) nonindustrial fugitive sources (roadway dust from paved and unpaved roads, wind

erosion of cropland, construction, etc.), and (iv) transportation activities with cars, ships, airplanes, and other vehicles. Therefore, anthropogenic aerosols contain sulfate, ammonium, nitrate, trace metals, carbonaceous material, and water. The carbonaceous fraction of this particulate matter consists of both EC and OC, the first emitted directly into the atmosphere from combustion processes and the second emitted directly or formed through atmospheric condensation of low-volatility organic gases.

Anthropogenic aerosols certainly contribute to the total tropospheric aerosol mass loading by more than 10%. The influence of this relatively small but increasing contribution on the climate system is not exactly known and needs to be assessed in future model studies and experiments. In their coupled aerosol and gas-phase chemistry transport model, Tsigaridis *et al.* (2006) used emission values relative to the year 1990 equal to (i) 73 Tg per year for anthropogenic SO₂, (ii) 45 Tg per year for NO_x, (iii) 44.1 Tg per year for NH₃, (iv) 1051.8 Tg per year for carbon monoxide, (v) 7.5 Tg per year for BC, (vi) 250.9 Tg per year for VOCs, (vii) 44.4 Tg per year for primary organic aerosols, (viii) 19.2 Tg per year for CH₂O, and (ix) 14.3 Tg per year for aromatic VOCs. These values are low in comparison with the annual emission flux values assumed by Tsigaridis *et al.* (2006) for natural dust (1704 Tg per year) and sea salt (7804 Tg per year) in their coupled model (see Table 1.1) but indicate that a considerable influence is exerted by humankind emissions on the current atmospheric composition. Use of biological materials by humans results in the emission of many chemical species into the atmosphere, such as (i) CO₂, CO, NO_x, N₂O, NH₃, SO₂, and hydrogen chloride (HCl) arising from the combustion of oil, gas, coal, and wood; (ii) hydrocarbons from vehicles, refineries, paints, and solvents; (iii) H₂S and DMS from paper mills and oil refineries; (iv) COS from natural gas; and (v) chloroform CHCl₃ from combustion of petroleum, bleaching of woods, and solvents. The change in trace gases can have negative effects on the stability of the climate system, favoring global warming, and nonreversible processes in the Earth–atmosphere system. Therefore, it is of basic importance to monitor the columnar contents of trace gases and the aerosol concentration along the vertical atmospheric path on a global scale using satellite measurements. Although the increased gaseous concentrations lead to stronger atmospheric absorption effects and, therefore, to a more pronounced warming of the atmosphere, it is worth considering that airborne aerosol load could increase or decrease the overall albedo of the Earth–atmosphere system, to an extent closely depending on the ground albedo. For the low albedo typical of ocean and dark vegetation in the visible, additional anthropogenic aerosols induce an increase in the planetary albedo and therefore favor a cooling of the atmosphere. Aerosols with a high soot content appear dark and hence reduce planetary albedo, especially in the polar regions presenting bright snow surfaces. Consequently, additional warming is expected to occur due to current efforts to clean polluted areas of the planet, because this could reduce the pollution load but increase the risks related to heat waves (Meehl and Tebaldi, 2004).

The global input of anthropogenic particles into the atmosphere is ~20% (by mass) of that from natural sources. For particles with diameters $a > 5 \mu\text{m}$, direct emissions from anthropogenic sources dominate over secondary aerosols, which mainly originate in the atmosphere through g-to-p conversion of anthropogenic gases. The opposite case applies to most small particles, for which g-to-p conversion is the largely prevailing source favoring the increase in the concentration of anthropogenic aerosols. About 35% of the number concentration of atmospheric aerosols is estimated to be given by sulfates formed through oxidation of SO_2 . The worldwide direct emission into the atmosphere of primary anthropogenic particles with sizes smaller than $10 \mu\text{m}$ was estimated to be ~350 Tg per year (Jaenicke, 1988), excluding the secondary particles formed through g-to-p conversion. On the basis of these remarks, the primary anthropogenic aerosols can be subdivided into the three following classes: (i) industrial dust, (ii) particles from fossil fuel combustion that include an important fraction of carbonaceous (soot) aerosols, and (iii) particles from waste and biomass burning.

1.5.1

Industrial Dust

The main anthropogenic sources of industrial dust are given by (i) transportation vehicular traffic and dust from roads, (ii) coal and fuel combustion in industrial processes, (iii) cement manufacturing, (iv) metallurgy, and (v) waste incineration. Wind erosion of tilled land can contribute to yield supplementary amounts of dust. In fact, three broad categories account in general for nearly all of the potential fugitive emissions including mineral dust and food agricultural products. Primary metals are also included in the first category and have a considerable impact considerably on environmental quality. Industrial dust has been widely monitored and regulated in developed countries, verifying that such an impact of fugitive dust emissions is relatively limited because they consist mostly of giant particles, which settle a short distance from the source. Fugitive dust sources are most efficient in rural areas. Relatively low nonindustrial fugitive dust emissions are caused by traffic entrainment of dust from paved and unpaved roads, agricultural activities, building construction, and fires.

During the twentieth century, the emission of particles from anthropogenic sources into the atmosphere was a small fraction of the overall particulate mass emitted from natural sources. Currently, the aforementioned aerosol sources are responsible for the most conspicuous impact of anthropogenic aerosols on environmental quality and were monitored and regulated over the past 20 years in North America and Europe. The result was that the emission of industrial dust aerosols has decreased significantly in these areas during the past two decades, obtaining a general improvement of air quality. On the other hand, the anthropogenic emission of aerosols has considerably increased over the past 50 years in world areas where industrialization has grown without stringent emission controls, especially in Asia. It is estimated that such a growth in industrialization could lead to a considerable increase in the industrial dust emission flux until

reaching values of particulate mass global emission flux higher than 300 Tg per year by 2040 (Wolf and Hidy, 1997) with respect to evaluations of industrial dust emission estimated in the 1990s to vary from about 100 Tg per year excluding carbonaceous matter (Kiehl and Rodhe, 1995) to 200 Tg per year (Wolf and Hidy, 1997), as also shown in Table 1.5. The previous limitations are probably not of crucial importance for the current climatic conditions, considering the source strength of these emissions and the fact that many industrial dust particles have sizes $<1\ \mu\text{m}$ and hence can cause only relatively weak extinction effects on the incoming solar radiation.

1.5.2

Anthropogenic Aerosols from Fossil Fuel Combustion and Carbonaceous (Soot) Particles

Particulate matter emissions worldwide have been dominated by fossil fuel combustion (primarily coal) and biomass burning. These emissions are projected to double by the year 2040, largely due to anticipated increases in fossil fuel combustion, which are predicted to occur mainly in China and India. The combustion of all carbon-containing particles leads to the formation of EC particles, partially combusted fuel components, and products of the high-temperature reactions in the flame. These primary EC particles are very small (mostly with sizes smaller than $2\ \mu\text{m}$), but they rapidly aggregate through coagulation, starting already in the flame. In the case of solid fuels, there are several pathways leading to a variety of particle sizes, shapes, and composition. To give an idea of the variety of physicochemical processes taking place during the combustion of pulverized coal, a schematic representation of the pathways of particle formation during the combustion of a pulverized coal particle of $70\ \mu\text{m}$ size is shown in Figure 1.10 (Okazaki, 1993).

It can be seen that the particle may be subject to two initial pathways of swelling or shrinking: (a) in the first case, the particle breaks into various fragments after swelling, forming a large number of particles with sizes ranging mainly from 0.5 to $30\ \mu\text{m}$; and (b) in the second case, the shrinking of the particle leads to (i) vaporization and condensation, until surface enrichment of very small particles is obtained; (ii) vaporization followed by nucleation and coalescence (and also coagulation, after Heintzenberg (1994)), to form a large number of particles with sizes ranging from 0.02 to $0.2\ \mu\text{m}$; (iii) direct agglomeration and coagulation, producing particles that may grow up to $30\ \mu\text{m}$ sizes; (iv) expansion and quenching, yielding particles of 10 – $90\ \mu\text{m}$ sizes; and (v) expansion and disintegration, generating particles with sizes $a < 30\ \mu\text{m}$. The high-temperature fragmentation of burning coal and other solid fuels is a special case of the b-to-p conversion process. Supersaturated vapors are formed in all combustion processes described earlier. Therefore, the g-to-p conversion processes are also expected to occur during combustion.

Some SEM images of industrial aerosol particles formed through fossil fuel combustion (oil, coal, and distilled oil) are shown in Figure 1.11, presenting nearly spherical shapes. These images present a characterization of combustion particles

Table 1.5 Estimates of the annual emission fluxes of anthropogenic aerosols on a global scale from various sources and their precursors, as found in the literature of the past two decades.

Anthropogenic direct emission fluxes	Estimates (in teragram per year, being $1 \text{ Tg yr}^{-1} = 10^6 \text{ ton yr}^{-1}$) and references
Sulfates from industrial activities and fossil fuel combustion	75 (Hobbs, 2000)
Anthropogenic sulfates (as NH_4HSO_4)	122 (IPCC, 2001)
Secondary sulfates from SO_2	48.6 (in Tg(S) yr^{-1}) (Liao <i>et al.</i> , 2003)
Anthropogenic SO_2	73.0 (Tsigaridis <i>et al.</i> , 2006)
Nitrates from N_2O (fossil fuel combustion and industrial activities)	10 (Hobbs, 2000)
Nitrates from NO_x (fertilizers and fossil fuel combustion)	26 (Hobbs, 2000), 45 (Tsigaridis <i>et al.</i> , 2006)
Nitrates from NH_3 (fertilizers and agricultural activities)	12 (Hobbs, 2000)
Nitrates from NH_3 (breeding activities)	23 (Hobbs, 2000)
Anthropogenic nitrates (as NO_3^- ions)	14.2 (IPCC, 2001)
Secondary nitrates from NO_x (NO_3^- ions only)	21.3 (Liao <i>et al.</i> , 2004)
Secondary nitrates from NH_3	44.1 (Tsigaridis <i>et al.</i> , 2006)
Carbonaceous aerosols from biomass burning (sizes $< 2 \mu\text{m}$)	54 (IPCC, 2001)
Carbonaceous aerosols from fossil fuel (sizes $< 2 \mu\text{m}$)	28.4 (IPCC, 2001)
Fossil fuel organic matter (sizes $< 2 \mu\text{m}$)	6.60 (IPCC, 2001)
Biomass burning black carbon (sizes $< 2 \mu\text{m}$)	5.7 (IPCC, 2001)
Anthropogenic organic compounds	0.6 (IPCC, 2001)
Carbonaceous aerosols from aircraft	0.006 (IPCC, 2001)
Industrial dust, etc. (sizes $> 1 \mu\text{m}$)	100 (IPCC, 2001)
Industrial dust	40–130 (Andreae and Rosenfeld, 2008)
Biomass burning black carbon (sizes $< 2 \mu\text{m}$)	5.6 (IPCC, 2001)
Black carbon	7.5 (Tsigaridis <i>et al.</i> , 2006)
Black carbon (soot)	Ranging from 8 to 14 Tg yr^{-1} (Andreae and Rosenfeld, 2008)
Subtotal (anthropogenic)	440 (IPCC, 2001)
Total (natural + anthropogenic)	6315 (IPCC, 2001)

sampled in the Po Valley (Italy) area, as emitted by an oil fuel-fired power plant (Bacci *et al.*, 1983), a coal-fueled power plant (Del Monte and Sabbioni, 1984), and a domestic heating unit fueled by distilled oil (Sabbioni and Zappia, 1992). An analysis of these samples indicated that (a) oil-fired aerosol particles have spherical shapes presenting a porous surface, internal cavities, and a spongy structure,

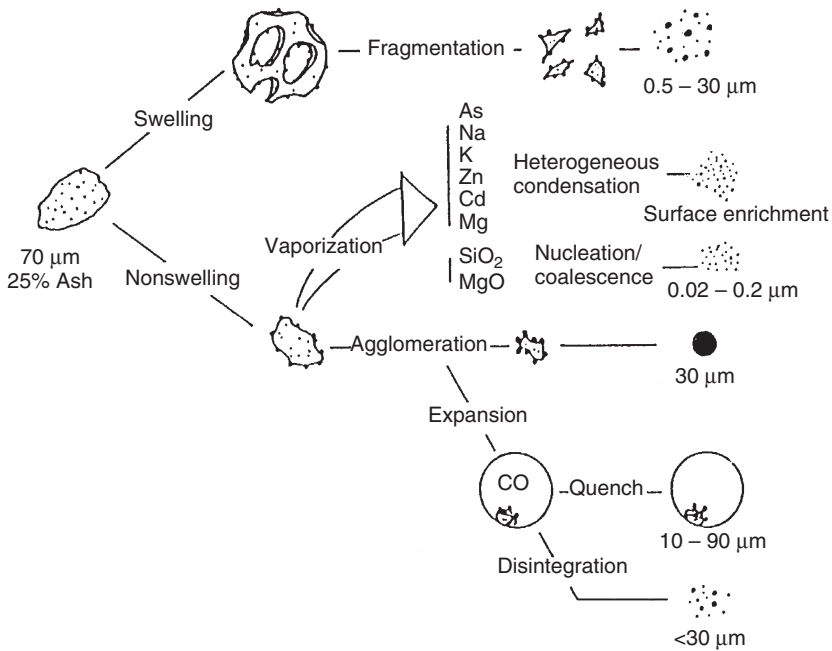


Figure 1.10 Pathways of particle formation during the combustion of pulverized coal through different combinations of swelling, shrinking, fragmentation, vaporization,

condensation, nucleation, coagulation, expansion, quenching, and disintegration processes. (Adapted from a graph of Okazaki (1993).)

as can be seen in Figure 1.11a and b, which often contain sodium and vanadium oxide hydrate crystals having prismatic shapes and presenting relatively high elemental concentrations for all size classes over the 0.01–50 μm range (mainly with traces of Na, Al, Mg, S, K, V, Fe, Ni, Cu, Zn, and Pb elements); (b) fly ash particles emitted by a coal-fired power plant, such as that shown in Figure 1.11c, which may include different components of particulate matter, such as (i) glassy aluminosilicates of variable composition, (ii) spongy carbonaceous matter, (iii) spherical metallic particles containing different iron oxide phases (magnetite, hematite, maghemite), (iv) spherical rutile particles, (v) spherical lime particles, and (vi) mineral formless particles, containing mainly quartz and mullite; and (c) particles generated by domestic heating units fueled by distilled oil exhibit different morphological typologies (irregular, rounded to spherical, spherical with circular pores, smooth spherical particles, and spherical agglomerated particles, as presented in the example of Figure 1.11d); they often host crystals with different structural shapes, such as “rosettes” composed of twinned crystals with hexagonal habit or elongated crystals, in which the elemental composition is mainly given by S, Fe, Pb, Ti, V, Mn, Cu, Zn, Cd, Ni, Co, Ca, Si, and Cr.

Figure 1.11 clearly indicates that these soot particles change appreciably in shape passing from fractal-like fresh diesel soot particles to more compact aggregates of spherical shape soot particles. Schnaiter *et al.* (2005) pointed out that

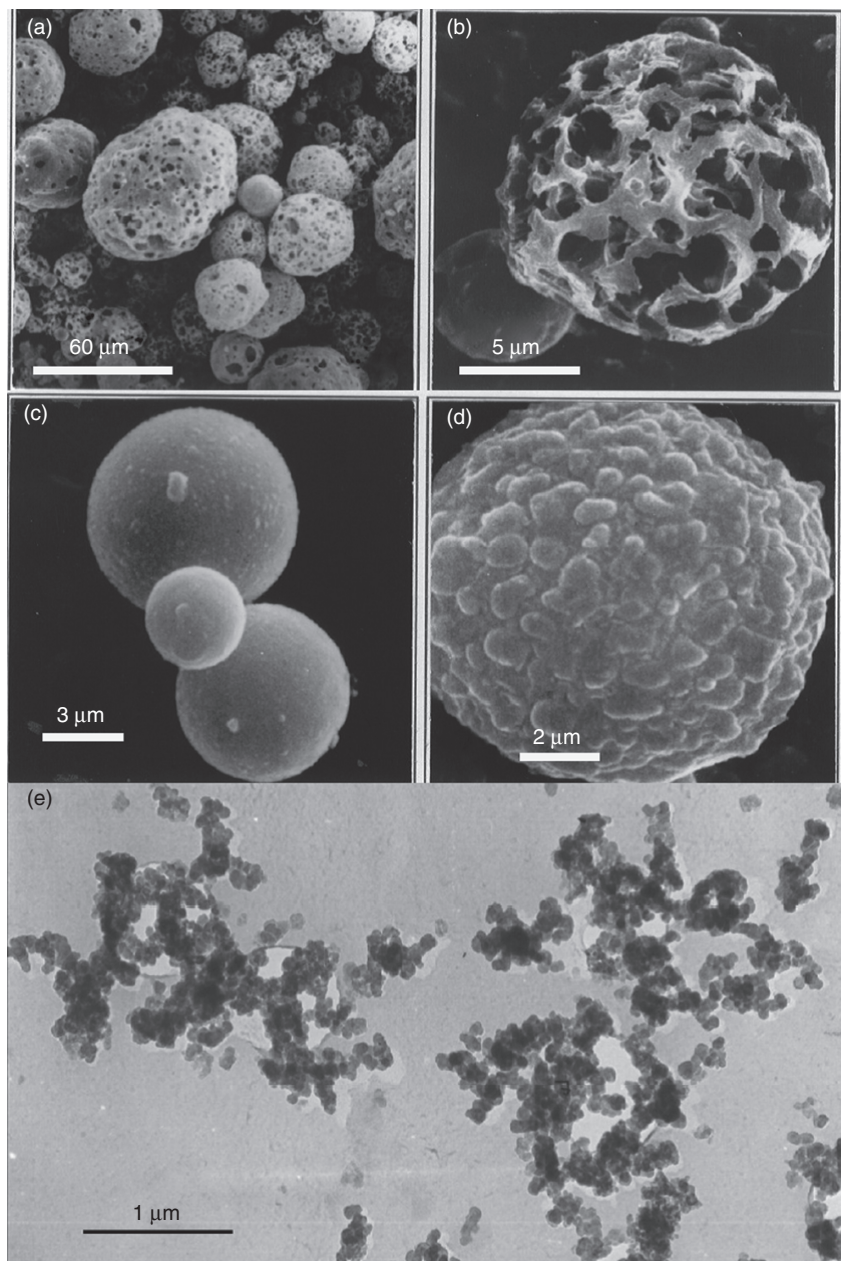


Figure 1.11 SEM images of industrial aerosol particles: (a, b) particles formed from fuel oil combustion, (c) soot particles from coal combustion, (d) particle from distilled oil fuel combustion, and (e) atmospheric diesel soot particles. ((a)–(d) Reproduced with

permission and courtesy of Cristina Sabbioni, ISAC-CNR Institute, Bologna, Italy. (e) Reproduced with permission and courtesy of Annie Gaudichet (LISA, Paris, France) and H el ene Cachier.)

particle growth after the initial aggregate restructuring was reflected by a clear decrease in Ångström's (1964) exponent and in the hemispheric backscattering ratio measured in the laboratory, in accordance with the Mie (1908) theory. Considering that these combustion particles exhibit nearly spherical shapes in most cases, it seems not difficult to calculate the radiative effects induced by these particles applying the Mie (1908) theory directly to spherical particle polydispersions, provided that realistic values of the real and imaginary parts of complex refractive index are known. On this matter, the most reliable estimates available in the literature indicate that the real part of the refractive index for soot particles is equal to 1.74 at 0.30 μm wavelength, 1.75 at wavelengths increasing from 0.40 to 1.06 μm and slowly increasing at the longer wavelengths, assuming values equal to 1.76 at 1.30 μm and 1.83 at 2.5 μm . Correspondingly, the imaginary part was estimated to assume values decreasing from 0.47 at 0.30 μm to 0.43 at 0.694 and 0.860 μm wavelengths and then increasing from 0.44 at 1.06 μm to 0.51 at 2.50 μm .

The problem of BC influence on the planetary radiative budget (in terms of solar radiation absorption by aerosols and subsequent direct aerosol-induced radiative forcing effects) is a hot topic in modern research. In particular, aerosols transported from highly polluted areas in Europe toward the Arctic can lead to a decrease in the planetary albedo over areas where these soot aerosols are deposited, rendering the snow and ice surfaces dirtier and more polluted. These changes in the surface albedo lead to variations in the local radiation budget that can be associated with a more intense absorption of solar radiation due to such absorbing aerosol particles (Hansen and Nazarenko, 2004). Among the atmospheric aerosols of natural and anthropogenic origin, those emitted by combustion sources such as industrial plants, heating units, and vehicular traffic can cause major damage to buildings, bridges, monuments, and other human constructions through deposition on surfaces and the subsequent formation of substances, most commonly gypsum (calcium sulfate dihydrate), calcite (calcium carbonate), and noncarbonated carbon (Sabbioni, 1992).

As mentioned before, the carbonaceous fraction of ambient particulate matter consists of EC and various organic compounds (mainly OC): (i) EC is also often called BC and has a chemical structure similar to impure graphite, being emitted directly into the atmosphere during combustion processes, and (ii) OC can be emitted directly by primary sources or formed *in situ* by condensation of low-volatility products formed through photooxidation of hydrocarbons (secondary OC). It refers to only a part of the organic material mass, the rest being given by hydrogen, oxygen, nitrogen, and so on. Additional small quantities of particulate carbon may exist either as carbonates (e.g., CaCO_3) or CO_2 adsorbed onto particulate matter such as soot. Therefore, atmospheric carbonaceous particles consist of two major components, that is, BC (which is the most abundant light-absorbing aerosol species in the atmosphere and sometimes referred to as EC or free carbon) and OM. EC can be produced only in combustion processes and is therefore solely primary. Organic particulate matter is a complex mixture of many classes of compounds either directly emitted from sources or produced through atmospheric

reactions involving gaseous organic precursors. A major reason for the study of OM is the possibility that such compounds pose a health hazard. Specifically, certain fractions of particulate OM, especially those containing polycyclic aromatic hydrocarbons (PAHs), were found to be carcinogenic in animals and mutagenic in *in vitro* bioassays.

Carbonaceous compounds make up a large but highly variable fraction of atmospheric aerosols. Organics are the largest single component of biomass burning aerosols, which can contribute to light scattering at least as much as the sulfate component. They are also important constituents of aerosols suspended in the upper troposphere. The presence of polar functional groups, particularly carboxylic and dicarboxylic acids, makes many of the organic compounds in aerosols water soluble and allows them to play a role in cloud droplet nucleation, acting as efficient cloud nuclei and hence having a major indirect effect on climate. Carbonaceous particles are produced by the combustion of liquid or gaseous fuels and consist of both EC and OC, presenting a wide variety of shapes assumed by soot, fly ash, and OC particles of anthropogenic (industrial and urban) origins. Various SEM and TEM images of such complex particle shapes are available in the literature. Pósfai *et al.* (1999) showed some TEM images of particles collected in the boundary layer of the North Atlantic Ocean (Azores islands), in which ammonium sulfate particles include small soot particles and fly ash spheres, and some TEM images of a typical chain-like soot aggregate, in which a carbon film connects individual small spherules within the aggregate and fly ash spheres consisting of amorphous silica, having sizes of 1–2 μm , clearly indicating that soot particles are mainly agglomerates of small nearly spherical carbonaceous particles forming typical chains. Other TEM and SEM images were shown by Li, Anderson, and Buseck (2003a) during the ACE-2 conducted at Sagres in southern Portugal, in which soot particles aggregated to form particles of different composition, such as silica or sea salt: (i) a TEM image showing, for instance, a typical chain-like soot aggregate of soot spheres having sizes of more than 10 μm , (ii) a SEM image showing a soot aggregate mixed with sea-salt crystals, (iii) a high-resolution TEM image showing an example of typical discontinuous onion-like structure of graphitic particle layers, and (iv) a TEM image illustrating an aggregate of rounded amorphous carbonaceous particles, sampled at Sagres, providing evidence under high magnification that these carbonaceous particles sometimes do not show the graphitic layers characterizing soot particles. Some SEM images of OC and fly ash particles sampled in the urban area of Mainz (Germany) have been also shown by Sinha *et al.* (2008), such organic aerosols being mainly formed during *in cloud* processes.

On the basis of the previous analyses, it can be stated that the industrial and urban aerosols are in general agglomerates of small roughly spherical elementary carbonaceous particles, in which the size and morphology of the clusters may vary widely. The small spherical elementary particles are remarkably consistent from one to another and have sizes ranging from 20 to 30 nm. They can cluster with each other, forming straight or branched chains, which can then agglomerate to

form soot particles having sizes up to a few micrometers. Soot formed in combustion processes is not a unique substance, since it consists mainly of carbon atoms but also contains up to 10% moles of hydrogen as well as traces of other elements. The composition of a soot particle aged at the high temperatures of a flame is typically C_3H (Flagan and Seinfeld, 1988). Soot particles usually contain more hydrogen earlier in the flame. Subsequently, they absorb organic vapors when the combustion products cool down and frequently accumulate significant mass fractions of organic compounds. Thus, soot substances consist in general of a mixture of EC, OC, and other elements such as oxygen, nitrogen, and hydrogen incorporated in its graphitic structure (Chang, Brodzinsky, and Gundel, 1982). The EC found in atmospheric particles is not usually present in the large-size particles of highly structured pure graphite but tends to form three-dimensional arrays of carbon with small fractions of other elements, containing a high number of crystallites having sizes of 2–3 nm, all consisting of several carbon layers presenting the hexagonal structure of graphite. Therefore, the density of these soot particles is around 2 g cm^{-3} .

Soot forms in a flame as the result of a sequence of events starting with the oxidation and/or pyrolysis of the fuel into small molecules, such as those of acetylene, C_2H_2 , and PAHs, which are considered the main molecular intermediates for soot formation and growth (McKinnon and Howard, 1990). These particles grow through the initial formation of soot nuclei and the subsequent rapid effects of surface reactions (Harris and Weiner, 1983a,b). However, the soot nuclei represent only a small fraction of the overall soot mass produced. The formation of soot particles depends strongly on the fuel composition, because the rank ordering of the sooting tendency of fuel components is naphthalenes \rightarrow benzenes \rightarrow aliphatics, and the order of sooting tendencies of the aliphatics (alkanes, alkenes, alkynes) varies dramatically depending on the flame type (Flagan and Seinfeld, 1988), and soot formation depending critically on the carbon–oxygen ratio in the hydrocarbon–air mixture (Wagner, 1981).

The typical layered structure of soot spherules can be successfully investigated using the HRTEM techniques for identifying the soot components in complex internally mixed particles, as evidenced by Pósfai *et al.* (1999), since the nanostructural features of primary soot spherules reflect their distinct sources (from oil boilers, jet aircraft, and diesel engines) (Hays and Vander Wal, 2007). In addition, the fractal properties of soot aggregates are influenced by fuel type and combustion conditions, this allowing a source apportionment in some cases from the structure variations and fractal parameters of atmospheric soot (Wentzel *et al.*, 2003; van Poppel *et al.*, 2005).

Together with wood burning fires, diesel vehicles are effective sources of EC, estimated to emit particulate matter consisting of more than 90% submicron particles, generally distributed within a mode centered at diameter $a_c \approx 0.1 \mu\text{m}$. EC mass concentration usually varies from 0.2 to $2.0 \mu\text{g m}^{-3}$ in rural and remote areas and from 1.5 to $20 \mu\text{g m}^{-3}$ in urban areas, where values often higher than $10 \mu\text{g m}^{-3}$ can be found in the PM_{10} samples. Conversely, EC concentration is very low over the remote oceans, where values ranging mainly from 5 to 20 ng m^{-3} are

usually measured, and assumes values not exceeding a few nanograms per cubic meter in the coastal areas of Antarctica (Wolff and Cachier, 1998). The organic component of ambient particles in both polluted and remote areas is a complex mixture of hundreds of organic compounds (including *n*-alkanes, *n*-alkanoic acids, *n*-alkanals, aliphatic dicarboxylic acids, diterpenoid acids and retene, aromatic polycarboxylic acids, PAHs, polycyclic aromatic ketones and quinones, steroids, N-containing compounds, regular steranes, pentacyclic triterpanes, and iso- and anteiso-alkanes), as pointed out by Seinfeld and Pandis (1998, 2006). Most studies have assumed in the past decades that OC concentration was simply given by the concentration of carbon measured in microgram(C) per cubic meter, therefore without including the contribution to the aerosol mass of the other elements, namely, oxygen, hydrogen, and nitrogen, present in the organic aerosol compounds. It was suggested in the early 1990s that measured OC values should therefore be multiplied by a factor of 1.5 to calculate the total organic mass associated with OC, while alternative values of such a conversion factor varying between 1.2 and 2.0 were proposed in the literature. The mass size distributions of OC particles sampled in urban polluted areas usually present bimodal features, with the first mode centered at an aerodynamic diameter of around 0.1 μm and the second mode centered over the 0.5–1 μm aerodynamic diameter range. In remote marine areas, the ambient aerosol OC concentration was found to vary from 0.1 $\mu\text{g m}^{-3}$ (in the Samoa archipelago and New Zealand) to 0.8 $\mu\text{g m}^{-3}$ (Enewetak Atoll in the Pacific Ocean). Primary carbonaceous particles are produced by combustion (pyrogenic), chemical (commercial products), geologic (fossil fuel), and natural (biogenic) sources. Annual global primary OC emissions were estimated to vary from 15 to 80 Tg per year, with open burning contributions around 75% of the total, while fossil fuel combustion was estimated to provide a partial contribution of about 7%. Several hundred organic compounds have been identified in primary organic aerosol emissions, due to a variety of sources: the major constituents of the resolved urban aerosol mass are normal alkanolic acids (with annual average concentrations of 0.25–0.30 $\mu\text{g m}^{-3}$), aliphatic dicarboxylic acids (0.20–0.30 $\mu\text{g m}^{-3}$), and aromatic polycarboxylic acids ($\sim 0.10 \mu\text{g m}^{-3}$).

1.5.3

Anthropogenic Aerosols from Waste and Biomass Burning

Although the controlled technological burning of fossil fuels emits almost pure soot, a much greater variety of carbonaceous particles results from biofuel, agricultural, and uncontrolled biomass fires (Reid *et al.*, 2005). Biomass burning produces atmospheric particles in amounts and concentrations that can affect both the regional and global climate (Forster *et al.*, 2007). In the past 10 years, individual particle TEM studies have greatly improved our knowledge of particle formation from biomass fires and revealed that agricultural fires severely affect atmospheric composition and air quality, even in developed regions such as Europe (Niemi *et al.*, 2006) and North America (Hudson *et al.*, 2004). In addition to soot particles, the major types of particulate matter generated by waste and biomass burning

include organic particles, many of which also contain inorganic salt inclusions (Martins *et al.*, 1998; Li *et al.*, 2003b) and the so-called tar balls (Pósfai *et al.*, 2004), which are spherical and have sizes greater than individual soot spherules. They not only consist mainly of carbon and oxygen but sometimes also contain nitrogen and traces of sulfur, silicate, and other elements. The distribution of carbon is homogeneous, and oxygen is enriched in the ~ 30 nm outer layer of the spherules (Hand *et al.*, 2005) where the organic compositions resemble those of atmospheric humic-like substances (Tivanski *et al.*, 2007).

The intentional burning of biomass is the major source of combustion products suspended in the atmosphere. Most of these burning episodes take place in the tropics where emissions from burning vegetation arise from any uncontrolled combustion process and include both EC and OM, besides CO_2 , CO, NO_x , CH_4 , and NMHCs. The quantity and type of emissions from an intentional biomass fire depend not only on the type of vegetation but also on its moisture content, ambient temperature, RH conditions, and local wind speed. Other sources of biomass burning aerosols are the human-induced burning, such as wood or agricultural wastes, which together with intentional forest fires are estimated to produce about 40% of carbonaceous particulate matter emissions over a global scale. The overall annual emissions from fossil fuel and biomass burning are gauged to be 10–30 Tg per year and 45–80 Tg per year, respectively (IPCC, 2001). Combustion processes constitute the dominant source of BC, which contribute to emit the prevailing particulate mass fraction in the submicron size fraction and furnish an overall annual emission of 12–17 Tg per year (with an average value of 14 Tg per year on the global scale), of which 6–9 Tg per year is mainly from intentional biomass burning and 6–8 Tg per year from fossil fuel combustion (IPCC, 2001).

1.6

Secondary Anthropogenic Aerosols

Secondary liquid particles are usually quite small and exhibit shapes that can be correctly approximated by spheres in radiative transfer calculations. However, many anthropogenic aerosols show irregular shapes, since they originate and grow through two basic processes which both regulate the mass transfer from the gas phase to the particulate phase (g-to-p conversion) where (i) preexisting particles may grow through material condensation from the gas phase and (ii) new particles may form through homogeneous nucleation. In these g-to-p conversion processes, three major families of chemical species are involved, containing sulfur or nitrogen or organic and carbonaceous substances. The most important role in these processes is played by the following two reactions:



forming molecules of sulfuric acid and nitric acid, respectively. The subsequent conversion of the H_2SO_4 vapor to liquid H_2SO_4 occurs through the following mechanisms, already considered in Section 1.4.4 to describe the formation of volcanic sulfuric acid droplets in the stratosphere: (i) the combination of H_2SO_4 and H_2O molecules in *homogeneous bimolecular nucleation* processes and/or the combination of H_2SO_4 , H_2O , and HNO_3 in *homogeneous heteromolecular nucleation* processes to form new primarily sulfuric acid droplets and (ii) the vapor condensation of H_2SO_4 , H_2O , and HNO_3 onto the surfaces of preexisting particles with sizes no greater than $0.3\ \mu\text{m}$ in *heterogeneous heteromolecular nucleation* processes. These *in situ* chemical reactions are classified as *homogeneous* or *heterogeneous* according to the following concepts: (i) a homogeneous reaction involves reactants that are all in the same phase, and (ii) a heterogeneous reaction involves reactants that are in two or more phases, such as that occurring in a mixing of an inorganic aerosol (like sulfuric acid or nitric acid) with organic compounds (like aldehydes).

The formation of SOA particles is in part due to the VOCs emitted from anthropogenic sources and in part to sulfur- and nitrogen-containing gases. The nucleation of nanometer-sized sulfate particles has been observed in rural, urban, and coastal environments (Kulmala *et al.*, 2004), probably enhanced by the presence of aromatic acids (Zhang *et al.*, 2004). This suggests that organics are already present in the nucleation of small sulfate particles. In particular, SOA/sulfate mixed particles were formed through a further condensation of organics onto freshly nucleated particles (Adachi and Buseck, 2008; Smith *et al.*, 2008). In general, SOA particles are amorphous and composed of light elements, so that it is very difficult to study their structural characteristics using the TEM and SEM techniques and adopting the related methodologies (Pósfai and Buseck, 2010).

Secondary anthropogenic aerosols are transported by the airflows they encounter during their life in the atmosphere, until covering the global scale. In fact, aerosols formed through g-to-p conversion processes can be transported over long distances, since the time required for g-to-p conversion and the relatively small sizes of the particles formed during such a process lead to long atmospheric residence times for such aerosols. This is, for instance, the case of acidic aerosols such as sulfates and nitrates, which contribute to the so-called acid rains: it was found in the 1980s that SO_2 emitted from power plants in the United Kingdom were most intensely deposited as sulfate particles far inland in continental Europe.

1.6.1

Secondary Particles from SO_2

About 35% of the number density concentration of airborne aerosols consists of sulfates forming through oxidation of anthropogenic SO_2 emissions, in large part originated from fossil fuel combustion (primarily coal and oil). Therefore, these emissions can lead to dramatic pollution effects in urban areas where the consumption of coal and oil is very strong, causing high local concentrations of

aerosols that are commonly termed “smog.” The term *smog* derives from *smoke* and *fog* and was originally coined to refer to heavily polluted air that can form in cities (generally in winter under calm, stable, and moist conditions of air) due to emissions of SO_2 and aerosols from fossil fuel burning. The term is now applied to all forms of severe air pollution, particularly to those occurring in urban areas and causing a strong reduction of visibility.

Prior to the introduction of air pollution abatement laws in the latter part of the twentieth century, many of the most populated cities in Europe and North America regularly suffered from severe and frequent smog episodes. The London event was notorious and known as *London smog*: in the presence of smog, where particles swelled in size under high air RH conditions and acted in part as condensation nuclei on which fog droplets formed. In these cases, sulfur dioxide gas dissolves in the fog droplets, in which it is oxidized to form sulfuric acid. After the London smog episode, laws were passed in the United Kingdom and elsewhere banning the use of coal in open fires for domestic heating and the emission of black smoke and requiring industries to switch to cleaner burning fuels. Nevertheless, pollution is still a serious problem in some cities in Europe and in the United States as well as in many large cities of developing countries (China, India) due to the burning of coal and wood and the lack of strict air pollution controls.

Sulfuric acid is important in aerosol formation for humid air conditions, as emphasized in a number of studies (Kiang *et al.*, 1973; Mirabel and Katz, 1974; Kulmala and Laaksonen, 1990). The efficiency of this process can be first studied considering the simplified binary *sulfuric acid–water system* before discussing more complicated atmospheric aerosol systems. Sulfuric acid is very hygroscopic and absorbs significant amounts of water even at extremely low values of air RH. If RH exceeds 50%, the H_2SO_4 concentration in solution will be lower than 40% by mass, and the H_2SO_4 mole fraction smaller than 0.1. For a temperature of 20 °C, this corresponds to equilibrium vapor pressures lower than 10–12 mm Hg. Under all conditions, the concentration of H_2SO_4 in the gas phase is much less than the aerosol sulfate concentration. For particles having sizes $<0.1 \mu\text{m}$, the H_2SO_4 mole fraction in the droplet is highly dependent on particle size. Thus, for each fixed small droplet size, the water concentration increases as RH increases.

The reaction



can often be neglected in atmospheric aerosol calculations in all cases where the vapor pressure of $\text{H}_2\text{SO}_4(\text{g})$ is practically null over atmospheric particles. The whole system is therefore described by the bisulfate dissociation reaction



with an equilibrium constant at 298 K. Since the molar ratio of HSO_4^- to SO_4^{2-} is proportional to the hydrogen ion concentration, it is expected that HSO_4^- ions will be present in acidic particles.

In the *sulfuric acid–ammonia–water system*, aerosol composition depends mainly on air temperature, air RH, and concentrations of ammonia and sulfuric

acid. However, a series of compounds may exist in the aerosol phase, including both solids (like letovicite $((\text{NH}_4)_3\text{H}(\text{SO}_4)_2)$, $(\text{NH}_4)_2\text{SO}_4$, and NH_4HSO_4) and aqueous solutions of NH_4^+ , SO_4^{2-} , HSO_4^- , and NH_3 (aq.). For environments in which NH_3 is poorly available, sulfuric acid exists in the aerosol phase in the form of H_2SO_4 . As the NH_3 availability increases, H_2SO_4 is converted to HSO_4^- and its salts and finally, if there is an abundance of NH_3 , to SO_4^{2-} and its salts. For total (gas and aerosol) ammonia concentrations lower than $0.8 \mu\text{g m}^{-3}$, the aerosol phase consists mainly of H_2SO_4 (aq.), while some molecules of NH_4HSO_4 (s) are also present. A significant amount of water accompanies the H_2SO_4 (aq.) even for low RH conditions. This regime is characterized by an ammonia/sulfuric acid molar ratio lower than ~ 0.5 . For higher values of this ratio, the following aerosol composition features are found: (i) when the ammonia/sulfuric acid molar ratio varies from 0.5 to 1.25, NH_4HSO_4 (s) is the dominant aerosol component for this system; (ii) when the ratio reaches unity (for ammonia concentration equal to $1.8 \mu\text{g m}^{-3}$), the salt $(\text{NH}_4)_3\text{H}(\text{SO}_4)_2$ (s) (letovicite) is formed in the aerosol phase, gradually replacing NH_4HSO_4 (s); (iii) for a molar ratio of 1.25, $(\text{NH}_4)_3\text{H}(\text{SO}_4)_2$ (s) is the dominant aerosol component, and for a value equal to 1.5 the aerosol phase consists almost exclusively of letovicite; (iv) for even higher ammonia concentrations, $(\text{NH}_4)_2\text{SO}_4$ starts to form; (v) for an ammonia concentration equal to $3.6 \mu\text{g m}^{-3}$ (molar ratio 2), the aerosol consists of only $(\text{NH}_4)_2\text{SO}_4$ in the solid state; (vi) when the total ammonia concentration is lower than $3.6 \mu\text{g m}^{-3}$, aerosol almost completely exists in the form of sulfate salts; and (vii) further increases in the available ammonia do not change the aerosol composition, but the excess ammonia remains in the gas phase as NH_3 (g).

It is expected that an increased availability of NH_3 would result in a monotonic increase in the total aerosol mass. This is not the case observed for ammonia-poor environmental conditions, that is, for ammonia/sulfuric acid molar ratio lower than unit. An increase in NH_3 concentration results in a reduction of the H_2SO_4 (aq.) and water. The overall aerosol mass decreases mainly because of the water loss, reaching a minimum for an ammonia concentration of $1.8 \mu\text{g m}^{-3}$. A further increase in the ammonia concentration leads to a corresponding increase in the overall aerosol mass.

At the 298 K temperature, the deliquescence RH values for the NH_4HSO_4 and $(\text{NH}_4)_3\text{H}(\text{SO}_4)_2$ salts are 40% and 69%, respectively. A system characterized by higher RH (equal to 75%, for instance) is that the aerosol consists of a liquid solution of H_2SO_4 , HSO_4^- , SO_4^{2-} , and NH_4^+ over the usual ammonia concentration range in which the formation of these salts is favored. It is important to bear in mind that (i) H_2SO_4 dominates for ammonia/sulfuric acid molar ratios lower than 0.5, (ii) HSO_4^- is the main aerosol component for values of the above ratio ranging from 0.5 to 1.5, and (iii) sulfate is formed for higher ammonia concentrations. When there is enough ammonia to completely neutralize the available sulfate forming $(\text{NH}_4)_2\text{SO}_4$, the liquid aerosol loses its water content and becomes solid. The deliquescence RH for $(\text{NH}_4)_2\text{SO}_4$ is equal to 80% at this temperature. Therefore, assuming it is on the deliquescence branch of the hysteresis curve, the

aerosol will exist as solid matter only. These changes in the particulate chemical composition and the accompanying phase transformation significantly modify the hygroscopic characteristics of aerosol particles, resulting in a monotonic decrease of their water mass. The net result is a significant reduction of the overall aerosol mass with increasing ammonia for this system and an abrupt change accompanying the phase transition from liquid to solid. Summarizing, in very acidic atmospheres (i.e., for $\text{NH}_3/\text{H}_2\text{SO}_4$ molar ratios lower than 0.5), aerosol particles exist primarily as H_2SO_4 solutions, while in acidic atmospheres (in which the $\text{NH}_3/\text{H}_2\text{SO}_4$ molar ratio ranges from 0.5 to 1.5), the particles consist mainly of bisulfate. If there is a sufficient ammonia concentration to neutralize the available sulfuric acid, $(\text{NH}_4)_2\text{SO}_4$ or NH_4^+ and SO_4^{2-} solution constitutes the prevailing composition of the aerosol phase. For acidic atmospheres, all the available ammonia is taken up by the aerosol phase, and only for $\text{NH}_3/\text{H}_2\text{SO}_4$ molar ratios higher than 2 can ammonia also exist in the gas phase.

Numerous SEM and TEM images of ammonium sulfate aerosols with different sizes can be found in the literature, mixed with smaller soot particles or nearly spherical silica particles and with soot inclusions or surrounded by numerous tiny satellite droplets. For instance, Li, Anderson, and Buseck (2003a) showed images of ammonium sulfate particles mixed with small soot particles and silica spheres sampled at Sagres (Portugal) during the ACE-2 campaign and ammonium sulfate particles with soot inclusions as well as a particle consisting of NaCl with a mixed-cation sulfate rim, both sampled at Punta del Hidalgo (Canary Islands). The morphologic characteristics of some ammonium sulfate particles surrounded by numerous tiny satellite droplets were described by Kojima, Buseck, and Reeves (2005). Ammonium sulfate particles collected in the free troposphere near Pietersburg (South Africa) were shown by Li *et al.* (2003b), exhibiting both round and elongated shapes, in some cases aggregated with soot when larger in size. Various ammonium sulfate particles sampled in the urban environment of Mainz (Germany) were shown by Sinha *et al.* (2008), providing evidence of their mixed composition in such a polluted ambient.

The nearly spherical shape characteristics of sulfate ammonium particles facilitate the calculations based on the Mie (1908) theory of the radiative effects produced by these aerosol particles that scatter and absorb solar radiation. In fact, ammonium sulfate particles are highly hygroscopic and therefore gradually tend to assume more spherical shapes as the RH of the surrounding air increases to exceed 70–75% (Hänel, 1976). In order to better study the radiative effects of sulfate particles, the evaluations of the sulfate particulate matter refractive index proposed by Toon, Pollack, and Khare (1976) and Shettle and Fenn (1979) can be conveniently used. On the basis of these data, the real part of refractive index was estimated to have a stable value of 1.53 over the 0.30–0.70 μm wavelength range and to decrease with wavelength until reaching a value of 1.42 within the 2.0–2.5 μm spectral interval, while the imaginary part was in general very low at all the visible and near-infrared wavelengths, assuming values varying from 5×10^{-3} to 8×10^{-3} over the 0.3–0.7 μm wavelength range and slightly higher values in

the near-infrared 0.86–2.50 μm range, varying from 8×10^{-3} to 2×10^{-2} , with a maximum at 1.30 μm and a pronounced minimum at around 2.00 μm .

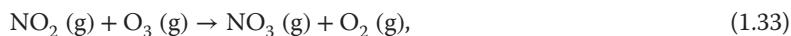
Anthropogenic emissions constitute the main source of SO_2 over continents and in polluted marine air masses, where most sulfur compounds are lost by deposition before oxidation. Therefore, anthropogenic aerosols are mainly formed from SO_2 emitted by industrial activities, domestic heating, and vehicular traffic. As shown in Table 1.2, they predominate in concentration over those formed in the troposphere from natural SO_2 . Being mostly generated by fossil fuel burning, the source distribution and magnitude of anthropogenic SO_2 are fairly well known, and recent estimates differ one from the other by no more than 30% (Lelieveld *et al.*, 1997). Anthropogenic SO_2 emissions were estimated to have decreased by ~25% from 1980 to 2000 when the major emitting regions shifted from Europe and North America to Southeast Asia (Liu, Penner, and Herzog, 2005).

1.6.2

Secondary Particles from NO_x

Nitrate particles generally exhibit larger sizes than sulfate particles suspended in marine air. Because seawater contains negligible nitrate concentrations, the nitrate in these particles must derive from the condensation of gaseous HNO_3 , possibly through g-to-p conversion in the liquid phase. Nitrates are also common in continental aerosols, mainly formed from agricultural activities and deriving in part from the condensation of HNO_3 onto larger and more alkaline mineral particles, with sizes predominantly ranging from about 0.2 to 20 μm . The *in situ* chemical reactions involving and generating many important atmospheric trace constituents lead to the formation of nitrate aerosols. Most of such gaseous reactions are initiated by photolysis involving radicals and occur with one to three different molecules. These reactions can be classified as *homogeneous* or *heterogeneous*, according to the aforementioned definitions.

One of the most important homogeneous reactions is the following:



which constitutes in practice the major source of the nitrate radical (NO_3) in the atmosphere. Mixing an inorganic aerosol, like nitric acid (HNO_3), with organic compounds (aldehydes) which can appreciably increase the rate of aerosol growth is an example of a heterogeneous reaction.

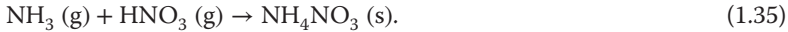
Odd nitrogen (NO_y), or total reactive nitrogen as it is sometimes called, refers to the sum of NO_x plus all the compounds produced by the atmospheric oxidation of NO_x , including HNO_3 , NO_3 , dinitrogen pentoxide (N_2O_5), and peroxyacetyl nitrate (PAN for short). Nitric acid can form from N_2O_5 in cloud water, and subsequently the evaporation of cloud water releases nitrate particles into the air. The main sources of NO_y are anthropogenic emissions, but away from pollution sources, soils and lightning can also play dominant roles. Interactions between NO_y and NMHC can lead to photochemical smogs in cities. On regional and global scales, interactions of NO_y with odd hydrogen have a strong influence on

OH concentrations. Even with rigorous pollution controls, increasing numbers of cars in urban centers can produce high concentrations of NO, which can then be converted to NO₂ through the following reaction:



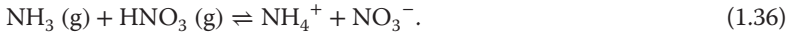
The NO₂ can then be involved in the production of O₃. Because the rate coefficient of the reaction represented in Eq. (1.34) increases as temperature decreases, the production of NO₂ can become significant in urban areas during cold winters.

In the *ammonia–nitric acid–water system*, NH₄NO₃ is found in the aqueous state for air RH higher than the deliquescence point. In fact, ammonia and nitric acid react in the atmosphere to form ammonium nitrate (NH₄NO₃):



Ammonium nitrate is formed in areas characterized by high ammonia and nitric acid concentrations in the presence of low sulfate concentrations. Depending on the ambient RH, ammonium nitrate may exist as a solid or aqueous solution of NH₄⁺ and NO₃⁻. Equilibrium concentrations of gaseous NH₃ and HNO₃ and the resulting concentration of solid or aqueous NH₄NO₃ can be calculated on the basis of fundamental thermodynamic principles using the method of Stelson and Seinfeld (1982a,b). For low air RH conditions, at which NH₄NO₃ is in the solid state, the dissociation constant is equal to the product of the partial pressures of NH₃ and HNO₃. This parameter increases almost linearly as a function of temperature and therefore is quite sensitive to temperature changes, varying by more than two orders of magnitude for typical ambient conditions. Lower temperatures correspond to lower values of the dissociation constant and, hence, to lower equilibrium values of the NH₃ and HNO₃ gas-phase concentrations. Thus, lower temperatures shift the equilibrium of the system toward the aerosol phase, inducing an increase in the aerosol mass concentration of NH₄NO₃.

In ammonium nitrate solutions for RH higher than that of deliquescence, NH₄NO₃ is found in the aqueous state. The corresponding dissociation reaction is



Solution concentrations with 8–26 molalities can be expected in wetted atmospheric aerosol. These concentrations depend not only on the aerosol nitrate and ammonium but also on the amount of water in the aerosol phase. Therefore, calculation of the aerosol solution composition requires estimation of the aerosol water content.

In the *ammonia–nitric acid–sulfuric acid–water system*, gaseous components (NH₃, HNO₃, H₂SO₄, H₂O) are present together with aqueous-phase components (NH₄⁺, H⁺, HSO₄⁻, SO₄²⁻, NO₃⁻, and H₂O) and solid components (NH₄HSO₄, (NH₄)₂SO₄, NH₄NO₃, (NH₄)₂SO₄ · 2NH₄NO₃, (NH₄)₂SO₄ · 3NH₄NO₃, and (NH₄)₃H(SO₄)₂). Two remarks are useful to determine a priori the composition of the aerosol existing in such a system: (i) sulfuric acid possesses an extremely low vapor pressure, and (ii) (NH₄)₂SO₄ in the solid or aqueous state is the

preferred form of sulfate. The first note implies that the amount of sulfuric acid in the gas phase will be negligible, and the second means that, if possible, each mole of sulfate will remove two moles of ammonia from the gas phase. Based on these observations, two regimes of interest can be considered that are ammonia poor and ammonia rich, respectively:

1. In the ammonia-poor case, there is insufficient NH_3 to neutralize the available sulfate, and therefore the aerosol phase will be acidic. The vapor pressure of NH_3 will be low, and the sulfate will tend to drive the nitrate to the gas phase. Since the NH_3 partial pressure will be low, the $\text{NH}_3 - \text{HNO}_3$ partial pressure product will also be low, so that ammonium nitrate levels tend to be low or null, and sulfate may exist as bisulfate.
2. In the ammonia-rich case, there is an excess of ammonia, so that the aerosol phase will be largely neutralized. The ammonia that does not react with sulfate is thus available for reacting with nitrate until producing NH_4NO_3 .

Therefore, at very low ammonia concentrations, sulfuric acid and bisulfate constitute the aerosol composition. As ammonia increases, ammonium nitrate becomes a significant aerosol constituent. The aerosol LWC varies nonlinearly as a function of these variations, reaching a minimum close to the transition between the two regimes. The formation of ammonium nitrate is often limited by the availability of one of the reactants. Rural areas with significant ammonia emissions are often in this regime, where NH_4NO_3 formation is nitric acid limited. The boundary between the nitric acid-limited and ammonia-limited regimes depends on temperature, air RH, sulfate concentrations, and concentrations of the other major inorganic aerosol components.

Reductions in the sulfate concentration affect the inorganic particle concentration in two different ways: (i) part of the sulfate may be replaced by nitric acid, leading to an increase in the ammonium nitrate content of the aerosol, while sulfate decrease frees up ammonia to react with nitric acid and transfers it to the aerosol phase; (ii) if the particles are aqueous, there is also a second effect, for which the reduction of the sulfate ions in solution increases the equilibrium vapor pressure product of the ammonia and nitric acid in the particles, shifting the ammonium nitrate partitioning toward the gas phase. In this second scenario for aqueous particles, the substitution of sulfate by nitrate is in general relatively small: sulfate reductions are accompanied by an increase in the aerosol nitrate and a reduction of the aerosol ammonium, water, and total mass. However, such a reduction of the mass is in general nonlinear. For example, a reduction of total sulfate from 30 to $10 \mu\text{g m}^{-3}$ results in a net reduction of the dry aerosol mass (excluding water) of only $12.9 \mu\text{g m}^{-3}$, because of the increase in the aerosol nitrate concentration by $10 \mu\text{g m}^{-3}$, while ammonium decreases by only $2.9 \mu\text{g m}^{-3}$.

These g-to-p conversion processes caused dramatic episodes of urban pollution during the second half of the twentieth century, when emissions of vehicle exhausts constituted an important source of pollutants in many urban areas. For sunlight and stagnant meteorological conditions, the combination of chemical species in the strongly polluted urban air can lead to *photochemical smog* cases,

which are also called *Los Angeles-type smogs*. They are characterized by high concentrations of a wide variety of pollutants, such as nitrogen oxides, O₃, CO, hydrocarbons, aldehydes (and other eye-irritant materials), and sometimes sulfuric acid. The chemical reactions leading to photochemical smog are very complex, due to the interactions of a large number of organic pollutants (e.g., hydrocarbons such as ethylene and butane) with nitrogen oxides. The reactions start with the photolysis process



induced with rate coefficient j by the incoming solar radiation with wavelength $\lambda < 430$ nm, which is followed by the reaction



forming O₃ molecules with rate coefficient k_1 . However, O₃ is then depleted by the rapid reaction



characterized by a high rate coefficient k_2 . If there are no other reactions, the reactions in Eqs (1.37–1.39) are expected to lead to a steady-state concentration of O₃ given by

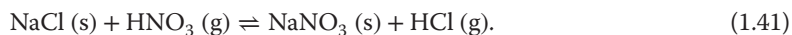
$$[\text{O}_3] = j[\text{NO}_2]/k_2[\text{NO}]. \quad (1.40)$$

Equation (1.40) predicts O₃ concentrations in urban-polluted air of only ~0.03 ppmv, whereas typical values are well above this concentration and can exceed 0.5 ppmv. Therefore, other chemical reactions need to be involved to explain the photochemical smog occurrence. Most effective are reactions that oxidize NO to NO₂ without consuming O₃, since this would allow a net O₃ production, favoring a buildup of ozone concentrations during the day. The reactions leading to photochemical smog and due to organic compounds are examined in the next section dedicated to the SOAs.

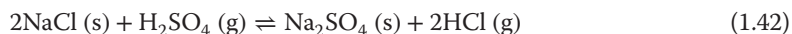
In marine air, the main contributors to the mass of inorganic aerosols are the ions Na⁺, Cl⁻, Mg²⁺, SO₄²⁻, K⁺, and Ca²⁺. Apart from SO₄²⁻, these compounds are contained primarily in particles with sizes of no more than a few micrometers, because they originate from sea-salt particles derived from bubble bursting. Sulfate mass concentrations exhibit the highest values over the 0.1–1 μm size range. As mentioned before, nitrates constitute the particles with sizes larger than those of sulfates in marine air. Therefore, seawater contains negligible concentrations of nitrate-containing particles, which are formed by condensation of gaseous HNO₃, mainly through g-to-p conversion in the liquid phase. For this reason, nitrate particles are common in continental aerosols, formed through condensation of HNO₃ onto larger and more alkaline mineral particles, assuming sizes varying mainly from 0.2 to 20 μm.

Considering other *inorganic aerosol species*, aerosol particles exhibit considerably high concentrations in regions close to seawater, consisting mainly of Na⁺ and

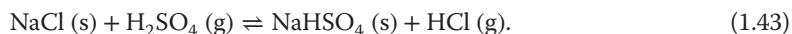
Cl^- ions. Sodium and chloride interact with several aerosol components, generating a variety of particles formed during these reactions, including ammonium chloride, sodium nitrate, sodium sulfate, and sodium bisulfate, while $\text{HCl}(\text{g})$ may be released to the gas phase. The addition of NaCl to an urban aerosol can have a series of interesting effects, including the following reaction of NaCl with HNO_3 :



As a result of this reaction (see, for instance, De Bock, Van Maldered, and Van Grieken (1994)), more nitrate is transferred to the aerosol phase and is associated with the coarse sea-salt particles. At the same time, hydrochloric acid is liberated and the aerosol particles appear to be chloride deficient. As found by Pakkanen (1996) examining particulate samples collected in the urban area of Helsinki (Finland), high atmospheric concentrations of coarse nitrate particles can be formed in the reaction of nitric acid with sea- and soil-derived coarse particles. In particular, the reaction with sea-salt particles resulted in the evaporation of chlorine ions as HCl . The presence of nss sulfate ions indicates that also H_2SO_4 and/or SO_2 can react with sea salt and contribute to the loss of chlorine ions. In fact, such a chloride deficiency substantially results from the following pair of reactions:



and



The overall percentage of evaporated chlorine ions was found to decrease as the particle size increases, so that Cl^- evaporation was found to be almost complete over the $1-2 \mu\text{m}$ size range, indicating that all major sea-derived chlorides (NaCl , MgCl_2 , CaCl_2 , and KCl) may react with acidic species in the atmosphere (Pakkanen, 1996).

1.6.3

Secondary Organic Aerosols

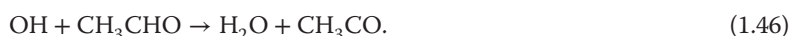
SOA particles originate in the atmosphere through the mass transfer of low-pressure products given by the oxidation of organic gases to the aerosol phase. Carbonaceous particles emitted directly into the atmosphere derive mainly from biomass fires. Organic and carbonaceous aerosols are produced by g-to-p conversion of gases released from the biosphere and from volatile compounds, such as crude oil leaking to the Earth's surface. The organic gases are oxidized in the gas phase by species such as the hydroxyl radical (OH), ozone (O_3), and the nitrate radical (NO_3), so that such oxidation products gradually accumulate. Some of these products have low volatilities and condense on the available particles in an effort to establish equilibrium between the gas and aerosol phases. The mass transfer flux of these products to the aerosol phase is proportional to the difference between their gas-phase concentration and their concentration in the gas phase at the particle surface. Thus, there are two separate steps involved

in the production of SOAs: (i) the organic aerosol compound is produced in the gas phase during the reaction of parent organic gases, with rates closely depending on the gas-phase chemistry of the organic aerosol precursors, and (ii) the organic compound partitions between the gas and particulate phases form SOA, occurring through variable interactions among the various compounds present in both phases.

In the formation of photochemical smog, the OH radical can initiate a chain reaction, which attacks the hydrocarbon pollutants in urban air, through one of the following three reactions:



or

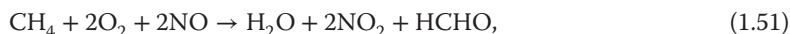


The resulting radicals – CH_3 in Eq. (1.44), H in Eq. (1.45), and CH_3CO in Eq. (1.46) – are then involved in reactions that oxidize NO to NO_2 and regenerate OH. For example, CH_3 formed through the reaction given in Eq. (1.44) can initiate the following sequence of reactions:



to form OH and oxidize NO to NO_2 .

The net result of these four reactions together with the reaction described in Eq. (1.44) is given by



where the oxidation of CH_4 results in the oxidation of NO to NO_2 without consuming O_3 .

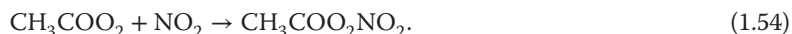
The reaction defined in Eq. (1.51) produces formaldehyde (HCHO), which is an eye irritant and constitutes an efficient source of HO_x , as can be seen in the sequence of the two following reactions producing HO_2 :



and



Similarly, the acetyl radical (CH_3CO) formed in the reaction described in Eq. (1.46) is involved in a series of reactions leading to the formation of the methyl radical CH_3 and the peroxyacetyl radical (CH_3COO_2). The methyl radical oxidizes NO through the reactions defined in Eqs. (1.47–1.50), and the peroxyacetyl radical reacts with nitrogen dioxide, as follows:



The chemical species on the right-hand side of the reaction represented in Eq. (1.54) is the vapor of a colorless and dangerously explosive liquid called PAN, an important component of photochemical smog and another major eye irritant. Other alkenes oxidize NO to NO_2 without consuming O_3 and regenerate OH, doing this much faster than the previously reported reactions. The concentrations of some of the major components of photochemical smog in Los Angeles vary typically throughout the day. For these high-pollution conditions, ozone precursors, such as NO_x and hydrocarbons, build up during the morning rush hour, and aldehydes, O_3 , and PAN peak in the early afternoon.

The role of PAHs in air pollution and public health was first studied in the early 1940s following the discovery that organic extracts of particles from polluted air (e.g., benzo[*a*]pyrene ($\text{C}_{20}\text{H}_{12}$), a five-ring PAH) produced cancer in laboratory experiments on animals, its metabolites being mutagenic and highly carcinogenic. The PAHs are emitted by diesel and gasoline engines, coal-fired electric power-generating plants, biomass burning, and cigarettes and are present in air as volatile particulates and gases. Reactions initiated by OH in the day and NO_3 during the night convert gaseous PAHs to nitro-PAH derivatives, which are responsible for about 50% of the mutagenic activity of respirable airborne particles monitored in southern California.

1.7

Concluding Remarks on the Global Annual Emission Fluxes of Natural and Anthropogenic Aerosol Mass

The previous sections showed that significant contributions are made by primary and secondary sources of natural and anthropogenic particulate matter to the global airborne aerosol loading. Table 1.1 presents the estimates of the average annual emissions of the various aerosol types on a global scale, due to the primary and secondary natural sources, chosen among those proposed in the literature over the past decades. Similarly, Table 1.5 provides the estimates of the average global annual emissions from the primary and secondary sources of anthropogenic aerosols evaluated since 2000. Examining the data reported in Table 1.1, it can be stated that the global annual emission flux Φ_e of natural primary particulate matter into the atmosphere varies:

1. over the $3 \times 10^3 - 2.0 \times 10^4$ Tg per year range (Andreae and Rosenfeld, 2008) for the sea-salt particles formed by wind forcing on the oceanic surfaces, with

- average annual values of 1.01×10^4 Tg per year (Gong, Barrie, and Lazare, 2002), 3.3×10^3 Tg per year (Jaenicke, 2005), and 7.8×10^3 Tg per year (Tsigaridis *et al.*, 2006), for which an arithmetic mean value of about 7×10^3 Tg per year was reported in Table 1.6;
2. over the 1.0×10^3 – 2.15×10^3 Tg per year range (Andreae and Rosenfeld, 2008) for the mineral dust mobilized by winds in desert regions and more generally on arid soil and rock debris, with average annual values of 1.49×10^3 Tg per year (Zender, Brian, and Newman, 2003), 2×10^3 Tg per year (Jaenicke, 2005), and 1.7×10^3 Tg per year (Tsigaridis *et al.*, 2006), for which an arithmetic mean value of 1.73×10^3 Tg per year was reported in Table 1.6;
 3. from 15 to 70 Tg per year (Andreae and Rosenfeld, 2008) for the primary organic aerosol emitted from the various biological sources, with an average value of 50 Tg per year estimated by Kiehl and Rodhe (1995) for biological debris;
 4. from 26 to 70 Tg per year (Andreae and Rosenfeld, 2008) for the biomass burning organic aerosol, with an average annual value of 44.4 Tg per year proposed by Tsigaridis *et al.* (2006) in good agreement with the IPCC (2001) estimate equal to 56 Tg per year;
 5. from 4 to 90 Tg per year (Jaenicke, 1988) for primary and secondary aerosol fluxes injected into the troposphere by volcanic eruptions, with an average annual value of 30 Tg per year (Kiehl and Rodhe, 1995) (see Table 1.1), this quantity varying largely from one year to another, since it depends closely on the number frequency and intensity of volcanic eruptions;
 6. from 4 to 10^4 Tg per year (Seinfeld and Pandis, 1998) for volcanic aerosol formed in the stratosphere from volcanic SO_2 , with an average annual estimate of 20 Tg per year (Kiehl and Rodhe, 1995) comparable to those of (i) 21 Tg per year (IPCC, 2001), (ii) 30 Tg per year (Seinfeld and Pandis, 1998) – which are considerably higher than the value of 9.2 Tg per year proposed by Tsigaridis *et al.* (2006) – and (iii) the average value of 10 Tg per year derived by Toohey *et al.* (2011) over the last 20 years (see Table 1.1); and
 7. from 1.5×10^{-4} to 4×10^{-2} Tg per year (Gardner *et al.*, 2014) for the global flux of cosmic dust entering the Earth's atmosphere, which are several orders of magnitude smaller than those attributed to sea salt and mineral dust sources, these evaluations implying an estimate of the average global flux of cosmic dust equal to 2×10^{-2} Tg per year, as reported in Table 1.6.

In addition, significant emission fluxes of secondary aerosol particles of natural origins need to be taken into account:

1. The overall sulfate aerosol flux Φ_e was estimated to vary from 107 to 374 Tg per year by Andreae and Rosenfeld (2008), including the flux of sulfate aerosols formed from natural DMS, which was estimated to be equal to 12.4 Tg per year by Liao *et al.* (2003) and 18.5 Tg per year by Tsigaridis *et al.* (2006). In agreement with the evaluations of Andreae and Rosenfeld

Table 1.6 Ranges and average values of global emission fluxes (measured in teragram per year, being $1 \text{ Tg yr}^{-1} = 10^6 \text{ ton yr}^{-1}$) of the most important aerosol types due to natural, anthropogenic, and overall mixed (natural + anthropogenic) sources, as derived from the data given in Tables 1.1 and 1.5 for natural and anthropogenic particles and derived from the evaluations available in the literature of the past 20 years.

Aerosol particle type	Natural sources		Anthropogenic sources		Overall mixed sources	
	Range	Average	Range	Average	Range	Average
Sea salt	3000–20 000	7068	—	—	3000–20 000	7068
Mineral dust	1000–2150	1731	50–250	150	1050–2400	1881
Biogenic primary organic	15–70	50	—	—	15–70	50
Biomass burning organic	26–70	44	12–270	90	38–340	134
Tropospheric volcanic	4–90	30	—	—	4–90	30
Stratospheric volcanic	2–17	10	—	—	2–17	10
Cosmic dust in the middle atmosphere	2×10^{-4} to 4×10^{-2}	2×10^{-2}	—	—	2×10^{-4} to 4×10^{-2}	2×10^{-2}
Sulfates	107–374	165	50–122	73	157–496	238
Nitrates	12–27	25	90–118	95	102–145	115
Overall biogenic from isoprene, monoterpenes, and VOCs	835–1000	900	—	—	835–1000	900
Biogenic secondary organic	3–83	11	—	—	3–83	11
Industrial dust	—	—	40–130	100	40–130	100
Carbonaceous from hydrocarbons and VOCs	—	—	15–90	29	15–90	29
Black carbon (soot)	—	—	8–14	12	8–14	12

(2008), an average annual value of 165 Tg per year was assumed in Table 1.6, according to the SMIC (1971) evaluations.

2. The overall nitrate aerosol flux was estimated by Andreae and Rosenfeld (2008) to range from 12 to 27 Tg per year, with an average annual value of 25 Tg per year determined by the IPCC (2001) and reported in Table 1.6.
3. From about 3 to 83 Tg per year (Andreae and Rosenfeld, 2008) for the SOA, mainly given by the SOA formed from biogenic VOCs, estimated to provide an average global annual flux of about 11 Tg per year (Chung and Seinfeld, 2002). In reality, the overall emission of biogenic aerosol was estimated to be equal to 8.35×10^2 Tg per year by Tsigaridis *et al.* (2006), due to isoprenes, monoterpenes, and nonaromatic and aromatic VOCs, thus indicating that the overall annual flux of biological aerosol should be with good approximation equal to 10^3 Tg per year, as estimated by Jaenicke (2005) (see also Table 1.6).

For all the above average annual global estimates of natural primary and secondary particles, the overall annual emission of natural aerosol on the global scale was evaluated to be 5875 Tg per year on average (IPCC, 2001) but to vary from one year to another between 4185 and more than 2.2×10^4 Tg per year if the evaluations of Andreae and Rosenfeld (2008) are taken into account and the volcanic debris estimates proposed by the United Nations (1979) are included. More than 80% of the overall global annual emission flux of particulate mass turns out to be given by sea-salt particles.

The global annual emissions of particulate matter due to man-made activities arise primarily from four source categories that are (i) fuel combustion, (ii) industrial processes, (iii) nonindustrial fugitive sources (such as roadway dust from paved and unpaved roads, wind erosion of cropland, construction, etc.), and (iv) transportation sources (cars, ships, airplanes, etc.). Fugitive particles are those not emitted from a definable point such as a stack. Industrial fugitive dust emissions result from wind erosion of storage piles and unpaved plant roads and from vehicular traffic over plant roads. Fugitive process emissions are related to industrial activities, such as materials handling, loading, and transfer operations. Transportation source emissions occur mainly as vehicle exhaust and vehicle-related particles from tire, clutch, and brake wear. Engine-related particulate emissions are composed primarily of lead halides, sulfates, and carbonaceous matter and have sizes mostly smaller than $1 \mu\text{m}$. About 40% of particles from tire wear are less than $10 \mu\text{m}$ and about 20% less than $1 \mu\text{m}$, being primarily composed of carbon. Particles from brake linings are less than $1 \mu\text{m}$ and are composed mainly of carbon and asbestos.

The estimate of emissions of a certain aerosol species from a source is based on a technique using “emission factors” based on source-specific emission measurements evaluated as a function of activity level (e.g., amount of annual production at an industrial facility) with regard to each source. For example, to sample a power plant’s emissions of SO_2 or NO_x at the stack, knowing the plant’s boiler design and its consumption rate, the sulfur and nitrogen content of fuel burned can be used to calculate an emission factor of kilograms of SO_2 or NO_x emitted per metric

ton (Mg) of fuel consumed. Emission factors currently in use are developed from only a limited sampling of the emissions source population for any given category, and the values reported are an average of those limited samples and might not be statistically representative of populations. The formulation of emission factors for mobile sources, the major sources of VOCs and NO_x , is based on rather complex emission estimation models used in conjunction with data from laboratory testing of representative groups of motor vehicles.

Anthropogenic activities emit rather high number concentrations of particles into the atmosphere, both directly and through g-to-p conversion. For particles with $a \geq 2.5 \mu\text{m}$ (coarse particles), human activities worldwide are estimated to produce $\sim 15\%$ of natural emissions, with industrial processes, fuel combustion, and g-to-p conversion accounting for $\sim 80\%$ of the anthropogenic emissions. However, anthropogenic sources in urban areas are much more important. For particles with $a < 2 \mu\text{m}$ (fine particles), human activities produce $\sim 20\%$ of the overall natural emissions, with g-to-p conversion accounting for $\sim 90\%$ of the anthropogenic emissions. Table 1.5 summarizes the estimates of the annual global emissions of particulate matter due to anthropogenic activities, as estimated through various studies reported in the literature. From these data, it can be stated that the annual global emissions of particulate mass due to anthropogenic activities vary:

1. from 50 to 250 Tg per year (SMIC, 1971) for the dust from soil erosion and wind-forced mobilization associated with agricultural activities, with an average annual value of 150 Tg per year;
2. from 12 to 270 Tg per year (Lioussse *et al.*, 1996; IPCC, 2001) of carbonaceous aerosols from deforestation activities and biomass burning, with an average annual value of 90 Tg per year (Seinfeld and Pandis, 1998);
3. from about 50 to 122 Tg per year (IPCC, 2001; Liao *et al.*, 2003) for anthropogenic sulfates, with an average annual value of 73 Tg per year (Tsigaridis *et al.*, 2006);
4. from 40 to 118 Tg per year (IPCC, 2001) for anthropogenic nitrates, with an average annual value of 44 Tg per year (Tsigaridis *et al.*, 2006);
5. from 40 to 130 Tg per year (Seinfeld and Pandis, 1998) for industrial dust, with an average annual value of 100 Tg per year (Kiehl and Rodhe, 1995);
6. from 15 to 90 Tg per year (SMIC, 1971; Lioussse *et al.*, 1996) of carbonaceous aerosols from hydrocarbons, anthropogenic VOCs, and industrial activities, with an average annual value of 29 Tg per year (IPCC, 2001); and
7. from 8 to 14 Tg per year (Andreae and Rosenfeld, 2008) for BC (soot) aerosols, with an average annual value of 12 Tg per year (Lioussse *et al.*, 1996).

For these average estimates of the annual global emissions of various anthropogenic aerosol types, an overall emission of ~ 580 Tg per year can be assumed on average for the anthropogenic particulate matter. Thus, for the overall contribution of natural aerosols determined previously, the total (natural + anthropogenic) annual emissions over a global scale provide approximatively an overall average annual flux of about 6.5×10^3 Tg per year, which does not

differ appreciably from the estimate of 6.3×10^3 Tg per year established by the IPCC (2001).

Abbreviations

BC	black carbon
CCN	cloud condensation nuclei
EC	elemental carbon
HRTEM	high-resolution transmission electron microscope
LWC	liquid water content
NTP	normal temperature and pressure
OC	organic carbon
PAHs	polycyclic aromatic hydrocarbons
SEM	scanning electron microscope
TEM	transmission electron microscope
VOCs	volatile organic compounds

List of Symbols

Latin

Δt_L	atmospheric lifetime of aerosol particles
a	“equivalent” diameter of an aerosol particle assumed to have a spherical shape
a_c	mode diameter of an aerosol size-distribution curve
B	shape parameter used by Monahan <i>et al.</i> (1986) in their size-dependent production rate formula
h	Planck’s constant, defining the quantum of action, that is, the proportionality constant between the energy of a photon and its frequency ν : It is estimated to be equal to 6.626×10^{-34} J s
J_{s-s}	production rate of sea salt particles at the surface level (measured in $\text{m}^{-2} \mu\text{m}^{-1} \text{s}^{-1}$)
M_c	airborne mass concentration of crustal material near the surface
M_S	vertical mass loading M_S of volcanic aerosols in the stratosphere
M_{s-s}	total mass concentration of sea salt particles, measured in $\mu\text{g m}^{-3}$ and produced by wind forcing on the sea surface
RH	relative humidity of air (measured in %)
WS	wind speed (measured in m s^{-1})
z	altitude above mean sea level (measured in m a.m.s.l.)

Greek

ν	frequency of the incoming solar irradiance
$\tau_a(\lambda)$	aerosol optical thickness at wavelength λ

Φ_e	annual global emission flux of aerosol particulate mass (measured in Tg per year)
α	Ångström exponent (i.e., first atmospheric turbidity parameter given by the Ångström's formula)
β	second atmospheric turbidity parameter (giving the best-fit value of $\tau_a(\lambda)$ at the wavelength $\lambda = 1 \mu\text{m}$)

References

- Adachi, K. and Buseck, P.R. (2008) Internally mixed soot, sulfates, and organic matter in aerosol particles from Mexico City. *Atmos. Chem. Phys.*, **8** (21), 6469–6481. doi: 10.5194/acp-8-6469-2008
- Adams, P.J., Seinfeld, J.H., and Koch, D.M. (1999) Global concentrations of tropospheric sulfate, nitrate and ammonium aerosol simulated in a general circulation model. *J. Geophys. Res.*, **104** (D11), 13791–13823. doi: 10.1029/1999JD900083
- Adams, P.J., Seinfeld, J.H., Koch, D.M., Mickley, L., and Jacob, D. (2001) General circulation model assessment of direct radiative forcing by the sulfate-nitrate-ammonium-water inorganic aerosol system. *J. Geophys. Res.*, **106** (D1), 1097–1111. doi: 10.1029/2000JD900512
- Andreae, M.O. (1995) Climatic effects of changing atmospheric aerosol levels, in *World Survey of Climatology: Future Climates of the World*, vol. **16** (ed. A. Henderson-Sellers), Elsevier, Amsterdam, pp. 341–392.
- Andreae, M.O. and Crutzen, P.J. (1997) Atmospheric aerosols: biogeochemical sources and role in atmospheric chemistry. *Science*, **276** (5315), 1052–1056. doi: 10.1126/science.276.5315.1052
- Andreae, M.O. and Gelencsér, A. (2006) Black carbon or brown carbon? The nature of light-absorbing carbonaceous aerosols. *Atmos. Chem. Phys.*, **6** (10), 3131–3148. doi: 10.5194/acp-6-3131-2006
- Andreae, M.O. and Jaeschke, W.A. (1992) Exchange of sulphur between biosphere and atmosphere over temperate and tropical regions, in *Sulphur Cycling on the Continents: Wetlands, Terrestrial Ecosystems and Associated Water Bodies*, SCOPE 48 (eds R.W. Howarth, J.W.B. Stewart, and M.V. Ivanov), John Wiley & Sons, Ltd, Chichester, pp. 27–61.
- Andreae, M.O. and Rosenfeld, D. (2008) Aerosol-cloud-precipitation interactions. Part 1. The nature and sources of cloud-active aerosols. *Earth Sci. Rev.*, **89** (1-2), 13–41. doi: 10.1016/j.earscirev.2008.03.001
- Andres, R.J. and Kasgnoc, A.D. (1998) A time-averaged inventory of subaerial volcanic sulfur emissions. *J. Geophys. Res.*, **103** (D19), 25251–25261. doi: 10.1029/98JD02091
- Ångström, A. (1964) The parameters of atmospheric turbidity. *Tellus*, **16** (1), 64–75. doi: 10.1111/j.2153-3490.1964.tb00144.x
- Bacci, P., Del Monte, M., Longhetto, A., Piano, A., Prodi, F., Redaelli, P., Sabbioni, C., and Ventura, A. (1983) Characterization of the particulate emission by a large oil fuel fired power plant. *J. Aerosol Sci.*, **14** (4), 557–572. doi: 10.1016/0021-8502(83)90011-3
- Bates, T.S., Lamb, B.K., Guenther, A., Dignon, J., and Stoiber, R.E. (1992) Sulphur emissions to the atmosphere from natural sources. *J. Atmos. Chem.*, **14** (1-4), 315–337. doi: 10.1007/BF00115242
- Benkovitz, C.M., Berkowitz, C.M., Easter, R.C., Nemesure, S., Wagner, R., and Schwartz, S.E. (1994) Sulfate over the North Atlantic and adjacent continental regions: evaluation of October and November 1986 using a three-dimensional model driven by observation-derived meteorology. *J. Geophys. Res.*, **99** (D10), 20725–20756. doi: 10.1029/94JD01634
- Benkovitz, C.M., Scholtz, M.T., Pacyna, J., Tarrasón, L., Dignon, J., Voldner, E.C., Spiro, P.A., Logan, J.A., and Graedel, T.E. (1996) Global gridded inventories of anthropogenic emissions of sulfur and nitrogen. *J. Geophys. Res.*, **101** (D22), 29239–29253. doi: 10.1029/96JD00126

- Bigg, E.K. and Leck, C. (2008) The composition of fragments of bubbles bursting at the ocean surface. *J. Geophys. Res.*, **113**, D11209. doi: 10.1029/2007JD009078
- Blanchard, D.C. and Woodcock, A.H. (1957) Bubble formation and modification in the sea and its meteorological significance. *Tellus*, **9** (2), 145–158. doi: 10.1111/j.2153-3490.1957.tb01867.x
- Bond, T.C. and Bergstrom, R.W. (2006) Light absorption by carbonaceous particles: an investigative review. *Aerosol Sci. Technol.*, **40** (1), 27–67. doi: 10.1080/02786820500421521
- Bouman, A.F., Lee, D.S., Asman, W.A.H., Dentener, F.J., Van Der Hoek, K.W., and Olivier, J.G.J. (1997) A global high-resolution emission inventory for ammonia. *Global Biogeochem. Cycles*, **11** (4), 561–588. doi: 10.1029/97GB02266
- Budyko, M.I. (1977) *Climatic Changes*, American Geophysical Union, Waverly Press, Inc., Washington, DC (USA), p. 261.
- Bush, B.C. and Valero, F.P.J. (2002) Spectral aerosol radiative forcing at the surface during the Indian Ocean Experiment (INDOEX). *J. Geophys. Res.*, **107** (D19), 8003. doi: 10.1029/2000JD000020
- Cadle, R.D. (1966) *Particles in the Atmosphere and Space*, Reinhold, New York.
- Campanelli, M., Estelles, V., Smyth, T., Tomasi, C., Martinez-Lozano, M.P., Claxton, B., Muller, P., Pappalardo, G., Pietruczuk, A., Shanklin, J., Colwell, S., Wrench, C., Lupi, A., Mazzola, M., Lanconelli, C., Vitale, V., Congeduti, F., Dionisi, D., Cardillo, F., Cacciani, M., Casasanta, G., and Nakajima, T. (2012) Monitoring of Eyjafjallajökull volcanic aerosol by the new European Skynet Radiometers (ESR) network. *Atmos. Environ.*, **48**, 33–45. doi: 10.1016/j.atmosenv.2011.09.070
- Chang, S.G., Brodzinsky, R., Gundel, L.A., and Novakov, T. (1982) Chemical and catalytic properties of elemental carbon, in *Particulate Carbon: Atmospheric Life Cycle* (eds G.T. Wolff and R.L. Klimsch), Plenum Press, New York, pp. 158–181.
- Charlson, R.J., Langner, J., Rodhe, H., Leovy, C.B., and Warren, S.G. (1991) Perturbation of the northern hemisphere radiative balance by backscattering from anthropogenic sulfate aerosols. *Tellus B*, **43** (4), 152–163. doi: 10.1034/j.1600-0870.1991.00013.x
- Charlson, R.J., Lovelock, J.E., Andreae, M.O., and Warren, S.G. (1987) Oceanic phytoplankton, atmospheric sulphur, cloud albedo and climate. *Nature*, **326** (6114), 655–661. doi: 10.1038/326655a0
- Charlson, R.J., Schwartz, S.E., Hales, J.M., Cess, R.D., Coakley, J.A. Jr., Hansen, J.E., and Hofmann, D.J. (1992) Climate forcing by anthropogenic aerosols. *Science*, **255** (5043), 423–430. doi: 10.1126/science.255.5043.423
- Chung, S.H. and Seinfeld, J.H. (2002) Global distribution and climate forcing of carbonaceous aerosols. *J. Geophys. Res.*, **107**, D19, AAC 14-1–AAC 14-33. doi: 10.1029/2001JD001397
- Chylek, P. and Coakley, J.A. Jr. (1974) Aerosols and climate. *Science*, **183** (4120), 75–77. doi: 10.1126/science.183.4120.75
- Claeys, M., Graham, B., Vas, G., Wang, W., Vermeylen, R., Pashynska, V., Cafmeyer, J., Guyon, P., Andreae, M.O., Artaxo, P., and Maenhaut, W. (2004) Formation of secondary organic aerosols through photooxidation of isoprene. *Science*, **303** (5661), 1173–1176. doi: 10.1126/science.1092805
- Crutzen, P. (2006) Albedo enhancement by stratospheric sulfur injections: a contribution to resolve a policy dilemma? *Clim. Change*, **77** (3-4), 211–220. doi: 10.1007/s10584-006-9101-y
- Cwiertny, D.M., Baltrusaitis, J., Hunter, G.J., Laskin, A., Scherer, M.M., and Grassian, V.H. (2008) Characterization and acid-mobilization study of iron-containing mineral dust source materials. *J. Geophys. Res.*, **113**, D05202. doi: 10.1029/2007JD009332
- De Bock, L.A., Van Maldered, H., and Van Grieken, R.E. (1994) Individual aerosol particle composition variations ion air masses crossing the North Sea. *Environ. Sci. Technol.*, **28** (8), 1513–1520. doi: 10.1021/es00057a021
- Del Monte, M. and Sabbioni, C. (1984) Morphology and mineralogy of fly ash from a coal-fueled power plant. *Arch. Meteorol. Geophys. Bioclimatol., Ser. B*, **35** (1-2), 93–104. doi: 10.1007/BF02269412

- Deuzé, J.L., Herman, M., Goloub, P., Tanré, D., and Marchand, A. (1999) Characterization of aerosols over ocean from POLDER/ADEOS-1. *Geophys. Res. Lett.*, **26** (10), 1421–1424. doi: 10.1029/1999GL900168
- Duce, R. (1995) Distributions and fluxes of mineral aerosol, in *Aerosol Forcing on Climate* (eds R.J. Charlson and J. Heintzenberg), John Wiley & Sons, Ltd, Chichester, pp. 43–72.
- Elbert, W., Taylor, P.E., Andreae, M.O., and Pöschl, U. (2007) Contribution of fungi to primary biogenic aerosols in the atmosphere: wet and dry discharged spores, carbohydrates, and inorganic ions. *Atmos. Chem. Phys.*, **7** (17), 4569–4588. doi: 10.5194/acp-7-4569-2007
- Erickson, D.J. III, and Duce, R.A. (1988) On the global flux of atmospheric sea salt. *J. Geophys. Res.*, **93** (c011), 14079–14088. doi: 10.1029/JC093ic011p14079
- Falkovich, A.H., Ganor, E., Levin, Z., Formenti, P., and Rudich, Y. (2001) Chemical and mineralogical analysis of individual mineral dust particles. *J. Geophys. Res.*, **106** (D16), 18029–18036. doi: 10.1029/2000JD900430
- Flagan, R.C. and Seinfeld, J.H. (1988) *Fundamentals of Air Pollution Engineering*, Prentice-Hall, Englewood Cliffs, NJ.
- Flanner, M.G., Shell, K.M., Barlage, M., Perovich, D.K., and Tschudi, M.A. (2011) Radiative forcing and albedo feedback from the Northern Hemisphere cryosphere between 1979 and 2008. *Nat. Geosci.*, **4** (3), 151–155. doi: 10.1038/ngeo1062
- Forster, P., Ramaswamy, V., Artaxo, P., Bernsten, T., Betts, R., Fahey, D.W., Haywood, J., Lean, J., Lowe, D.C., Myhre, G., Nganga, J., Prinn, R., Raga, G., Schulz, M., and Van Dorland, R. (2007) Changes in atmospheric constituents and radiative forcing, in *Climate Change 2007: The Physical Science Basis. Contribution of Working Group I to the Fourth Assessment Report of the Intergovernmental Panel on Climate Change* (eds S. Solomon, D. Qin, M. Manning, Z. Chen, M. Marquis, K.B. Averyn, M. Tignor, and H.L. Miller), Cambridge University Press, Cambridge, pp. 129–234.
- Gao, Y., Anderson, J.R., and Hua, X. (2007) Dust characteristics over the North Pacific observed through shipboard measurements during the ACE-Asia experiment. *Atmos. Environ.*, **41** (36), 7907–7922. doi: 10.1016/j.atmosenv.2007.06.060
- Gardner, C.S., Liu, A.Z., Marsh, D.R., Feng, W., and Plane, J.M.C. (2014) Inferring the global cosmic dust influx to the Earth's atmosphere from lidar observations of the vertical flux of mesospheric Na. *J. Geophys. Res.*, **119** (9), 7870–7879. doi: 10.1002/2014JA020383
- Gelencsér, A. (2004) *Carbonaceous Aerosol*, Springer-Verlag, New York and Berlin, p. 350.
- Gong, S.L., Barrie, L.A., Blanchet, J.-P., and Spacek, L. (1998) Modeling size-distributed sea salt aerosols in the atmosphere: an application using Canadian climate models, in *Air Pollution Modeling and Its Applications XII*, NATO, Challenges of Modern Society, vol. **22** (eds S.-E. Gryning and N. Chaumerliac), Plenum Press, New York, pp. 337–345. doi: 10.1007/978-1-4757-9128-0_35
- Gong, S.L., Barrie, L.A., and Lazare, M. (2002) Canadian Aerosol Module (CAM): a size-segregated simulation of atmospheric aerosol processes for climate and air quality models. 2. Global sea-salt aerosol and its budgets. *J. Geophys. Res.*, **107** (D24), 4779. doi: 10.1029/2001JD002004
- Graf, H.-E., Feichter, J., and Langmann, B. (1997) Volcanic sulfur emissions: estimates of source strength and its contribution to the global sulfate distribution. *J. Geophys. Res.*, **102** (D9), 10727–10738. doi: 10.1029/96JD03265
- Graham, B., Mayol-Bracero, O.L., Guyon, P., Roberts, G.C., Decesari, S., Facchini, M.C., Artaxo, P., Maenhaut, W., Köll, P., and Andreae, M.O. (2002) Water-soluble organic compounds in biomass burning aerosols over Amazonia. *J. Geophys. Res.*, **107** (D20), 8047. doi: 10.1029/2001JD000336
- Guenther, A., Hewitt, C.N., Erickson, D., Fall, R., Geron, C., Graedel, T., Harley, P., Klinger, L., Lerdau, M., McKay, W.A., Pierce, T., Scholes, B., Steinbrecher, R., Tallamraju, R., Taylor, J., and Zimmerman, P. (1995) A global model of natural volatile

- organic compound emissions. *J. Geophys. Res.*, **100** (D5), 8873–8892. doi: 10.1029/94JD02950
- Hand, J.L., Malm, W.C., Laskin, A., Day, D., Lee, T., Wang, C., Carrico, C., Carrillo, J., Cowin, J.P., Collett, J. Jr., and Iedema, M.J. (2005) Optical, physical, and chemical properties of tar balls observed during the Yosemite Aerosol Characterization Study. *J. Geophys. Res.*, **110**, D21210. doi: 10.1029/2004JD005728
- Hänel, G. (1976) The properties of atmospheric aerosol particles as functions of the relative humidity at thermodynamic equilibrium with the surrounding moist air. *Adv. Geophys.*, **19**, 73–188. doi: 10.1016/S0065-2687(08)60142-9
- Hansen, J.E. and Nazarenko, L. (2004) Soot climate forcing via snow and ice albedos. *Proc. Natl. Acad. Sci. U.S.A.*, **101** (2), 423–428. doi: 10.1073/pnas.2237157100
- Harris, S.J. and Weiner, A.M. (1983a) Surface growth of soot particles in premixed ethylene/air flames. *Combust. Sci. Technol.*, **31** (3-4), 155–167. doi: 10.1080/00102208308923637
- Harris, S.J. and Weiner, A.M. (1983b) Determination of the rate constant for soot surface growth. *Combust. Sci. Technol.*, **32** (5-6), 267–275. doi: 10.1080/00102208308923661
- Havers, N., Burba, P., Lambert, J., and Klochow, D. (1998) Spectroscopic characterization of humic-like substances in airborne particulate matter. *J. Atmos. Chem.*, **29** (1), 45–54. doi: 10.1023/A:1005875225800
- Hays, M.D. and Vander Wal, R.L. (2007) Heterogeneous soot nanostructure in atmospheric and combustion source aerosols. *Energy Fuels*, **21** (2), 801–811. doi: 10.1021/ef060442h
- Heintzenberg, J. (1994) The life cycle of the atmospheric aerosol, in *Topics in Atmospheric and Interstellar Physics and Chemistry*, Vol. 1, Chapter XII (ed. F. Boultron), Les Editions de Physique, Sciences, Les Ulis, France ERCA, pp. 251–270.
- Hinds, W.C. (1999) *Aerosol Technology: Properties, Behavior, and Measurement of Airborne Particles*, 2nd edn, John Wiley & Sons, Inc., New York, pp. 504.
- Hobbs, P.V. (2000) *Introduction to Atmospheric Chemistry*, Cambridge University Press, New York, p. 182.
- Hudson, P.K., Murphy, D.M., Cziczo, D.J., Thomson, D.S., de Gouw, J.A., Warneke, C., Holloway, J., Jost, H.-J., and Hübner, G. (2004) Biomass-burning particle measurements: characteristics composition and chemical processing. *J. Geophys. Res.*, **109**, D23S27. doi: 10.1029/2003JD004398
- IPCC (Intergovernmental Panel on Climate Change) (2001) *Climate Change 2001. The Scientific Basis* (eds J.T. Houghton, Y. Ding, D.J. Griggs, M. Noguer, P.J. van der Linden, X. Dai, K. Maskell, and C.A. Johnson), Cambridge University Press, Cambridge and New York, p. 881.
- Jacobson, M.Z. (2001) Global direct radiative forcing due to multicomponent anthropogenic and natural aerosols. *J. Geophys. Res.*, **106** (D2), 1551–1568. doi: 10.1029/2000JD900514
- Jaenicke, R. (1988) Aerosol physics and chemistry, in *Landolt-Börnstein Numerical Data and Functional Relationship in Science and Technology*, New Series Group V, Geophysics and Space Research, Meteorology, vol. 4 (ed. G. Fischer), Springer-Verlag, Heidelberg, pp. 391–457.
- Jaenicke, R. (2005) Abundance of cellular material and proteins in the atmosphere. *Science*, **308**, 73. doi: 10.1126/science.1106335
- Jensen, E.J. and Toon, O.B. (1997) The potential impact of soot particles from aircraft exhaust on cirrus clouds. *Geophys. Res. Lett.*, **24** (3), 249–252. doi: 10.1029/96GL03235
- Jickells, T.D., An, Z.S., Andersen, K.K., Baker, A.R., Bergametti, C., Brooks, N., Cao, J.J., Boyd, P.W., Duce, R.A., Hunter, K.A., Kawahata, H., Kubilay, N., la Roche, J., Liss, P.S., Mahowald, N., Prospero, J.M., Ridgwell, A.J., Tegen, I., and Torres, R. (2005) Global iron connections between desert dust, ocean biogeochemistry, and climate. *Science*, **308** (5718), 67–71. doi: 10.1126/science.1105959
- Jones, P.R., Charlson, R.J., and Rodhe, H. (1994) Aerosols, in *Climate Change 1994: Radiative Forcing of Climate Change and An Evaluation of the IPCC 1992 Emission Scenarios* (eds J.T. Houghton,

- L.G. Meira Filho, J.P. Bruce, H. Lee, B.A. Callander, and E.F. Haites), Cambridge University Press, Cambridge, pp. 131–162.
- Junge, C.E. (1963) *Air Chemistry and Radioactivity*, Academic Press, New York, p. 382.
- Junge, C. (1979) The importance of mineral dust as an atmospheric constituent, in *Saharan Dust: Mobilization, Transport, Deposition*, SCOPE Report No. 14 (ed. C. Morales), John Wiley & Sons, Ltd, Chichester, pp. 49–60.
- Karam, D.B., Flamant, C., Cuesta, J., Pelon, J., and Williams, E. (2010) Dust emission and transport associated with a Saharan depression: February 2007 case. *J. Geophys. Res.*, **115** (D4), D00H27. doi: 10.1029/2009JD012390
- Kettle, A.J. and Andreae, M.O. (2000) Flux of dimethylsulfide from the oceans: a comparison of updated data sets and flux models. *J. Geophys. Res.*, **105** (D22), 26793–26808. doi: 10.1029/2000JD900252
- Kiang, C.S., Stauffer, D., Mohnen, V.A., Bricard, J., and Vigla, D. (1973) Heteromolecular nucleation theory applied to gas-to-particle conversion. *Atmos. Environ.*, **7** (12), 1279–1283. doi: 10.1016/0004-6981(73)90137-6
- Kiehl, J.T. and Rodhe, H. (1995) Modeling geographical and seasonal forcing due to aerosols, in *Aerosol Forcing of Climate* (eds R.J. Charlson and J. Heintzenberg), John Wiley & Sons, Inc., New York, pp. 281–296.
- Kojima, T., Buseck, P.R., and Reeves, J.M. (2005) Aerosol particles from tropical convective systems: 2. Cloud bases. *J. Geophys. Res.*, **110**, D09203. doi: 10.1029/2004JD005173
- Kokhanovsky, A.A. (2003) *Polarization Optics of Random Media*, Springer-Praxis, Chichester, p. 224.
- Krueger, B.J., Grassian, V.H., Cowin, J.P., and Laskin, A. (2004) Heterogeneous chemistry of individual mineral dust particles from different dust source regions: the importance of particle mineralogy. *Atmos. Environ.*, **38** (36), 6253–6261. doi: 10.1016/j.atmosenv.2004.07.010
- Kulmala, M. and Laaksonen, A. (1990) Binary nucleation of water sulfuric acid system. Comparison of classical theories with different H₂SO₄ saturation vapor pressures. *J. Chem. Phys.*, **93** (1), 696–701.
- Kulmala, M., Vehkamäki, H., Petäjä, T., Dal Maso, M., Lauri, A., Kerminen, V.-M., Birmili, W., and McMurry, P.H. (2004) Formation and growth rates of ultrafine atmospheric particles: a review of observations. *J. Aerosol Sci.*, **35** (2), 143–176. doi: 10.1016/j.jaerosci.2003.10.003
- Kwok, S. and Zhang, Y. (2011) Mixed aromatic–aliphatic organic nanoparticles as carriers of unidentified infrared emission features. *Nature*, **479** (7371), 80–83. doi: 10.1038/nature10542
- Leck, C. and Bigg, E.K. (2005) Source and evolution of the marine aerosol - A new perspective. *Geophys. Res. Lett.*, **32** (L19803), 1–4. doi: 10.1029/2005GL023651
- Lelieveld, J., Roelofs, G.J., Ganzeveld, L., Feichter, J., and Rodhe, H. (1997) Terrestrial sources and distribution of atmospheric sulphur. *Philos. Trans. R. Soc. London, Ser. B*, **352**, 149–158. doi: 10.1098/rstb.1997.0010
- Li, J., Anderson, J.R., and Buseck, P.R. (2003a) TEM study of aerosol particles from clean and polluted marine boundary layers over the North Atlantic. *J. Geophys. Res.*, **108** (D6), 4189. doi: 10.1029/2002JD002106
- Li, J., Pósfai, M., Hobbs, P.V., and Buseck, P.R. (2003b) Individual aerosol particles from biomass burning in southern Africa: 2. Compositions and aging of inorganic particles. *J. Geophys. Res.*, **108** (D13), 8484. doi: 10.1029/2002JD002310
- Liao, H., Adams, P.J., Seinfeld, J.H., Mickley, L.J., and Jacob, D.J. (2003) Interactions between tropospheric chemistry and aerosols in a unified GCM simulation. *J. Geophys. Res.*, **108** (D1), 4001. doi: 10.1029/2001JD001260
- Liao, H., Seinfeld, J.H., Adams, P.J., and Mickley, L.J. (2004) Global radiative forcing of coupled tropospheric ozone and aerosols in a unified general circulation model. *J. Geophys. Res.*, **109**, D16207. doi: 10.1029/2001JD002004
- Lin, Y., Sim, M.S., and Ono, S. (2011) Multiple-sulfur isotope effects during

- photolysis of carbonyl sulfide. *Atmos. Chem. Phys.*, **11** (19), 10283–10292. doi: 10.5194/acp-11-10283-2011
- Lioussé, C., Penner, J.E., Chuang, C., Walton, J.J., Eddleman, H., and Cachier, H. (1996) A global three-dimensional model study of carbonaceous aerosols. *J. Geophys. Res.*, **101** (D14), 19411–19432. doi: 10.1029/95JD03426
- Liu, X., Penner, J.E., and Herzog, M. (2005) Global modeling of aerosol dynamics: model description, evaluation, and interactions between sulfate and nonsulfate aerosols. *J. Geophys. Res.*, **110**, D18206. doi: 10.1029/2004JD005674
- Lohmann, U. and Lesins, G. (2002) Stronger constraints on the anthropogenic indirect aerosol effect. *Science*, **298** (5595), 1012–1015. doi: 10.1126/science.1075405
- McCormick, M.P., Thomason, L.W., and Trepte, C.R. (1995) Atmospheric effects of the Mt. Pinatubo eruption. *Nature*, **373** (6513), 399–404. doi: 10.1038/373399a0
- McKinnon, J.T. and Howard, J.B. (1990) Application of soot formation model: effects of chlorine. *Combust. Sci. Technol.*, **74** (1-6), 175–197. doi: 10.1080/00102209008951687
- Mandrioli, P., Negrini, M.G., Scarani, C., Tampieri, F., and Trombetti, F. (1980) Mesoscale transport of Corylus pollen grains in winter atmosphere. *Grana*, **19** (3), 227–233. doi: 10.1080/00173138009425007
- Mårtensson, E.M., Nilsson, E.D., de Leeuw, G., Cohen, L.H., and Hansson, H.-C. (2003) Laboratory simulations and parameterization of the primary marine aerosol production. *J. Geophys. Res.*, **108** (D9), 4297. doi: 10.1029/2002JD002263
- Martcorena, B., Bergametti, G., Aumont, B., Callot, Y., N'Doumé, C., and Legrand, M. (1997) Modeling the atmospheric dust cycle. 2. Simulation of Saharan dust sources. *J. Geophys. Res.*, **102** (D4), 4387–4404. doi: 10.1029/96JD02964
- Martins, J.V., Hobbs, P.V., Weiss, R.E., and Artaxo, P. (1998) Sphericity and morphology of smoke particles from biomass burning in Brazil. *J. Geophys. Res.*, **103** (D24), 32051–32057. doi: 10.1029/98JD01153
- Matsuki, A., Iwasaka, Y., Shi, G., Zhang, D., Trochkin, D., Yamada, M., Kim, Y.-S., Chen, B., Nagatani, T., Miyazawa, T., Nagatani, M., and Nakata, H. (2005) Morphological and chemical modification of mineral dust: observational insight into the heterogeneous uptake of acidic gases. *Geophys. Res. Lett.*, **32**, L22806. doi: 10.1029/2005GL024176
- Matthias-Maser, S. and Jaenicke, R. (1994) Examination of atmospheric bioaerosol particles with radii > 0.2 μm . *J. Aerosol Sci.*, **25** (8), 1605–1613. doi: 10.1016/0021-8502(94)90228-3
- Matthias-Maser, S. and Jaenicke, R. (1995) The size distribution of primary biological aerosol particles with radii > 0.2 μm in an urban-rural influenced region. *Atmos. Res.*, **39** (4), 279–286. doi: 10.1016/0169-8095(95)00017-8
- Meehl, G.A. and Tebaldi, C. (2004) More intense, more frequent, and longer lasting heat waves in the 21st century. *Science*, **305** (5686), 994–997. doi: 10.1126/science.1098704
- Middlebrook, A.M., Murphy, D.M., and Thomson, D.S. (1998) Observations of organic material in individual marine particles at Cape Grim during the First Aerosol Characterization Experiment (ACE 1). *J. Geophys. Res.*, **103** (D13), 16475–16483. doi: 10.1029/97JD03719
- Mie, G. (1908) Beiträge zur Optik trüber Medien, speziell kolloidaler Metallösungen. *Ann. Phys., Vierte Folge*, **25** (3), 377–445.
- Mirabel, P. and Katz, J.L. (1974) Binary homogeneous nucleation as a mechanism for the formation of aerosols. *J. Chem. Phys.*, **60** (3), 1138–1144. doi: 10.1063/1.1681124
- Molinarioli, E., Pistolato, M., Rampazzo, G., and Guerzoni, S. (1999) Geochemistry of natural and anthropogenic fall-out (aerosol and precipitation) collected from the NW Mediterranean: two different multivariate statistical approaches. *Appl. Geochem.*, **14** (4), 27–36. doi: 10.1016/S0883-2927(98)00062-6

- Monahan, E.C., Spiel, D.E., and Davidson, K.L. (1986) Model of marine aerosol generation via whitecaps and wave disruption, in *Oceanic Whitecaps and their Role in Air-Sea Exchange Processes* (eds E.C. Monahan and G. McNiocail), D. Reidel Publishing, Dordrecht, pp. 167–174.
- Morris, C.E., Sands, D.C., Bardin, M., Jaenicke, R., Vogel, B., Leyronas, C., Ariya, P.A., and Psenner, R. (2011) Microbiology and atmospheric processes: research challenges concerning the impact of airborne micro-organisms on the atmosphere and climate. *Biogeosciences*, **8** (17-25), 91–212. doi: 10.5194/bg-8-17-2011
- Moulin, C., Lambert, C.E., Dulac, E., and Dayan, U. (1997) Control of atmospheric export of dust from North Africa by the North Atlantic Oscillation. *Nature*, **387** (6634), 691–694. doi: 10.1038/42679
- Mullins, M.E., Michaels, L.P., Menon, V., Locke, B., and Ranade, M.B. (1992) Effect of geometry on particle adhesion. *Aerosol Sci. Technol.*, **17** (2), 105–118. doi: 10.1080/02786829208959564
- Muñoz, O., Volten, H., Hovenier, J.W., Veihelmann, B., van der Zande, W.J., Waters, L.B.F.M., and Rose, W.I. (2004) Scattering matrices of volcanic ash particles of Mount St. Helens, Redoubt, and Mount Spurr Volcanoes. *J. Geophys. Res.*, **109**, D16201. doi: 10.1029/2004JD004684
- Niemi, J.V., Saarikoski, S., Tervahattu, H., Mäkelä, T., Hillamo, R., Vehkamäki, H., Sogacheva, L., and Kulmala, M. (2006) Changes in background aerosol composition in Finland during polluted and clean periods studied by TEM/EDX individual particle analysis. *Atmos. Chem. Phys.*, **6** (12), 5049–5066. doi: 10.5194/acp-6-5049-2006
- O'Dowd, C.D., Smith, M.H., Consterdine, I.E., and Lowe, J.A. (1997) Marine aerosol, sea-salt, and the marine sulphur cycle: a short review. *Atmos. Environ.*, **31** (1), 73–80. doi: 10.1016/S1352-2310(96)00106-9
- Okada, K. and Kai, K. (2004) Atmospheric mineral particles collected at Qira in the Taklamakan Desert, China. *Atmos. Environ.*, **38** (40), 6927–6935. doi: 10.1016/j.atmosenv.2004.03.078
- Okazaki, K. (1993) Submicron particle formation in pulverized coal combustion. *J. Aerosol Res. Jpn.*, **7**, 289–291.
- Pakkanen, T.A. (1996) Study of formation of coarse particle nitrate aerosol. *Atmos. Environ.*, **30** (14), 2475–2482. doi: 10.1016/1352-2310(95)00492-0
- Paris, J.-D., Stohl, A., Nédélec, P., Arshinov, M.Y., Panchenko, M.V., Shmargunov, V.P., Law, K.S., Belan, B.D., and Ciais, P. (2009) Wildfire smoke in the Siberian Arctic in summer: source characterization and plume evolution from airborne measurements. *Atmos. Chem. Phys.*, **9** (23), 9315–9327. doi: 10.5194/acp-9-9315-2009
- Penner, J.E., Bergmann, D.J., Walton, J.J., Kinnison, D., Prather, M.J., Rotman, D., Price, C., Pickering, K.E., and Baughcum, S.L. (1998) An evaluation of upper tropospheric NO_x with two models. *J. Geophys. Res.*, **103** (D17), 22097–22113. doi: 10.1029/98JD01565
- Penner, J., Dickinson, R., and O'Neill, C. (1992) Effects of aerosols from biomass burning on the global radiation budget. *Science*, **256** (5062), 1432–1434. doi: 10.1126/science.256.5062.1432
- Penner, J.E., Lister, D., Griggs, D., Docken, D., and MacFarland, M.M. (eds) (1999) *Aviation and the Global Atmosphere*, Intergovernmental Panel on Climate Change, Special Report, Cambridge University Press, Cambridge, p. 373.
- Piccot, S.D., Watson, J.J., and Jones, J.W. (1992) A global inventory of volatile organic compound emissions from anthropogenic sources. *J. Geophys. Res.*, **97** (D9), 9897–9912. doi: 10.1029/92JD00682
- Plane, J.M.C. (2012) Cosmic dust in the earth's atmosphere. *Chem. Soc. Rev.*, **41** (19), 6507–6518. doi: 10.1039/C2CS35132C
- Pósfai, M. and Buseck, P.R. (2010) Nature and climate effects of individual tropospheric aerosol particles. *Annu. Rev. Earth Planet. Sci.*, **38**, 17–43. doi: 10.1146/annurev.earth.031208.100032
- Pósfai, M., Anderson, J.R., Buseck, P.R., and Sievering, H. (1995) Compositional variations of sea-salt-mode aerosol particles

- from the North Atlantic. *J. Geophys. Res.*, **100** (D11), 23063–23074. doi: 10.1029/95JD01636
- Pósfai, M., Anderson, J.R., Buseck, P.R., and Sievering, H. (1999) Soot and sulfate aerosol particles in the remote marine troposphere. *J. Geophys. Res.*, **104** (D17), 21685–21693. doi: 10.1029/1999JD900208
- Pósfai, M., Gelencsér, A., Simonics, R., Arató, K., Li, J., Hobbs, P.V., and Buseck, P.R. (2004) Atmospheric tar balls: particles from biomass and biofuel burning. *J. Geophys. Res.*, **109**, D06213. doi: 10.1029/2003JD004169
- Pósfai, M., Simonics, R., Li, J., Hobbs, P.V., and Buseck, P.R. (2003a) Individual aerosol particles from biomass burning in southern Africa: 1. Compositions and size distributions of carbonaceous particles. *J. Geophys. Res.*, **108** (D13), 8483. doi: 10.1029/2002JD002291
- Pósfai, M., Li, J., Anderson, J.R., and Buseck, P.R. (2003b) Aerosol bacteria over the Southern Ocean during ACE-1. *Atmos. Res.*, **66** (4), 231–240. doi: 10.1016/S0169-8095(03)00039-5
- Pósfai, M., Xu, H., Anderson, J.R., and Buseck, P.R. (1998) Wet and dry sizes of atmospheric aerosol particles: an AFM-TEM study. *Geophys. Res. Lett.*, **25** (11), 1907–1910. doi: 10.1029/98GL01416
- Price, C., Penner, J., and Prather, M. (1997) NO_x from lightning. 1. Global distribution based on lightning physics. *J. Geophys. Res.*, **102** (D5), 5929–5941. doi: 10.1029/96JD03504
- Prospero, J.M. (1999) Long-range transport of mineral dust in the global atmosphere: impact of African dust on the environment of the southeastern United States. *Proc. Natl. Acad. Sci. U.S.A.*, **96** (7), 3398–3403. doi: 10.1073/pnas.96.7.3396
- Prospero, J.M. and Nees, R.T. (1986) Impact of the North African drought and El Niño on mineral dust in the Barbados trade winds. *Nature*, **320** (6064), 735–738. doi: 10.1038/320735a0
- Pueschel, R.F., Kinne, S.A., Russell, P.B., Snetsinger, K.G., and Livingston, J.M. (1993) Effects of the 1991 Pinatubo volcanic eruption on the physical and radiative properties of stratospheric aerosols, in IRS '92: Current Problems in Atmospheric Radiation, Proceedings of the International Radiation Symposium, Tallinn (Estonia), 2-8 August 1992 (eds S. Keevallik and O. Kärner), A. Deepak Publishing, Hampton, VA, pp. 183–186.
- Reid, J.S., Koppmann, R., Eck, T.F., and Eleuterio, D.P. (2005) A review of biomass burning emissions. Part II: Intensive physical properties of biomass burning particles. *Atmos. Chem. Phys.*, **5** (3), 799–825. doi: 10.5194/acp-5-799-2005
- Rose, W.I. and Durant, A.J. (2009) Fine ash content of explosive eruptions. *J. Volcanol. Geotherm. Res.*, **186** (1-2), 32–39. doi: 10.1016/j.jvolgeores.2009.01.010
- Russell, P.B., Livingston, J.M., Dutton, E.G., Pueschel, R.F., Reagan, J.A., DeFoor, T.E., Box, M.A., Allen, D., Pilewski, P., Herman, B.M., Kinne, S.A., and Hofmann, D.J. (1993) Pinatubo and pre-Pinatubo optical-depth spectra: mauna Loa measurements, comparisons, inferred particle size distributions, radiative effects, and relationship to Lidar data. *J. Geophys. Res.*, **98** (D12), 22969–22985. doi: 10.1029/93JD02308
- Sabbioni, C. (1992) Characterization of atmospheric particles on monuments by scanning electron microscopy/energy dispersive X-ray analyses. Electron Microscopy 92. Material Sciences, Proceedings of 10th European Congress on Electron Microscopy (EUREM 92), Vol. 2, September 1992, Granada, Spain.
- Sabbioni, C. and Zappia, G. (1992) Characterization of particles emitted by domestic heating units fueled by distilled oil. *Atmos. Environ.*, **26** (18), 3297–3304. doi: 10.1016/0960-1686(92)90346-M
- Sassen, K. (1992) Evidence for liquid-phase cirrus cloud formation from volcanic aerosols: climatic implications. *Science*, **257** (5069), 516–519. doi: 10.1126/science.257.5069.516
- Sattler, B., Puxbaum, H., and Psenner, R. (2001) Bacterial growth in supercooled cloud droplets. *Geophys. Res. Lett.*, **28** (2), 239–242. doi: 10.1029/2000GL011684
- Schnaiter, M., Linke, C., Möhler, O., Naumann, K.-H., Saathoff, H., Wagner, R., Schurath, U., and Wehner, B. (2005)

- Absorption amplification of black carbon internally mixed with secondary organic aerosol. *J. Geophys. Res.*, **110**, D19. doi: 10.1029/2005JD006046
- Schnell, R.C. and Vali, G. (1976) Biogenic ice nuclei: Part I. Terrestrial and marine sources. *J. Atmos. Sci.*, **33** (8), 1554–1564. doi: 10.1175/1520-0469(1976)033<1554:BINPIT>2.0.CO;2
- Schumann, U., Weinzierl, B., Reitebuch, O., Schlager, H., Minikin, A., Forster, C., Baumann, R., Sailer, T., Graf, K., Mannstein, H., Voigt, C., Rahm, S., Simmet, R., Scheibe, M., Lichtenstern, M., Stock, P., Rüba, H., Schäuble, D., Tafferner, A., Rautenhaus, M., Gerz, T., Ziereis, H., Krautstrunk, M., Mallaun, C., Gayet, J.-F., Lieke, K., Kandler, K., Ebert, M., Weinbruch, S., Stohl, A., Gasteiger, J., Groß, S., Freudenthaler, V., Wiegner, M., Ansmann, A., Tesche, M., Olafsson, H., and Sturm, K. (2011) Airborne observations of the Eyjafalla volcano ash cloud over Europe during air space closure in April and May 2010. *Atmos. Chem. Phys.*, **11** (5), 2245–2279. doi: 10.5194/acp-11-2245-2011
- Schwartz, S.E., Arnold, F., Blanchet, J.-P., Durkee, P.A., Hofmann, D.J., Hoppel, W.A., King, M.D., Laci, A.A., Nakajima, T., Ogren, J.A., Toon, O.B., and Wendisch, M. (1995) Group report: connections between aerosol properties and forcing of climate, in *Aerosol Forcing of Climate* (eds R.J. Charlson and J. Heintzenberg), John Wiley & Sons, Inc., New York, pp. 251–280.
- Seinfeld, J.H. and Pandis, S.N. (1998) *Atmospheric Chemistry and Physics, from Air Pollution to Climate Change*, 1st edn, John Wiley & Sons, Inc., New York, p. 1326.
- Seinfeld, J.H. and Pandis, S.N. (2006) *Atmospheric Chemistry and Physics, from Air Pollution to Climate Change*, 2nd edn, John Wiley & Sons, Inc., Hoboken, NJ, p. 1225.
- Shen, T.L., Wooldrige, P.J., and Molina, M.J. (1995) Stratospheric pollution and ozone depletion, in *Composition, Chemistry, and Climate of the Atmosphere* (ed. H.B. Singh), Van Nostrand Reinhold, New York, pp. 394–442.
- Shettle, E.P. and Fenn, R.W. (1979) Models for the Aerosols of the Lower Atmosphere and the Effects of Humidity Variations on their Optical Properties. Environmental Research Papers, No. 676, Air Force Geophys. Lab., AFGL-Techn. Rep. 79-0214, Hanscom AFB, MA, 94 pp.
- Sievering, H., Boatman, J., Gorman, E., Kim, Y., Anderson, L., Ennis, G., Luria, M., and Pandis, S. (1992) Removal of sulphur from the marine boundary layer by ozone oxidation in sea-salt aerosols. *Nature*, **360** (6404), 571–573. doi: 10.1038/360571a0
- Simoneit, B.R.T., Cardoso, J.N., and Robinson, N. (1990) An assessment of the origin and composition of higher molecular weight organic matter in aerosols over Amazonia. *Chemosphere*, **21** (10-11), 1285–1301. doi: 10.1016/0045-6535(90)90145-J
- Sinha, B.W., Hoppe, P., Huth, J., Foley, S., and Andreae, M.O. (2008) Sulfur isotope analyses of individual aerosol particles in the urban aerosol at a central European site (Mainz, Germany). *Atmos. Chem. Phys.*, **8** (23), 7217–7238. doi: 10.5194/acp-8-7217-2008
- SMIC (1971) Inadvertent Climate Modification, Report of the Study of Man's Impact on Climate (SMIC), MIT Press, Cambridge, MA, pp. 185–232.
- Smith, J.N., Dunn, M.J., VanReken, T.M., Iida, K., Stolzenburg, M.R., McMurry, P.H., and Huey, L.G. (2008) Chemical composition of atmospheric nanoparticles formed from nucleation in Tecamac, Mexico: evidence for an important role for organic species in nanoparticle growth. *Geophys. Res. Lett.*, **35**, L04808. doi: 10.1029/2007GL032523
- Sobanska, S., Coeur, C., Maenhaut, W., and Adams, F. (2003) SEM-EDX characterisation of tropospheric aerosols in the Negev desert (Israel). *J. Atmos. Chem.*, **44** (3), 299–322. doi: 10.1023/A:1022969302107
- Song, N., Starr, D.O.'C., Wuebbles, D.J., Williams, A., and Larson, S.M. (1996) Volcanic aerosols and interannual variation of high clouds. *Geophys. Res. Lett.*, **23** (19), 2657–2660. doi: 10.1029/96GL02372

- Spiro, P.A., Jacob, D.J., and Logan, J.A. (1992) Global inventory of sulfur emissions with $1^\circ \times 1^\circ$ resolution. *J. Geophys. Res.*, **97** (D5), 6023–6036. doi: 10.1029/91JD03139
- Stelson, A.W. and Seinfeld, J.H. (1982a) Relative humidity and temperature dependence of the ammonium nitrate dissociation constant. *Atmos. Environ.*, **16** (5), 983–992. doi: 10.1016/0004-6981(82)90184-6
- Stelson, A.W. and Seinfeld, J.H. (1982b) Thermodynamic prediction of the water activity, NH_4NO_3 dissociation constant, density and refractive index for the system NH_4NO_3 - $(\text{NH}_4)_2\text{SO}_4$ - H_2O at 25 °C. *Atmos. Environ.*, **16** (10), 2507–2514. doi: 10.1016/0004-6981(82)90142-1
- Stohl, A., Andrews, E., Burkhardt, J.F., Forster, C., Herber, A., Hoch, S.W., Kowal, D., Lunder, C., Mefford, T., Ogren, J.A., Sharma, S., Spichtinger, N., Stebel, K., Stone, R., Ström, J., Tørseth, K., Wehrli, C., and Yttri, K.E. (2006) Pan-Arctic enhancements of light absorbing aerosol concentrations due to North American boreal forest fires during summer 2004. *J. Geophys. Res.*, **111**, D22214. doi: 10.1029/2006JD007216
- Stone, R.S., Anderson, G.P., Andrews, E., Dutton, E.G., Shettle, E.P., and Berk, A. (2007) Incursions and radiative impact of Asian dust in northern Alaska. *Geophys. Res. Lett.*, **34**, L14815. doi: 10.1029/2007GL029878
- Stone, R.S., Anderson, G.P., Shettle, E.P., Andrews, E., Loukachine, K., Dutton, E.G., Schaaf, C., and Roman, M.O. III, (2008) Radiative impact of boreal smoke in the Arctic: observed and modeled. *J. Geophys. Res.*, **113**, D14S16. doi: 10.1029/2007JD009657
- Tegen, I. and Fung, I. (1995) Contribution to the atmospheric mineral aerosol load from land surface modification. *J. Geophys. Res.*, **100** (D9), 18707–18726. doi: 10.1029/95JD02051
- Tegen, I., Hollrig, P., Chin, M., Fung, I., Jacob, D., and Penner, J. (1997) Contribution of different aerosol species to the global aerosol extinction optical thickness: estimates from model results. *J. Geophys. Res.*, **102** (D20), 23895–23915. doi: 10.1029/97JD01864
- Tegen, I. and Miller, R. (1998) A general circulation model study of the interannual variability of soil dust aerosol. *J. Geophys. Res.*, **103** (D20), 25975–25995. doi: 10.1029/98JD02345
- Thomason, L.W., Burton, S.P., Luo, B.-P., and Peter, T. (2008) SAGE II measurements of stratospheric aerosol properties at non-volcanic levels. *Atmos. Chem. Phys.*, **8** (4), 983–995. doi: 10.5194/acp-8-983-2008
- Tivanski, A.V., Hopkins, R.J., Tyliczszak, T., and Gilles, M.K. (2007) Oxygenated interface on biomass burn tar balls determined by single particle scanning transmission X-ray microscopy. *J. Phys. Chem. A*, **111** (25), 5448–5458. doi: 10.1021/jp070155u
- Tomasi, C., Vitale, V., and Tarozzi, L. (1997) Sun-photometric measurements of atmospheric turbidity variations caused by the Pinatubo aerosol cloud in the Himalayan region during the summer periods of 1991 and 1992. *Il Nuovo Cimento C*, **20** (1), 61–88.
- Tomasi, C., Vitale, V., Lupi, A., Di Carmine, C., Campanelli, M., Herber, A., Treffeisen, R., Stone, R.S., Andrews, E., Sharma, S., Radionov, V., von Hoyningen-Huene, W., Stebel, K., Hansen, G.H., Myhre, C.L., Wehrli, C., Aaltonen, V., Lihavainen, H., Virkkula, A., Hillamo, R., Ström, J., Toledano, C., Cachorro, V., Ortiz, P., de Frutos, A., Blindheim, S., Frioud, M., Gausa, M., Zielinski, T., Petelski, T., and Yamanouchi, T. (2007) Aerosols in polar regions: a historical overview based on optical depth and in situ observations. *J. Geophys. Res.*, **112**, D16205. doi: 10.1029/2007JD008432
- Toohey, M., Krüger, K., Niemeier, U., and Timmreck, C. (2011) The influence of eruption season on the global aerosol evolution and radiative impact of tropical volcanic eruptions. *Atmos. Chem. Phys.*, **11** (23), 12351–12367. doi: 10.5194/acp-11-12351-2011
- Toon, O.B., Pollack, J.B., and Khare, B.N. (1976) The optical constants of several atmospheric aerosol species: ammonium sulfate, aluminum oxide, and sodium chloride. *J. Geophys. Res.*, **81** (33), 5733–5748. doi: 10.1029/JC081i033p05733

- Trochkin, D., Iwasaka, Y., Matsuki, A., Yamada, M., Kim, Y.-S., Nagatani, T., Zhang, D., Shi, G.-Y., and Shen, Z. (2003) Mineral aerosol particles collected in Dunhuang, China, and their comparison with chemically modified particles collected over Japan. *J. Geophys. Res.*, **108** (D23), 8642. doi: 10.1029/2002JD003268
- Tsigaridis, K. and Kanakidou, M. (2007) Secondary organic aerosol importance in the future atmosphere. *Atmos. Environ.*, **41** (22), 4682–4692. doi: 10.1016/j.atmosenv.2007.03.045
- Tsigaridis, K., Krol, M., Dentener, F.J., Balkanski, Y., Lathière, J., Metzger, S., Hauglustaine, D.A., and Kanakidou, M. (2006) Change in global aerosol composition since preindustrial times. *Atmos. Chem. Phys.*, **6** (12), 5143–5162. doi: 10.5194/acp-6-5143-2006
- United Nations (1979) *Fine Particulate Pollution*, Pergamon Press, New York.
- van Poppel, L.H., Friedrich, H., Spinsby, J., Chung, S.H., Seinfeld, J.H., and Buseck, P.R. (2005) Electron tomography of nanoparticle clusters: implications for atmospheric lifetimes and radiative forcing of soot. *Geophys. Res. Lett.*, **32**, L24811. doi: 10.1029/2005GL024461
- Wagner, H.G. (1981) Soot formation - an overview, in *Particulate Carbon Formation During Combustion* (eds D.C. Siegl and G.W. Smith), Plenum Press, New York, pp. 1–29.
- Wallace, J.M. and Hobbs, P.V. (2006) *Atmospheric Science: An Introductory Survey*, 2nd edn, Elsevier Academic Press, Burlington, MA, pp. 153–208.
- Wentzel, M., Gorzawski, H., Naumann, K.H., Saathoff, H., and Weinbruch, S. (2003) Transmission electron microscopical and aerosol dynamical characterization of soot aerosols. *J. Aerosol Sci.*, **34** (10), 1347–1370. doi: 10.1016/S0021-8502(03)00360-4
- Winiwarter, W., Bauer, H., Caseiro, A., and Puxbaum, H. (2009) Quantifying emissions of primary biological aerosol particle mass in Europe. *Atmos. Environ.*, **43** (7), 1403–1407. doi: 10.1016/j.atmosenv.2008.01.037
- Wolf, M.E. and Hidy, G.M. (1997) Aerosols and climate: anthropogenic emissions and trends for 50 years. *J. Geophys. Res.*, **102** (D10), 11113–11121. doi: 10.1029/97JD00199
- Wolff, E.W. and Cachier, H. (1998) Concentrations and seasonal cycle of black carbon in aerosol at a coastal Antarctic station. *J. Geophys. Res.*, **103** (D9), 11033–11041. doi: 10.1029/97JD01363
- Yienger, J.J. and Levy, H. II, (1995) Empirical model of global soil-biogenic NO_x emissions. *J. Geophys. Res.*, **100** (D6), 11447–11464. doi: 10.1029/95JD00370
- Zender, C.S., Brian, H., and Newman, D. (2003) Mineral Dust Entrainment And Deposition (DEAD) model: description and 1990s dust climatology. *J. Geophys. Res.*, **107** (D24), 4416. doi: 10.1029/2002JD002775
- Zender, C.S., Miller, R.L., and Tegen, I. (2004) Quantifying mineral dust mass budgets: terminology, constraints, and current estimates. *Eos Trans. Am. Geophys. Union*, **85** (48), 509–512. doi: 10.1029/2004EO480002
- Zhang, R., Suh, I., Zhao, J., Zhang, D., Fortner, E.C., Tie, X., Molina, L.T., and Molina, M.J. (2004) Atmospheric new particle formation enhanced by organic acids. *Science*, **304** (5676), 1487–1490. doi: 10.1126/science.1095139
- Zook, H.A. (2001) Spacecraft measurements of the cosmic dust flux, in *Accretion of Extraterrestrial Matter Throughout Earth's History* (eds B. Peucker-Ehrenbrink and B. Schmitz), Springer US, Kluwer Academic/Plenum Publishers, New York, pp. 75–92. doi: 10.1007/978-1-4419-8694-8_5